SRI International

Final Report • August 1996

DIAGNOSTICS OF DIAMOND FILM DEPOSITION PLASMAS

Contract DAAH04-93-K-0001

Kenneth R. Stalder, Senior Research Physicist
Molecular Physics Laboratory

and

Jay B. Jeffries, Senior Research Chemical Physicist
Molecular Physics Laboratory

SRI Project PYU 4524
MP 96-108

Prepared for:

U.S. Army Research Office
P.O. Box 12211
Research Triangle Park, NC 27709-2211

333 Ravenswood Avenue • Menlo Park, CA 94025-3493 • (415) 326-6200 • FAX: (415) 326-5512 • Telex: 334486

SRI International

Final Report • August 1996

DIAGNOSTICS OF DIAMOND FILM DEPOSITION PLASMAS

Contract DAAH04-93-K-0001

Kenneth R. Stalder, Senior Research Physicist
Molecular Physics Laboratory

and

Jay B. Jeffries, Senior Research Chemical Physicist
Molecular Physics Laboratory

SRI Project PYU 4524
MP 96-108

Prepared for:

U.S. Army Research Office
P.O. Box 12211
Research Triangle Park, NC 27709-2211

333 Ravenswood Avenue • Menlo Park, CA 94025-3493 • (415) 326-6200 • FAX: (415) 326-5512 • Telex: 334486

REPORT DOCUMENTATION PAGE

Form Approved OMB No. 0704-0188

1. AGENCY USE ONLY *(Leave blank)*	2. REPORT DATE	3. REPORT TYPE AND DATES COVERED
	07/01/96	Final Progress 03/01/93 - 02/28/96

4. TITLE AND SUBTITLE

Diagnostics of Diamond Film Deposition Plasmas

5. FUNDING NUMBERS

DAAH04-93-K-0001

6. AUTHOR(S)

Kenneth R. Stalder and Jay B. Jeffries

7. PERFORMING ORGANIZATION NAME(S) AND ADDRESS(ES)

SRI International
Molecular Physics Laboratory
333 Ravenswood Avenue
Menlo Park, CA 94025-3493

8. PERFORMING ORGANIZATION REPORT NUMBER

Project 4524
MP 96-108

9. SPONSORING/MONITORING AGENCY NAME(S) AND ADDRESS(ES)

U.S. Army Research Office
P.O. Box 12211
Research Triangle Park, NC 27709-2211

10. SPONSORING/MONITORING AGENCY REPORT NUMBER

ARO 30665.1-PH

11. SUPPLEMENTARY NOTES

The views, opinions and/or findings contained in this report are those of the authors and should not be construed as an official Department of the Army position, policy or decision, unless so designated by other documentation.

12a. DISTRIBUTION/AVAILABILITY STATEMENT

Approved for public release; distribution unlimited.

12b. DISTRIBUTION CODE

13. ABSTRACT *(Maximum 200 words)*

Diagnostic measurements of diamond-depositing dc arcjet plasmas are described. Polycrystalline diamond films with high-quality Raman spectra are grown using both low-pressure (5 to 40 Torr) and high-pressure (200 Torr) plasma arcjets. A number of different techniques, including laser-induced fluorescence (LIF), optical emission spectroscopy, mass spectroscopy, and Langmuir probe methods were developed and applied to measure properties of the plasma's physical and chemical environment as it deposits diamond on a surface. Low-pressure arcjets are usually well out of thermal equilibrium even as they strike the substrate surface. LIF measurements show the gas temperature actually increases downstream of the arc, from 1800 to 2400 K, as a result of hydrogen atom recombination, whereas, Langmuir probe measurements show the electron temperature is roughly constant at 1 to 2 eV (12,000 to 24,000 K). Many species important for characterizing the physical environment have been detected with the optical methods (C_2, CH, C_3), and the mass spectroscopic measurements have focused on the species thought to be important for diamond growth (CH_3 and C_2H_2).

14. SUBJECT TERMS

Diamond, thin films, arcjets, plasmas, diagnostics, laser-induced fluorescence, Langmuir probes, mass spectroscopy, optical emission spectroscopy, spectroscopy

15. NUMBER OF PAGES

97 incl. Appendixes

16. PRICE CODE

17. SECURITY CLASSIFICATION OF REPORT	18. SECURITY CLASSIFICATION OF THIS PAGE	19. SECURITY CLASSIFICATION OF ABSTRACT	20. LIMITATION OF ABSTRACT
UNCLASSIFIED	UNCLASSIFIED	UNCLASSIFIED	UL

DIAGNOSTICS OF DIAMOND FILM DEPOSITION PLASMAS

FINAL PROGRESS REPORT

KENNETH R. STALDER AND JAY B. JEFFRIES

JULY 1, 1996

U.S. ARMY RESEARCH OFFICE

CONTRACT # DAAH04-93-K-0001

SRI INTERNATIONAL

CONTENTS

INTRODUCTION 1
STATEMENT OF THE PROBLEM STUDIED 1
SUMMARY OF THE MOST IMPORTANT RESULTS 2
Diamond Deposition by dc-Arcjet Plasmas 2
Low-Pressure Arcjet 3
Laser-Induced Fluorescence 4
Mass Spectroscopy 7
Langmuir Probe Measurements 8
RECOMMENDATIONS FOR FUTURE WORK 9
LIST OF PUBLICATIONS (1993-1996) 10
LIST OF CONFERENCE AND OTHER PRESENTATIONS 10
LIST OF PARTICIPATING SCIENTIFIC PERSONNEL 12
REPORT OF INVENTIONS 12
BIBLIOGRAPHY 13
APPENDIXES

- A: Understanding Plasma CVD of Diamond Films
- B: Observation and Spatial Distribution of C_3 in a dc-Arcjet Plasma During Diamond Deposition Using Laser-Induced Fluorescence
- C: Optical Diagnostics for Temperature Measurement in a dc-Arcjet Reactor Used for Diamond Deposition
- D: Electron Densities and Temperatures in a Diamond-Depositing dc-Arcjet Plasma

INTRODUCTION

The successful development and implementation of diamond-related products into Army systems hold great promise. Diamond is a unique material that has combined physical properties not found in any other material. It has a high electrical resistivity, normally associated with good electrical insulators, but also has extremely high thermal conductivity, normally found in metals. These combined properties are driving much research and development in the Army and in other DoD agencies to see if diamond can be exploited for military applications.

Diamond has been produced synthetically by high-pressure, high-temperature methods for many years, but only in the last decade or so has the low-pressure, plasma, chemical vapor deposition (CVD) method been studied as a means of producing diamond with properties good enough for useful applications.

The Army Research Office (ARO) has been supporting research related to CVD of diamond for at least the last six years. SRI's program is centered on developing diagnostic methods for understanding the CVD growth environment so that better diamond products can be produced. As a result of ARO support, we have developed a very good understanding of the diamond growth environment, and commercial diamond production applications are emerging that use the results of our research. We have expanded our understanding of the plasma CVD environment and improved the Army's position to exploit diamond technology.

STATEMENT OF THE PROBLEM STUDIED

The deposition of thin films of diamond hold great promise for applications relevant to the Army. Among these are improved hard coatings, thermal management materials, and a variety of electronic applications ranging from MMIC devices to radiation hard devices. Diamond has unique properties such as extremely high electrical resistivity yet extremely high thermal conductivity. This combination is not found in any other material to the degree found in diamond.

Synthetic diamond can be made by a variety of methods ranging from conventional high-pressure, high-temperature processes to the more recent advent of low-pressure CVD processes. Although low-pressure CVD can produce diamond coatings and free-standing plates of polycrystalline diamond, the growth rates are slow and only a tiny fraction of the feedstock carbon is incorporated into the diamond film. We wish to improve the efficiency of diamond deposition by developing sensors and models to provide real-time process control to improve diamond yield even for very long process times.

SRI's program under ARO sponsorship is to develop diagnostic methods to further the understanding of the physics and chemistry of diamond growth under plasma CVD conditions. Because arcjet plasmas have been shown by us, and others, to have properties that promote the high-rate deposition of diamond, our program is centered on the development of diagnostics that can probe this unique environment. We have developed diagnostics over the last six years in support of this program. This report describes our efforts for the last three years.

SUMMARY OF THE MOST IMPORTANT RESULTS

Most of our findings have been discussed in prior annual reports or in publications. During this project, we published 9 papers and presented 19 papers at scientific conferences and research institutes. In addition, we submitted an article to ARO's Research Highlights, a copy of which is included as Appendix A. Other appendixes contain preprints of articles soon to be published. The following sections review the most important findings discussed in our publications and presentations.

Diamond Deposition by DC-Arcjet Plasmas

Under ARO sponsorship, SRI has pursued the development of diagnostics suitable for understanding the plasma environment that exists when an arcjet plasma is impinged on a deposition substrate and diamond films are grown. When these plasmas are formed in approximately 99% hydrogen and 1% added hydrocarbon, a polycrystalline diamond film grows at rates that are quite high, exceeding 1 μm/min in many cases. As determined by Raman analysis, the diamond is usually of very good quality. We described the basic aspects of diamond growth in arcjet environments (our ARO-sponsored research) in three publications [Phelps and Stalder, 1990; Stalder and Sharpless, 1990; Stalder and Jeffries, 1993].

We used several arcjet designs and operating modes in our ARO projects. Our first generation arcjets operated at relatively high pressure, 200-400 Torr, and produced relatively small jets that consequently deposited diamond over small areas of a few square millimeters. Much of our recent work on arcjets focused on lower-pressure arcjet environments, 5-40 Torr, because other researchers and commercial producers use the low-pressure regime to spread out the arcjet and deposit diamond over larger areas. The plasma environment in these lower-pressure devices departs more strongly from equilibrium conditions and thus requires more extensive diagnostic development. Before describing the results of this research, we describe some of the operational aspects of low-pressure arcjets.

Low-Pressure Arcjet

The diameter of the diamond film deposited from the plume of a dc-arcjet significantly increases as the reactor pressure is lowered; a bigger plume is also driven by increasing the power dissipated in the dc-arc. The commercial dc-arcjet deposition reactors used, for example, by Norton and Crystalline Materials have reactor pressures between 5 and 40 Torr, and recently, new processes are being developed at pressures below 1 Torr. The low-pressure allows deposition of films greater than 10 cm in diameter with power dissipation in the 100-200 kW range. To ensure that the sensors we develop will be applicable to the commercial growth environments, we concentrated our optical diagnostics work on a low-pressure dc-arcjet reactor. We constructed a new dc-arcjet with primary support from an ARPA sponsored subcontract with the Naval Research Laboratory. ARO provided a modest contribution to the development of this facility to ensure adequate optical access for the ARO diagnostics work.

A stable dc-arcjet reactor places stringent requirements on the dc-power supply. The arc is struck in a high-pressure feedstock gas and forms a highly ionized column of gas. The temperature of this gas column increases as the current flow in the gas increases; however, the resistance of an ionized gas column decreases with increased gas temperature, so as current increases, the voltage drop across the arc decreases. Thus, the dc-arc has a region of negative resistance. The resistance also depends on the feedstock gases. Arc welding power supplies are designed for argon where the voltage drop for a typical arc is approximately 60 V. Diamond deposition is improved with a large fraction of hydrogen in the feedstock gas. The voltage drop for a typical arc in hydrogen is between 200 and 300 V. Therefore, an arcjet reactor for diamond deposition requires a dc-power supply capable of maintaining high frequency current control at voltages as high as 300 V. A 10 kW, current-controlled, dc-power supply was specially designed and built for the low-pressure SRI dc-arcjet reactor.

The arc is struck between a thoriated tungsten cathode tip and the apex of a converging/diverging nozzle in a feedstock mixture of argon and hydrogen at six atmospheres pressure. The nozzle is designed for subsonic arc attachment and for a gas flow of 5-7 standard liters per minute at an arc current of approximately 10 A. This produces a 500 W arc in pure argon and a 3.5 kW arc in pure hydrogen; mixtures of the feedstock have intermediate arc power requirements. The cathode-anode gap must be carefully adjusted to avoid restrike; during restrike the temperature increases, voltage drops, and the arc extinguishes, then the power supply increases the voltage to maintain constant current restoring the arc. This restrike phenomena produces oscillations between 500 Hz and 10 kHz. Restrike can be minimized by stable flow control, gas mixture, and the proper anode/cathode gap.

Optical measurements of the plume composition and temperature are made by directing a laser beam perpendicular to the gas plume and collecting the resulting laser-induced fluorescence (LIF) perpendicular to both plume and probe laser beam. The dc-arc and substrate are mounted in concert on an XYZ manipulator. This allows us to direct a probe laser or Langmuir probe into the arcjet plume and map the variation across the plume and along the axis between the exit plane of the nozzle and the substrate. These spatially resolved measurements can be made without disturbing the arcjet operation or moving the optical alignment of the optical collection.

We have grown high quality diamond film in this new, low-pressure, arcjet reactor. Figure 1 shows that the Raman spectrum of our low-pressure arcjet-grown material in the upper panel is nearly identical to the spectrum of a natural diamond stone in the lower panel. The CVD material shows broadband luminescence with an intensity of about 5% of the diamond Raman peak; this luminescence is not present in the spectrum of the natural material. The inset in the upper right corner of Figure 1 shows the line shape. We find the natural diamond has less pronounced wings of the Raman feature, indicating slightly less stress in the natural single crystal.

Laser-Induced Fluorescence

Laser-induced fluorescence is an ideal nonintrusive probe into chemically reactive systems. A laser beam directed into the reactive gas is tuned in wavelength to resonance with an allowed electronic transition, and some of the molecules absorb a photon and are promoted into an excited state. These excited molecules can fluoresce which produces the LIF signal. The signal is produced only for laser wavelengths in resonance with allowed transitions, and the pattern of these absorptions as the laser is tuned in wavelength provides an unambiguous identification of the specific species probed. The open-shell, highly reactive, free-radical, diatomic molecules have the most favorable spectroscopy for LIF, and they are important intermediates in reactive gas phase environments. Free radicals have allowed optical transitions in the visible or near ultraviolet regions of the spectrum where tunable lasers are readily available. Our work on diamond deposition has included the LIF detection of CH, C_2, and C_3.

The LIF of CH in our 220 Torr dc-arcjet plume discovered interference from a polyatomic species [Raiche and Jeffries, 1993]. We initially speculated that polycyclic aromatic hydrocarbons (PAH) formed in the reactive plume produced the interference LIF. The growth of hydrocarbon rings in a reaction time of a few hundred microseconds at 220 Torr is a reasonable expectation. However, we were quite surprised to discover the same interference in the 25 Torr arcjet plume with a reaction time of only a few microseconds [Jeffries, Raiche, and Brown, 1994]. Therefore, we more carefully investigated the source of the interference with the CH LIF.

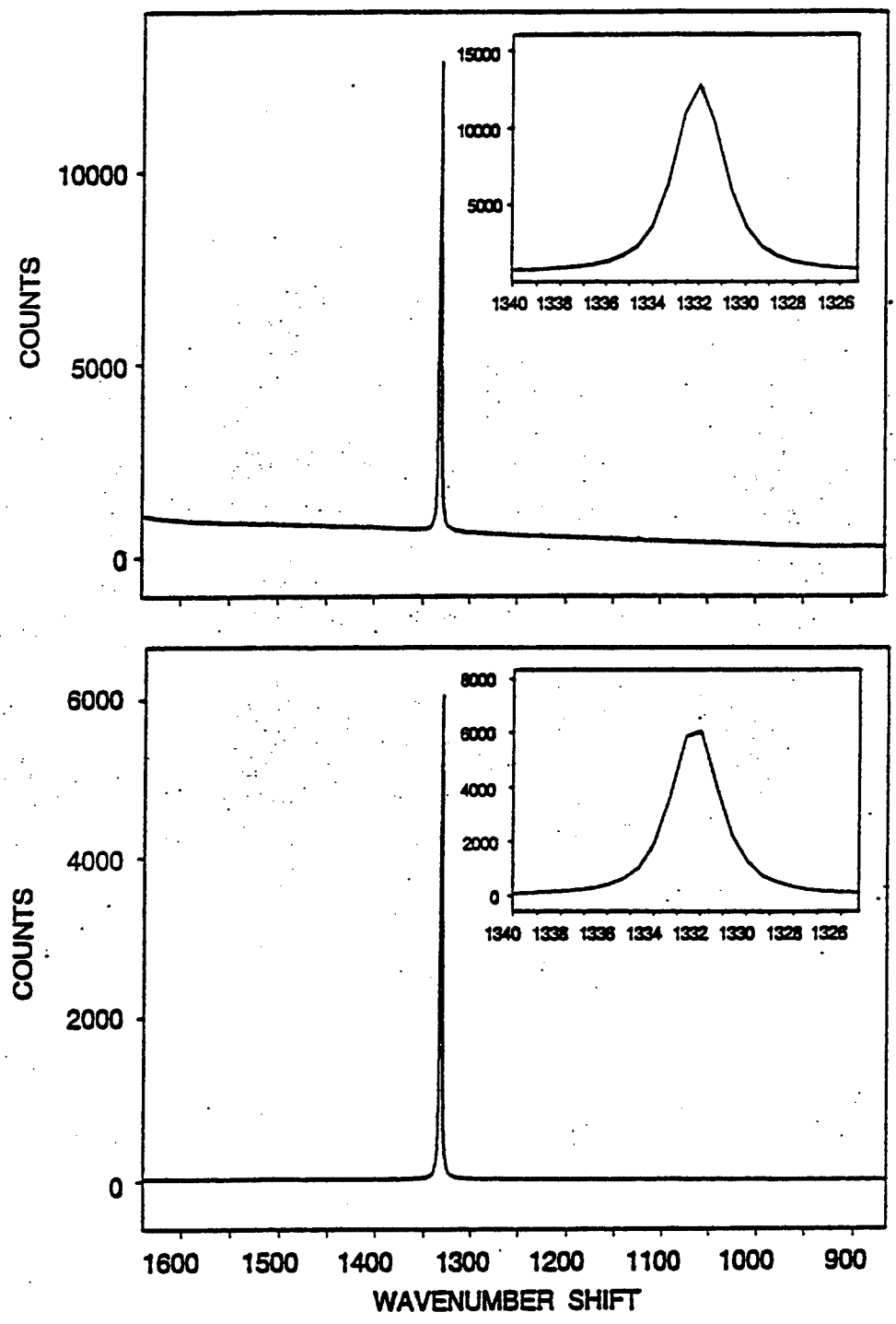

Figure 1. Raman spectrum of natural IIa diamond (lower panel) and CVD diamond (upper panel).

When we excited the interference with laser pulse energies of 1 mJ, we observed nearly no structure in the signal as we scanned the excitation wavelength. However, broad oscillations in the spectra reproduced from scan to scan. When we lowered the excitation pulse energy, we discovered an increase in this structure. At this point, we speculated that C_3 radicals might be the source of the interference.

The spectroscopy of C_3 is quite complex in the A-X transition near 400 nm. The A-state is Renner Teller split, with a larger splitting than the 67 cm^{-1}, low-frequency, vibrational mode. This produces a great deal of overlap between the many vibrational bands populated at the 2000 K level of the arcjet plume. These overtone bands have a very large variation in line strengths. If the excitation laser energy is sufficient to saturate the strongest of these transitions, then the weaker transitions appear to have a similar signal strength. If even the intermediate strength transitions are saturated, the spectrum begins to look continuous and unstructured. Such saturated C_3 LIF was the source of our observed interference for CH LIF in the arcjet plume. This work is described in detail in Appendix B.

Understanding the source of the CH interference has allowed us to develop successful strategies to greatly improve the CH LIF signal to noise. We have unambiguously shown that the interference for the CH LIF is C_3 LIF. We found that reducing the excitation laser pulse energy to on the order of 1 μJ/pulse dramatically increases the CH LIF signal to noise. We found that the C_3 molecules are spatially distributed in the cooler, outer edge of the plume. Thus, measurements of CH in the core of the plume are significantly improved by increasing the spatial resolution to exclude the regions of highest C_3 concentration.

Rotational distributions of CH are determined by LIF of CH in the ground X-state. In most reactive systems, we could be confident that the gas temperature is in equilibrium with the CH rotational distribution. However, in the arcjet plume, the large H atom concentration provides an environment so reactive that CH only sustains 3-5 nonreactive collisions before it is chemically reacted by atomic hydrogen to produce molecular hydrogen and atomic carbon. Therefore, to determine a gas temperature that could be used to chemically model this system, we must first determine if the CH distribution reflects the gas temperature.

We add NO to determine the gas temperature via LIF measurements of the NO rotational distribution; these measurements are discussed in detail in Appendix C. NO is not removed rapidly by chemical reaction with atomic H. However, NO does have the lowest ionization potential of any species in the plume. Therefore, we must separately determine if the NO addition alters the energy balance in the plume enough to change the gas temperature. From the Langmuir probe

measurements described below and in Appendix D, we find that although the NO addition increases the ion density by approximately a factor of two, the ion density is so low (< 10 ppm) that ionization of the NO does not alter the energy partition in the plume.

With the measurement of gas temperature and ionization we can now determine the atomic hydrogen concentration by conservation of energy. We carefully measure the electrical power dissipated in the arc by measuring the current and voltage of the arc. We then measure the temperature rise and flow rate of the cooling of the arcjet nozzle assembly. Recombination of ions and electrons or of atomic hydrogen on the walls of the nozzle heats the nozzle assembly and the cooling rate measures this path in the energy partition. We find nearly 30% of the feedstock hydrogen has been dissociated in the plume of the dc-arcjet, which makes this source of atomic hydrogen one with nearly the highest density of atoms.

Mass Spectroscopy

Mass spectroscopic sampling of the plasma is a useful method for characterizing the species that exist in the chemically reacting boundary layer of the arcjet. The fundamental idea is to sample the gases striking the substrate surface through a small hole in the substrate. Our first generation arcjet reactor produces diamond films at pressures near 200 Torr. The mass spectrometer requires pressures no higher than 10^{-4} Torr. Thus, significant differential pumping is needed right behind the substrate orifice. We built our system to achieve this pressure drop in just 1 cm with a two-stage pumping system. Because arcjet plasmas are commercially used for metal machining and cutting, significant water cooling of the deposition substrate was required to avoid erosion or melting of the sampling surface.

Our mass spectroscopic measurements began in earnest during the latter part of our first contract; during the last three years we have refined the measurements and obtained good mass spectra of the plasma under diamond growth conditions. Gas from the arc impinges on a tantalum substrate and some of the gas that diffuses through the boundary layer is sampled though a hole in a water-cooled substrate. The gas flowing through this hole is formed into a beam by a second skimmer before entering the high-vacuum analysis chamber. Sometimes a tuning fork chopper is used to modulate the beam, so that signal from background gas in the mass spectrometer chamber can be distinguished from the arc effluent in the beam. Diamond growth around the high-pressure sampling hole in the substrate has been confirmed by ex-situ Raman analysis and microscopic observation of the crystalline deposit.

As predicted by chemical models, we found a significant hydrogen dissociation fraction and a large acetylene production from 99% hydrogen and 1% methane feedstock. These results

were recently published [Stalder and Homsi, 1996]. We found that the acetylene was linearly proportional to the amount of methane in the feedstock; however, the observed methyl radical variation was erratic.

Our high-pressure arcjet is now free of air contamination; consequently our measurements show clear evidence of significant acetylene production, and the M/e peak at 29 is clearly C_2H_5. Even larger peaks at M/e = 27 and 28 suggest that C_2H_3 and C_2H_4 are being produced, although we are currently determining whether they are produced in the arcjet or are fragmentation products in the quadrupole mass spectrometer. Atomic carbon is also observed in small quantities, but the same fragmentation issues apply to these observations.

After acquiring a large XYZ translator stage suitable for mounting the arcjet, we spent a good deal of time conducting experiments on the spatial distribution of the various species flowing in the high-pressure arcjet. Because the plasma is primarily unionized compressible gas, its flow is subject to compressible gas dynamics, which is a well-understood field. We used compressible gas dynamic equations and our experimental measurements to determine the gas temperature of the boundary layer. We presented these measurements at several conferences and we prepared manuscripts for submittal to journals. The gas temperatures measured by this method are consistent with those obtained by the LIF methods described above.

Langmuir Probe Measurements

We conducted a brief set of experiments to measure the charged particle densities and electron temperatures in the low-pressure arcjet [Brinkman, Stalder, and Jeffries, 1996 (see Appendix D)]. This experiment was motivated by LIF measurements of this arcjet when NO was added as a gas temperature probe. Because NO has a very low ionization potential, we wanted to determine if the ionization level was significantly altered as a result of the addition of small amounts of NO gas to the arcjet. Although the NO addition was another effective indicator of gas temperature, its addition adversely affected the quality of the diamond. We tried to determine if altered plasma properties could have been a source of the reduced quality of the diamond in this case. Another motivation for the probe measurements was to determine additional aspects of the power balance in the arc to see if charged particles possessed a significant fraction of the energy dissipated in the arc. In addition, some of the optical emissions appear to be related to electron impact excitation.

The ion densities in the arcjet are about 10^{12}-10^{13} cm^{-3} 13 mm from the exit plane of the arcjet. The addition of NO causes the ion density to increase by a factor of fifty percent to a factor of seven, depending on argon/hydrogen mixtures and other factors. Downstream from this point,

at 42 mm from the exit plane, the ion density drops by about an order of magnitude, and the effect of the NO addition appears to be similar. At both locations, the electron temperatures usually are about 1-2 eV, corresponding to 10,000 to 25,000 K. The electrons clearly do not equilibrate to the gas temperature during its transit from the arc region to the substrate. This low-pressure arcjet plasma is significantly far from local thermodynamic equilibrium, in contrast to the plasma in the higher pressure (~ 200 Torr, early generation) arcjet that was studied extensively in the early stages of this program.

RECOMMENDATIONS FOR FUTURE WORK

We observed spatial structure in the CH, C_2, and C_3 in the arcjet plume. We determined the atomic hydrogen density by energy balance. We are now prepared to test the fundamental growth mechanisms of diamond. We can make measurements into the boundary layer, and from the gradients in concentration and temperature we observe, we can infer the gas-surface processes. This will allow us to distinguish between the many diamond growth mechanisms.

Continued work in spatially resolved mass spectroscopic sampling coupled with LIF will enable us to more completely characterize the chemical and physical nature of the boundary layer above a growing diamond surface. This region is where many of the deposition species vary strongly as a result of the hydrodynamics of the impinging arcjet. It is also a challenging but important region to probe to more accurately determine boundary conditions for the chemical growth models mentioned above.

LIST OF PUBLICATIONS (1993-1996)

1. Kenneth R. Stalder and Jay B. Jeffries, "Recent Results on the Deposition of Diamond Thin Films by Arcjet Plasmas and Diagnostic Measurements of the Plasma-Surface Region," Diamond and Related Materials **2**, 443 (1993).

2. G. A. Raiche and J. B. Jeffries, "Laser-Induced Florescence Detection of Polycyclic Aromatic Hydrocarbons in a dc-Arc-Jet Used for Diamond Deposition," Appl. Phys. Lett. **63**, 3002 (1993).

3. J. B. Jeffries, G. A. Raiche, and M. S. Brown, "Optical Diagnostics of Diamond CVD," in *Laser Techniques for State-Selected and State-to-State Chemistry II*, J. W. Hepburn, ed., SPIE Vol. **2124**, 1994, p. 270.

4. E. A. Brinkman and J. B. Jeffries, "Optical Diagnostics for Temperature Measurement in a Diamond CVD Reactor," in *Diamond Materials III*, K. V. Ravi, ed., Electrochemical Society Press, Pennington, NJ, 1995.

5. E. A. Brinkman and J. B. Jeffries, "Comparison of Optical Emission and Laser-Induced Fluorescence in Arcjet Thruster Plumes Used for Diamond Deposition," Proceedings of the 26th AIAA Plasmadynamics and Lasers Conference, AIAA 95-1955, Washington, DC, 1995.

6. K. R. Stalder and W. Homsi, "Mass Spectroscopic Investigations of a Hydrocarbon Arcjet Plasma Operating Under Diamond Deposition Conditions," Appl. Phys. Lett. **68**, 3710 (1996).

7. G. A. Raiche and J. B. Jeffries, "Observation and Spatial Distribution of C_3 in a dc-Arcjet Plasma During Diamond Deposition Using Laser-Induced Fluorescence," submitted to Appl. Phys. B, June 1996.

8. E. A. Brinkman, G. A. Raiche, M. S. Brown, and J. B. Jeffries, "Optical Diagnostics in a dc-Arcjet Reactor Used for Diamond Deposition," submitted to Appl Phys. B, July 1996.

9. E. A. Brinkman, K. R. Stalder, and J. B. Jeffries, "Electron Densities and Temperatures in a Diamond-Depositing dc-Arcjet Plasma," submitted to J. Appl. Phys., August 1996.

LIST OF CONFERENCE AND OTHER PRESENTATIONS

1. "Spatially Resolved Mass Spectroscopy of Hydrocarbon Species in the Boundary Layer During the Deposition of Diamond Thin Films," by K. R. Stalder and W. Homsi, 46th Annual Gaseous Electronics Conference, October 1993.

2. (invited) "Laser-Based Diagnostics of Diamond CVD," Jay B. Jeffries, Diamond Gordon Research Conference, Plymouth, NH, June 1994.

3. "Spatially Resolved Mass Spectroscopy of Hydrogen and Other Light Hydrocarbons in the Boundary Layer During the Deposition of Diamond Thin Films," K. R. Stalder, 47th Annual Gaseous Electronics Conference, October 1994. Also, Bull. Am. Phys. Soc. **39**, 1473 (1994).

4. (invited seminar) "Plasma Synthesis of Diamond--Understanding the Growth Environment," Kenneth R. Stalder, presented at Lawrence Livermore National Laboratory, 26 January 1995.

5. (invited) "Optical Diagnostics in dc-Arcjet Plasmas," Jay B. Jeffries, presented at the Optical Society of America Annual Meeting, 1995.

6. "Laser-Induced Fluorescence (LIF) Measurement of Gas Temperatures in a Diamond CVD Reactor," Elizabeth A. Brinkman and Jay. B. Jeffries, presented at the Optical Society of America Annual Meeting, 1995.

7. "LIF of Reactive Intermediate Species During Diamond Deposition," Michael S. Brown and Jay B. Jeffries, Laser Diagnostics Gordon Research Conference, Plymouth, NH, July 1995.

8. "Atomic Hydrogen Concentration Determined from LIF Temperature in a dc-Arcjet," Elizabeth A. Brinkman and Jay B. Jeffries, 48th Annual Gaseous Electronics Conference, Oct. 1995. Also, Bull. Am. Phys. Soc. **40**, 1556 (1995).

9. "Measurements of Electron Densities and Temperatures in Supersonic Arcjet Plasmas Operating Under Diamond Growth Conditions," K. R. Stalder, E. A. Brinkman, and J. B. Jeffries, 48th Annual Gaseous Electronics Conference, October 1995. Also, Bull. Am. Phys. Soc. **40**, 1578 (1995).

10. "Diagnostic Measurements of Gas Species, Temperatures and Plasma Properties of Subsonic and Supersonic Arcjet Plasmas Used to Deposit Diamond Thin Films," J. B. Jeffries and K. R. Stalder, 48th Annual Gaseous Electronics Conference, October 1995. Also, Bull. Am. Phys. Soc. **40**, 1577 (1995).

11. (invited seminar) "Laser-Induced Fluorescence Measurements in dc-Arcjet plasmas During Diamond CVD," Jay B. Jeffries, High Temperature Gas Dynamics Laboratory, Stanford University, October 1995.

12. (invited seminar) "Optical Diagnostics in a Diamond Depositing Plasma," Jay B. Jeffries, Army Research Laboratory, Aberdeen, MD, January 1996 (host Andrzej Miziolek).

13. "Measurements of Electron Densities and Temperatures in Low-Pressure Arcjet Plasmas Operating Under Diamond Growth Conditions," K. R. Stalder, E. A. Brinkman, and J. B. Jeffries, 1996 IEEE International Conference on Plasma Science, June 1996.

14. (invited departmental seminar) "dc-Arcjet CVD of Diamond Films," Jay B. Jeffries, Forschungsgruppe Reacktive Stroemung, University of Heidelberg, July 1996.

15. (invited seminar) "Optical Measurements to Characterize Diamond CVD," Jay B. Jeffries, University of Freiberg, July 1996.

16. (invited seminar) "dc-Arcjet CVD of Diamond Films," Jay B. Jeffries, University of Bielefeld, July 1996.

17. (invited seminar) "Optical Measurements to Characterize Diamond CVD," Jay B. Jeffries, DLR, Stuttgart, July 1996.

18. (invited) "Optical Measurements to Characterize a dc-Arcjet Plume During Diamond CVD," Jay B. Jeffries, Diamond Gordon Research Conference, Plymouth, NH, August 1996.

19. (invited) "Optical Measurements to Understand the Chemistry of Diamond CVD," Jay B. Jeffries, American Chemical Society, Orlando, FL, August 1996.

LIST OF PARTICIPATING SCIENTIFIC PERSONNEL

Dr. Kenneth R. Stalder, Sr. Research Physicist

Dr. Jay B. Jeffries, Sr. Research Chemical Physicist

Professor George Raiche, Assistant Professor, Chemistry Department, Hamilton College

Dr. Elizabeth A. Brinkman, Postdoctoral Fellow

Dr. Jorge Luque-Sanchez, Postdoctoral Fellow

Mr. Wolfgang Juchmann, International Fellow

Mr. Wadih Homsi, International Fellow

REPORT OF INVENTIONS

No inventions were reported during this contract.

BIBLIOGRAPHY

Brinkman, E. A., Stalder, K. R., and Jeffries, J. B., "Electron Densities and Temperatures in a Diamond-Depositing dc-Arcjet Plasma," submitted to J. Appl. Phys., August 1996.

Jeffries, J. B., Raiche, G. A., and Brown, M. S., *Laser Techniques for State-Selected and State-to-State Chemistry II*, J. W. Hepburn, ed., SPIE Vol. **2124**, 1994, p. 270.

Phelps, A. W. and Stalder, K. R., Appl. Phys. Lett. **57**, 1090 (1990).

Raiche, G. A. and Jeffries, J. B., Appl. Phys. Lett. **63**, 3002 (1993).

Stalder, K. R. and Sharpless, R. L., J. Appl. Phys. **68**, 6187 (1990).

Stalder, K. R. and Jeffries, J. B., Diamond and Related Materials **2**, 443 (1993).

Stalder, K. R. and Homsi, W., Appl. Phys. Lett. **68**, 3710 (1996).

APPENDIX A

UNDERSTANDING PLASMA CVD OF DIAMOND FILMS

Submitted to ARO's "Research Highlights"

April 1996

Understanding Plasma CVD of Diamond Films

Jay B. Jeffries and Kenneth R. Stalder
SRI International, Menlo Park, California

Chemical vapor deposition of diamond films in low-pressure plasmas could enable a wide variety of practical applications to exploit the unique properties of diamond. Diamond's unique combination of excellent thermal conductivity and high electrical resistivity would make it the material of choice for thermal management for high-speed electrical circuits, reliable laser communication diodes, and ultra-fast computers. Semiconductor diamond with its >5 eV band gap could be used to fabricate high-temperature, high-voltage electronics, and diamond LED's or diode lasers could emit ultra-violet light. These enticing features of diamond have driven a myriad of research projects in the past decade. Although semiconductor quality plasma deposition of diamond remains elusive, plasma CVD of thermal management diamond can produce free standing polycrystalline diamond wafers 15 cm in diameter and 500 μm thick. Unfortunately even the fastest deposition methods only deposit 10 μm/hour over large areas and only a tiny fraction of the feedstock carbon is incorporated into the diamond film. Thus, CVD diamond film remains expensive $10-100/carat and deposition applications are quite time consuming. The development of process models and control sensors will improve the yield of diamond films and perhaps will spawn the insight to develop more cost effective processes.

As part of SRI's program to understand diamond deposition, a diamond depositing arcjet plasma reactor has been constructed and polycrystalline diamond films have been deposited which have Raman spectra that rival natural IIa diamond stones. A high resolution Raman spectrum of natural IIa diamond stones in the lower panel of Fig. 1 were compared to a spectrum and synthetic diamond grown in our arcjet reactor in the upper panel. The synthetic diamond had a slightly higher luminescent background with a Raman lineshape which was comparable to the natural diamond. Faceted, polycrystalline diamond film was evident in the electron micrograph in Fig. 2 which indicated the surface morphology near the position on the film where the Raman spectrum was measured.

The feedstock gas in the arcjet reactor has a short, well-defined residence time with localized diamond growth[1], which made this an ideal technique to unravel the precursor chemistry of diamond deposition. To test the chemical model of diamond precursor chemistry and semi-empirical scaling laws developed for diamond deposition rate, the reactive gas plume in our dc-arcjet reactor was characterized. The degree of dissociation of feedstock hydrogen is crucial to the precursor chemistry of diamond CVD.[1] Calorimetry was proposed to determine the extent of hydrogen dissociation. The electrical power dissipated in the dc arc, the heating of the cooling water in the arc and expansion nozzle, and the gas temperature at the exit of the nozzle was measured. If the extent of ionization, the electron energy distribution, and the velocity of the gas jet were known, calorimetry can be used to determine the dissociation fraction of the feedstock hydrogen. A Langmuir probe has been used to determine the ion density and electron temperature. Even though the electron temperature was >10,000 K, the ion density was less than 10 ppm. Thus, only a small fraction of the input electrical energy was dissipated via ionization of the feedstock. Most of the energy dissipated was partitioned into hydrogen dissociation, gas heating, and directed velocity of the gas plume.

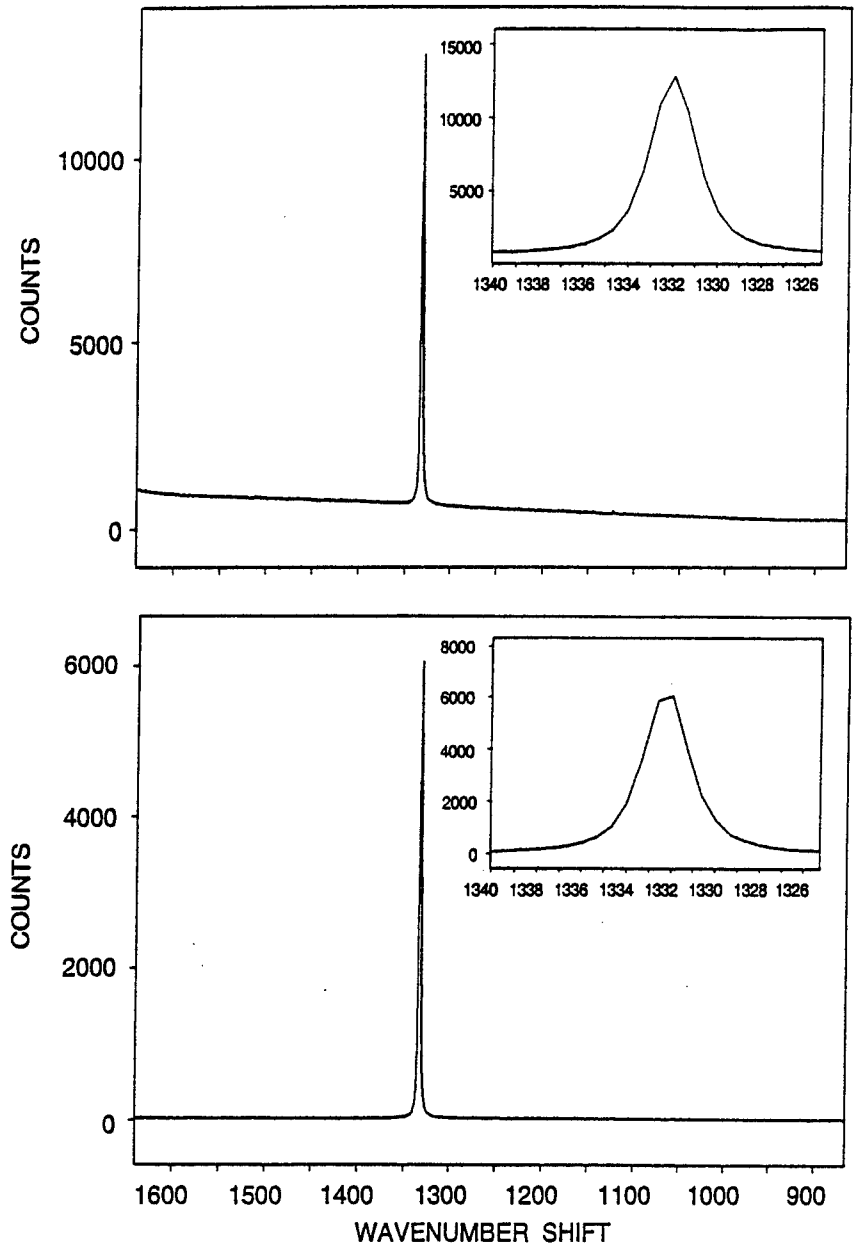

Figure 1. *Raman spectrum of natural IIa diamond (lower panel) and CVD Diamond (upper panel).*

Figure 2. *Electron micrograph of CVD diamond.*

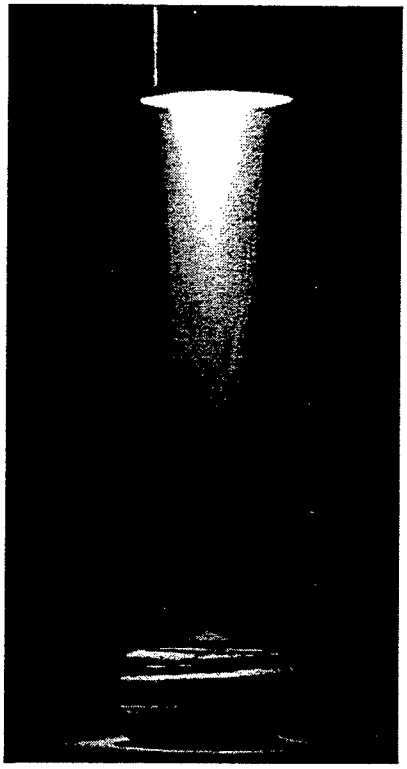

Figure 3. *Photo of arcjet gas plume striking substrate.*

A photo of the arcjet plume in Fig. 3 showed the luminous flow striking a water cooled molybdenum substrate with a reactor pressure of 4 Torr; intense optical emission from atomic hydrogen Balmer-α in the red, from CH A-X transitions in the blue, and C_2 Swan bands in the yellow/green were evident via visual observation. An arc discharge was struck in a hydrogen/argon mixture, and this plasma was expanded through a converging diverging nozzle into the low-pressure reactor. The exit of the expansion nozzle is visible in Fig. 3. Hydrocarbon feedstock is added to the reactive mixture in the diverging half of the nozzle. Diamond film characterized in Fig. 1 and 2 above was grown on a threaded molybdenum rod seen in Fig. 3. The substrate temperature was controlled length of rod extending from the water cooled holder and by the water flow volume.

The arcjet, diamond deposition reactor was designed to accommodate a wide variety of optical and electrical probes to evaluate diagnostics as process control sensors. The design exploited experience depositing diamond with a higher pressure dc-arcjet which was characterized with sampling mass spectrometry and optical diagnostics.[3] A laser beam passed through the arcjet plume normal to the flow between nozzle and substrate, optical emission and laser induced-fluorescence light was collected at right angles to both the gas flow and the laser beam, and Langmuir probes could be inserted into the plume. The arcjet nozzle and substrate assembly were translated with a precision manipulator to make spatially resolved measurements in the reactive gas plume as a function of distance between the nozzle and substrate and as a function of radius from the center of the luminous gas beam.

Laser-induced fluorescence (LIF) has been observed in the reactive gas plume from CH, C_2, and C_3 radicals.[4] LIF signals measured from a series of transitions was used to determine the rotational and/or vibrational population distribution in the ground electronic states of these radicals. The population in these energy levels was a Boltzmann distribution and gas temperature was deduced from an LIF spectrum scanning several different rotational transitions. With its large rotational energy spacing, CH was the best candidate for LIF temperature measurements.[5] Unfortunately, CH LIF in the arcjet plume was obscured by interference.[6] This interference LIF produced a very intense signal which had modest (±10%) variation with excitation wavelength and an example is shown in the lower panel of Fig. 4.

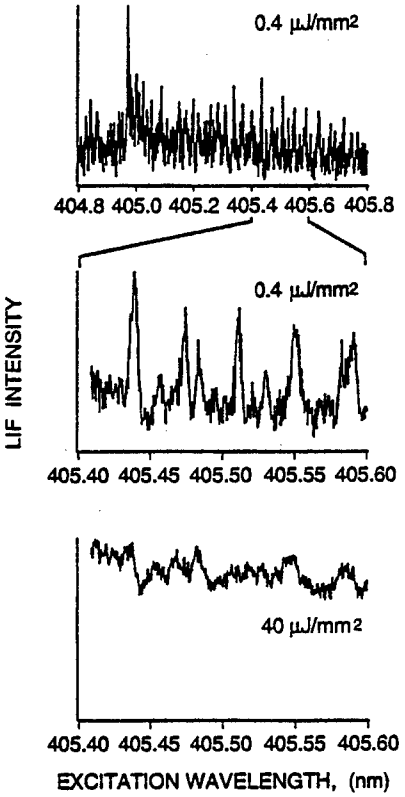

Figure 4. LIF excitation spectrum of C_3.

LIF from C_3 radicals has been identified as the source of interference. If the excitation pulse energy in an unfocused dye laser beam (1 mm diameter) was reduced from 40 µJ/pulse to 400 nJ/pulse, structure was resolved in the laser excitation spectrum of the A-X system shown in the middle and top panels of Fig. 4. The C_3 spectrum was complex due to the large Renner-Teller splitting of the electronic excited A-state and the large number of populated vibrational levels in the ground electronic state. The bending frequency in the X-state was only 63 cm^{-1} and many overtone and combination bands have significant thermal population in the high temperature reactive plume. Saturation of the fundamental 000-000 vibrational transition and excitation of these hot bands produces the nearly continuous background LIF signal shown in the bottom panel of Fig. 4. Therefore this interference could be minimized by greatly reducing the excitation laser pulse energy.

The spatial distribution of C_3 has been measured by LIF excitation of the A-X 000-000 transitions near 405 nm and detection of the 000-100 near 423 nm. The laser was scanned from 404.95-405.15 nm and the signal integrated for R-branch rotational transitions from J=0-52. Qualitatively different C_3 LIF signals were observed in different regions of the plume. Along the centerline of the plume very small C_3 signal intensity is measured, whereas near the outer edges of the plume large C_3 signals were

obtained. The integrated LIF intensities at different locations in the plasma plume were corrected for the temperature variation of the partition function. Integration over many rotational states mitigates the temperature dependence of the rotational partition function; the fraction of the rotational population detected in the integration varies from 0.95 at 1000 K to 0.78 at 2500 K. The vibrational partition function as a function of temperature was calculated by summing populations of the ground state vibrational levels observed experimentally by Rohlfing.[7]

The LIF signal has been normalized by the partition function to give a relative C_3 concentration as a function of position; the data in Fig. 5 indicated the C_3 was not uniformly distributed in the reactive gas plume. The C_3 was localized in a cone at the outer edge of the luminous plume of reactive gas. Near the nozzle the C_3 was in the center of the plume, and further downstream the C_3 distribution was localized at larger diameters producing a hollow cone. Thus, if the excitation laser pulse energy were reduced and the spatial resolution increased, CH LIF measurements free of C_3 interference were possible to map the temperature distribution in the arcjet plasma plume. With the temperature map and a velocity distribution, the precursor chemistry to diamond growth could be modeled. Concentration measurements of the radicals then would provide a test of these models.

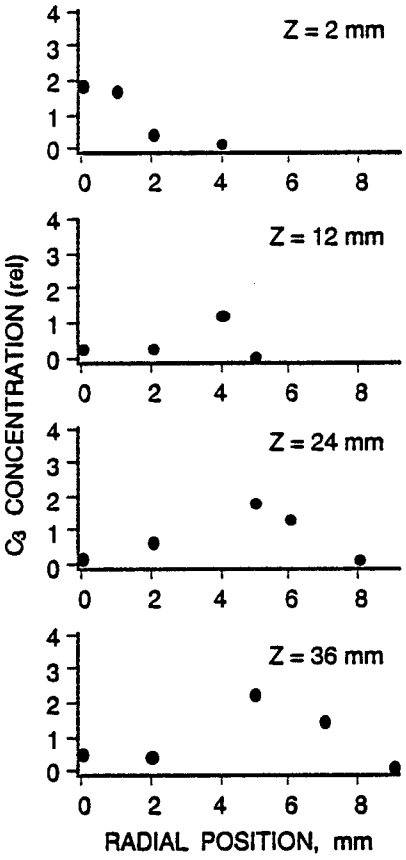

Figure 5. Relative C_3 concentration versus radical position at four different positions between nozzle and substrate.

References

1. A. W. Phelps and K. R. Stalder, Appl. Phys. Lett. **57**,1090 (1990).
2. D. G. Goodwin, J. Appl. Phys. **74**, 6888(1993).
3. K. R. Stalder and R. L. Sharpless, J. Appl. Phys. **68**, 6187 (1990).
4. G. A. Raiche and J. B. Jeffries, Appl. Opt. **32**, 4629 (1993).
5. J. B. Jeffries, G. A. Raiche, and M. S. Brown, "Optical Diagnostics of Diamond CVD Plasmas," in *Laser-Techniques for State-Selected and State-to-State Chemistry II,* Ed. J. W. Hepburn, SPIE, **2124**, (1994) pp. 270-277.
6. G. A. Raiche and J. B. Jeffries, Appl. Phys. Lett. **63**, 3002 (1993).
7. E. A. Rohlfing, J. Chem. Phys. **91**, 4531 (1989).

APPENDIX B

OBSERVATION AND SPATIAL DISTRIBUTION OF C_3 IN A DC-ARCJET PLASMA DURING DIAMOND DEPOSITION USING LASER-INDUCED FLUORESCENCE

G. A. Raiche and J. B. Jeffries

Submitted to *Applied Physics B*

June 1996

Observation and Spatial Distribution of C_3 in a dc Arcjet Plasma During Diamond Deposition Using Laser-Induced Fluorescence

George A. Raiche
Department of Chemistry
Hamilton College, Clinton NY 13323 USA

Jay B. Jeffries
Molecular Physics Laboratory
SRI International, Menlo Park CA 94025 USA

Abstract

We report on measurements of the spatial distribution of the concentration of the C_3 radical in the plume of an arcjet plasma during diamond film chemical vapor deposition. C_3, identified using laser-induced fluorescence, is distributed in a shell surrounding the diamond-depositing core of the arcjet plasma plume. PACS 52.70.K, 81.15.G

MP 96-020a
May 29, 1996

Introduction

Thin films of diamond-phase carbon enjoy an unusual pair of properties: high thermal conductivity and high electrical resistance, a combination valuable in the construction of high-speed and high-density integrated circuits with robust thermal management requirements. Of the several chemical vapor deposition (CVD) methods currently recognized for depositing diamond films [1], the DC arcjet technique is remarkable because of its large deposition rate and its ability to deposit over large surface areas of minimally-prepared substrates. Freestanding, 0.5 mm thick poly-crystalline wafers deposited using this technique are commercially available. Because the geometry, flow, electrical parameters, and film growth areas are well-defined and controllable in an arcjet reactor, this system is amenable to both correlation of reactor conditions to film quality, and chemical modeling based on well-known hydrocarbon reaction kinetics.

In an effort to refine real-time diagnostics for arcjet deposition and to understand the chemical processes necessary for high-quality diamond growth, we have constructed an arcjet reactor that is optimized for optical diagnostic studies. This reactor allows optical access to the plasma plume and the plume-substrate interface during diamond deposition. Laser-induced fluorescence (LIF), a sensitive and selective technique for measurement of species concentrations and state distributions, has previously been used to detect CH and C_2 radicals generated in the plasma plume and to measure their apparent temperatures [2,3]. These studies, combined with chemical modeling, indicate that the reactive species are in neither thermal nor chemical equilibrium.

In the CH studies a persistent laser-correlated fluorescence signal interfered with the observation of CH LIF, and based on its spectral characteristics we initially attributed it to the presence of polycyclic aromatic hydrocarbon (PAH) species [4]. Our further investigation with an optimized reactor design clearly demonstrates that the origin of this signal is the A-X system of the C_3 radical. Although C_3 is a familiar species in astronomy and hydrocarbon combustion, its

presence in the diamond plasma was unexpected and previously unknown, as is its significance for diamond film growth. Very similar background LIF was observed by Klein-Douwel et al. [5] when they measured CH B-X LIF in an oxygen/acetylene flame depositing diamond film. They also speculated this interference was due to the presence of PAH in these fuel rich flames. The large LIF background which they observe with a photomultiplier filtered at 430 nm to peak with a laser excitation energy near 400 nm is consistent with C_3 LIF. Here we report the relative concentrations and spatial distribution of C_3 in the diamond-depositing plasma plume, both to characterize its spectral properties under these conditions and to assist in elucidating its role in the diamond deposition process.

Experimental

This reactor deposits diamond by directing the effluent plasma plume of a hydrocarbon arcjet onto a water-cooled substrate. A 50% hydrogen/argon mixture at ~6 bar flows through an annular electrode assembly where it is activated by a 1-3 kW DC discharge, and this active mixture then expands through a converging/diverging nozzle. A small flow of methane (~0.5%) is injected into the divergent region. The resulting reactive plasma plume impinges on a water-cooled molybdenum substrate 42 mm downstream of the nozzle exit; the plasma plume is ~18 mm in diameter at the substrate, and the main apparatus chamber, containing the substrate assembly, is maintained at ~0.033 bar. During arcjet operation a substrate temperature of approximately 900 K results in film growth rates on the order of 1 μm/min. The entire arcjet/substrate assembly is mounted on an XYZ translation stage and is manipulable during diamond deposition. Optical access through ports and observation windows allows observation along two orthogonal axes perpendicular to the plasma effluent flow, and translation of the arcjet assembly relative to these ports allows spatial mapping of plume features with the optical excitation and collection axes fixed.

For LIF studies, we collect signal photons at right angles to the laser and plume axes using f/5 collection optics, a laser beam apertured to 2 mm diameter, and a spatial filter to limit the observation region to a cylinder approximately 2 × 3.0 mm. A photomultiplier tube converts these

photons, either dispersed with a 0.33 m monochromator or filtered to a selected bandpass, to a laser-correlated photocurrent amplified and integrated with a gated boxcar averager. The intensity of the pulsed dye laser used for excitation is also monitored, with a piezoelectric detector, to normalize the fluorescence signals. Because the (non-laser-correlated) plasma emission is strong and broadly distributed through the visible wavelengths, spatial filtering of the observed photons is necessary to avoid saturating the detection optics. We excited fluorescence by pumping in the region of the $A(^1\Pi_u)$–$X(^1\Sigma g^+)$ (000-000) transition near 405 nm, and observing (000-100) near 423 nm [6-8]; for the relative C_3 concentration studies a 420 ± 10 nm filter bandpass is sufficiently wide to pass the entire rotational envelope, and thus avoids detection bias from incomplete equilibration prior to emission. For this observation region, the primary source of non-C_3 spectral interference is the (intense) R-branch emission of the CH A–X system [3].

Results and Discussion

Several workers have characterized the spectroscopy of C_3, [6,8] and we identify C_3 in the arcjet plasma plume by comparison with known spectral features and work previously done in this laboratory. Figure 1 compares the LIF spectrum obtained in a room-temperature discharge flow apparatus [9] with that acquired in our arcjet plasma. Although the spectra were acquired with different laser linewidths and gas temperatures, the similarities in the spectra indicate that our signal is C_3 LIF. Because the room temperature species is rotationally cold the individual rotational branches are more prominent than at plasma temperatures, where the rotational distribution is broad and the spectrum is highly congested. The room temperature spectrum is power broadened from saturation of the rotational transitions. The arcjet spectrum is acquired with a narrower laser bandwidth and lower excitation pulse energy, which resolves more detail in the spectrum.

Figure 2 (top) shows a section of the C_3 LIF spectrum in the region of the A–X (000-000) origin, obtained using an unfocused, apertured laser beam pulse energy 0.4 $\mu J/mm^2$; the LIF signal is linear at this intensity and recognizable C_3 features are evident. The prominent feature near 404.96 nm is the red-degraded R bandhead, and structures to the blue are from features in

vibrational hot-bands. In the lower panel the pulse energy is 40 $\mu J/mm^2$, and the rotational features obvious in the low-intensity spectrum are effectively lost in the continuous baseline signal. The unstructured spectrum observed at higher laser pulse energy initially led us to speculate that the signal was attributable to PAH fluorescence [4]. The C_3 A-X (000-000) features are saturated and the underlying, less saturated hot bands effectively obscure the structured excitation spectrum.

The LIF from C_3 interferes with LIF detection of CH in either the A-X (0,0) band near 431 nm or the B-X (0,0) near 389 nm; CH molecules are an attractive candidate for LIF measurements of gas temperature and quantitative measurements test models of the diamond and CVD chemistry. This interference is illustrated in Fig. 3 by the wavelength resolved fluorescence from C_3 following excitation near 435 nm (top), 390 nm (bottom), and 405 nm (center), the C_3 A-X (000)-(000) origin is near 405. Scattered laser light is off-scale at the three excitation wavelengths, although with 405 nm the emission itself is very strongly peaked at 405 nm. Most of the emission intensity lies between 380 and 410 nm, with a weaker feature shifted approximately 1270 cm^{-1} (one symmetric stretch) [6] to the red of (000-000). The top panel indicates that excitation and detection of CH A-X (0,0) near 431 nm will simultaneously excite C_3 LIF, resulting in significant interference. Similarly, excitation of CH B-X (0,0) near 389 nm interferes with detection using either the (0,0) band near 389 nm or the (0,1) band near 418 nm. This combination of interference LIF led us in previous CH experiments [3] to excite the off-diagonal (0,1) band in the A-X system and observe the diagonal emission; although this reduces the total CH signal considerably, the C_3 interference is negligible when exciting near 494 nm.

Quantitative detection of C_3 LIF is complicated by the complex nature [6] of the C_3 A-X transition and the high temperature of the arcjet plasma plume. The A state has a very large Renner-Teller splitting. In addition, the A-X spectrum at high temperature is complicated by a bending frequency in the X-state of only 63 cm^{-1}. Previous studies indicate that the gas temperature of the arcjet diamond plasma ranges over approximately 1000-2500 K, depending on location in the flowfield [10]. Because of the relatively dense energy level structure of C_3, many rotational and vibrational levels of the X state are thermally populated in this system. In principle,

excitation of a single resolved rovibronic feature of the spectrum should yield a fluorescence signal with intensity proportional to species concentration. In the arcjet plasma, however, the energy level structure of C_3 results in severe rotational and vibrational congestion, which precludes isolation of single features given the Doppler broadening of the transition, our laser linewidth, and detector resolution.

To measure the relative C_3 concentration as a function of spatial location in the flowfield, we integrate the intensities of rotational transitions from J=0 to 52 in v=(000). Figure 4 shows LIF spectra acquired 12 mm above the substrate and at several points along a radius from the arcjet centerline. At the center of the jet (r=0 mm) the C_3 signal is small; it reaches a maximum at a radius of 5 mm, and declines at increasing radial separations. This general trend is evident in radial series acquired at several downstream positions. "Baseline" signal, the result of congested hot band excitation of the approximately 99% of the C_3 population in vibrationally excited states, is subtracted from each of these spectra prior to integration between 404.95 nm and 405.15 nm. This window covers the (000-000) R-branch to R(52) and provides the integrated LIF intensity excited from J=0 -52 in v = (000); the Q and P branches, just to the red of the integrated region, are excluded.

The fraction of C_3 we observe depends on the temperature dependence of the rotational-vibrational partition function. Assuming that C_3 in its X $^1\Sigma^+$ ground state is a linear rigid rotor and using a value of B_0=0.43 cm^{-1}, we sum directly over the J=0 to J=52 energy levels to generate a rotational partition function (because of state symmetry, odd J do not exist). Integration over many rotational states mitigates the temperature dependence of the rotational partition function; the fraction of rotational population detectable by excitation of $0 \leq J \leq 52$ varies from 0.95 at 1000 K to 0.78 at 2500 K. This small correction can be adequately estimated by our simplistic description of the rotational partition function. For vibration, calculation of the partition function is complicated by strong anharmonic coupling between the X-state vibrational modes, and simple anharmonic approximations do not adequately represent the vibrational level structure. To calculate the fraction of vibrational population in X (000) as a function of temperature, we summed over the

ground state vibrational levels experimentally determined by Rohlfing [8]. We approximate the full rotational-vibrational partition function as the product of the individual components and plot, in Figure 5, the temperature dependence of the fraction of C_3 X state that exists as (000), $0 \leq J \leq 52$. This fraction is on the order of 0.5% at typical plasma temperatures and varies approximately 80% over the full temperature range encountered in the plasma plume.

The C_3 fluorescence lifetime is dominated by collisional quenching in the plasma plume. However, spatially resolved lifetime measurements vary by less than 5% in the region of the plume examined by our plume studies. Therefore, collisional quenching corrections are not applied to the data presented here.

The spatial dependence of our plasma plume gas temperature has been determined [10,11] by LIF rotational distribution measurements on NO seeded into the plasma plume. We use this temperature distribution to generate relative C_3 concentrations from integrated LIF spectra by dividing each integrated excitation spectrum by the temperature-dependent fraction shown in Figure 5. The result is shown in Figure 6 for several positions both upstream of the cooled substrate (z) and radially separated from the centerline. At z=42 mm, immediately downstream of the nozzle exit, little structural detail is evident because the diameter of the LIF observation volume is approximately the same as that of the plasma stream. As the plasma stream expands radially on its way to the substrate, however, the shell-like distribution of C_3 concentration becomes apparent.

Conclusions

Our observation of C_3 in the diamond-depositing plume presents opportunities to improve our understanding of the deposition process. Experimentally, the identification of C_3 reduces the number of unknown plasma spectroscopic features, thus improving the prospects for conducting plume optical diagnostics of identified species (3). For modeling studies, C_3 provides a new experimental benchmark for validation of computer codes and chemical mechanisms [12-16]. Currently, the role of C_3 in diamond film deposition is not obvious. The bonding structure of C_3 indicates atomic orbital hybridization that is inconsistent with that of the diamond structure; since

hybridization changes are energetically expensive, formation of C_3 might represent a diversion of potential diamond precursor to "waste" carbon. However, Klein-Douwel et al. [5] used their non-resonant background LIF signal as a sensor for proper fuel-air stoichiometry to optimize diamond growth, and we hypothesize that their background LIF is due to C_3. An understanding of the significance of C_3 in the deposition process awaits chemical models that explicitly account for its formation and evolution.

Acknowledgments

This work was sponsored by the Army Research Office. We thank Prof. Mark Cappelli of Stanford University for the loan of an arcjet and his assistance in the design of our diamond CVD reactor.

References

[1] F. G. Celii and J. B. Butler, Ann. Rev. Phys. Chem. **42** (1991) 643.

[2] G. A. Raiche and J. B. Jeffries, Appl. Opt. **32** (1993) 4629.

[3] J. B. Jeffries, G. A. Raiche, and M. S. Brown, "Optical Diagnostics of Diamond CVD Plasmas," in *Laser-Techniques for State-Selected and State-to-State Chemistry II, Ed. J. W. Hepburn, SPIE, Vol, 2124, 1994, pp. 270-277.*

[4] G. A. Raiche and J. B. Jeffries, Appl. Phys. Lett. **63** (1993) 3002.

[5] R.J.H. Klein-Douwel, J.J.L. Spaanjaars, and J. J. ter Meulen, J. Appl. Phys. **78** (1995) 2086.

[6] G. Herzberg, Molecular Spectra and Molecular Structure III, Electronic Spectra and Electronic Structure of Polatomic Molecules, D. Van Nostrand, Inc., Princeton, NJ, 1966.

[7] E. A. Rohlfing and J.E.M. Goldsmith, JOS (B) **7** (1990) 1915.

[8] E. A. Rohlfing, J. Chem. Phys. **91** (1989) 4531.

[9] Rensberger and Smith, unpublished

[10] E. A. Brinkman and J. B. Jeffries, "Optical Diagnostics for Temperature Measurement in a Diamond CVD Reactor," in Diamond Materials IV, Ed., K. V. Ravi, Electrochemical Society Press, Pennington, NJ, 1995, pp. 461-466.

[11] E. A. Brinkman and J. B. Jeffries, "Comparison of Optical Emission and Laser-Induced Fluorescence in Arcjet Plumes Used for Diamond Deposition," American Institute of Aeronautics and Astronautics, WDC, Paper #95-1955.

[12] S. J. Harris, Appl. Phys. Lett. **56**, 2298 (1990).

[13] D. G. Goodwin, J. Appl. Phys. **74**, 6888 (1993); **74**, 6895 (1993).

[14] J. B. Butler and R. L. Woodin, Phil. Trans. R. Soc. London **342**, 209 (1993).

[15] P. K. Bachmann, D. Leers, and H. Lydtin, Diamond and Related Materials **1**, 1 (1991).

[16] M. Frenchlach and H. Wang, Phys. Rev. B **3**, 1520 (1991).

Figure Captions

Figure 1. Superposition of the C_3 $A(1\Pi u)$–$X(^1\Sigma g^+)$ (000)-(000) LIF versus excitation wavelength obtained in a discharge flow apparatus, top (T~300 K) and in the arcjet plasma plume, bottom (T~1600 K).

Figure 2. Plasma plume C_3 LIF excitation spectra obtained at "low" (top, center) and "high" (bottom) laser pulse energies. Saturation of the excitation spectrum generates a signal nearly featureless as the excitation wavelength is varied. The middle panel reveals the structure actually available in the spectrum.

Figure 3. Wavelength resolved fluorescence after exciting C_3 with laser near 435 nm (top), 405 nm (center) and 390 nm (bottom). Scattered laser light is off scale in each spectrum. LIF after exciting at 405 nm strongly peaked about 405 nm.

Figure 4. LIF excitation spectra of the (000)-(000) R-bandhead region, acquired at several points in the plasma plume. These spectra are integrated to yield relative concentrations, as described in the text.

Figure 5. A plot of the fraction of the population of C_3 molecules in the electronic ground state, which is in the (000) vibrational and the $0 \leq J \leq 52$ rotational states, versus temperature; these are the transitions covered by the integration window described in the text.

Figure 6. Spatial distributions of relative C_3 concentration, plotted at several heights above the film-deposition substrate, for several points along a radius of the plasma plume. A shell-like distribution becomes apparent as the plume evolves from nozzle to substrate. At z=42 mm, the plume radius is smaller than the spatial resolution for detection, and fine structure is obscured.

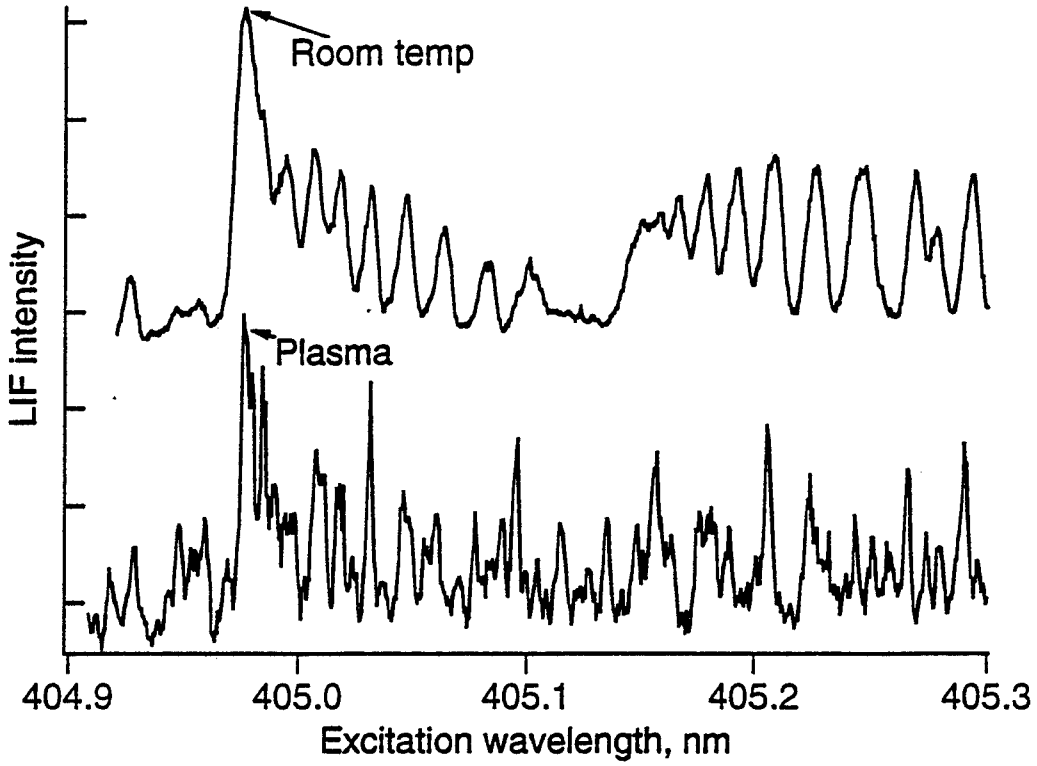
Room temp
Plasma
LIF intensity
404.9
405.0
405.1
405.2
405.3
Excitation wavelength, nm

Figure 1

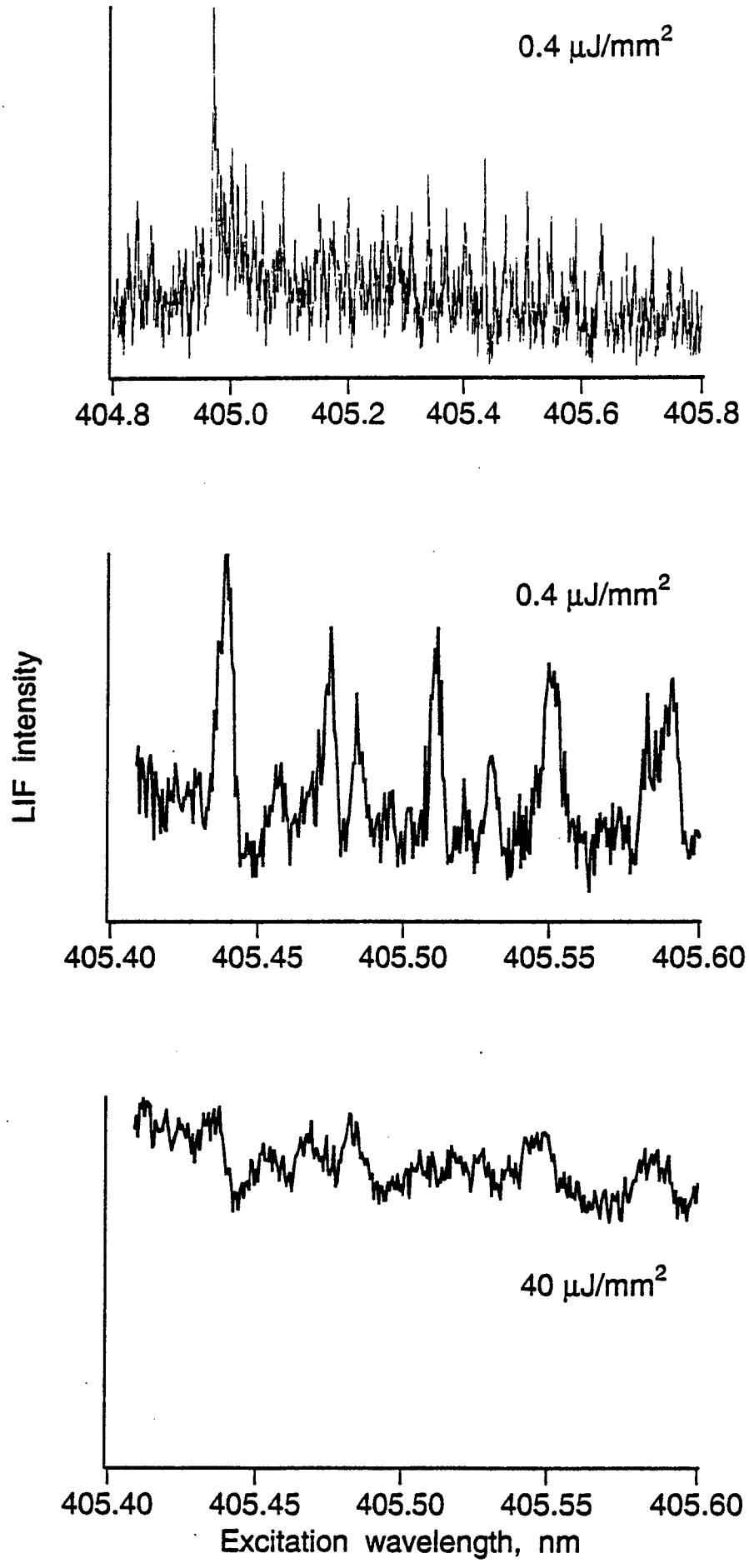
0.4 μJ/mm²
404.8
405.0
405.2
405.4
405.6
405.8
0.4 μJ/mm²
LIF intensity
405.40
405.45
405.50
405.55
405.60
40 μJ/mm²
405.40
405.45
405.50
405.55
405.60
Excitation wavelength, nm

Figure 2

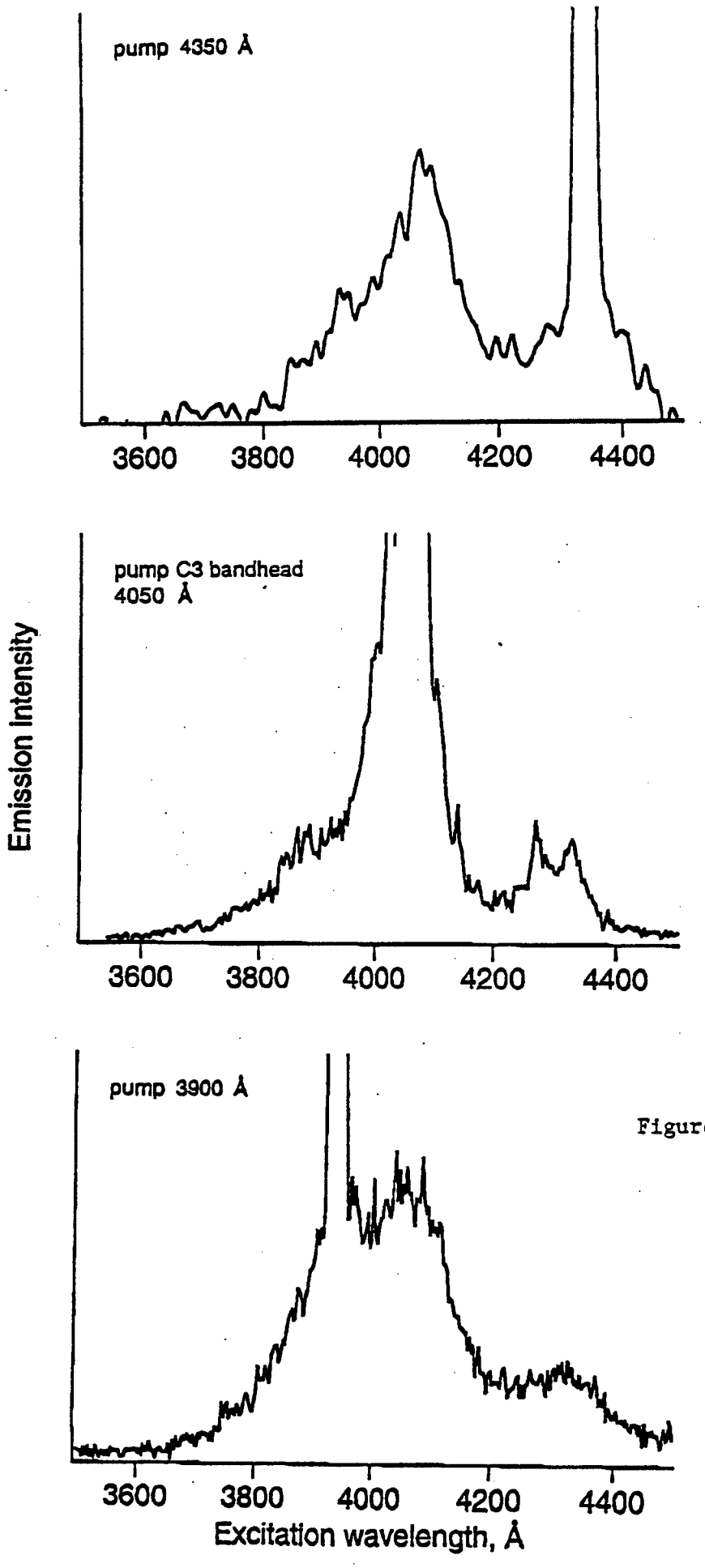
pump 4350 Å
3600
3800
4000
4200
4400
pump C3 bandhead
4050 Å
Emission Intensity
3600
3800
4000
4200
4400
pump 3900 Å
3600
3800
4000
4200
4400
Excitation wavelength, Å

Figure 3

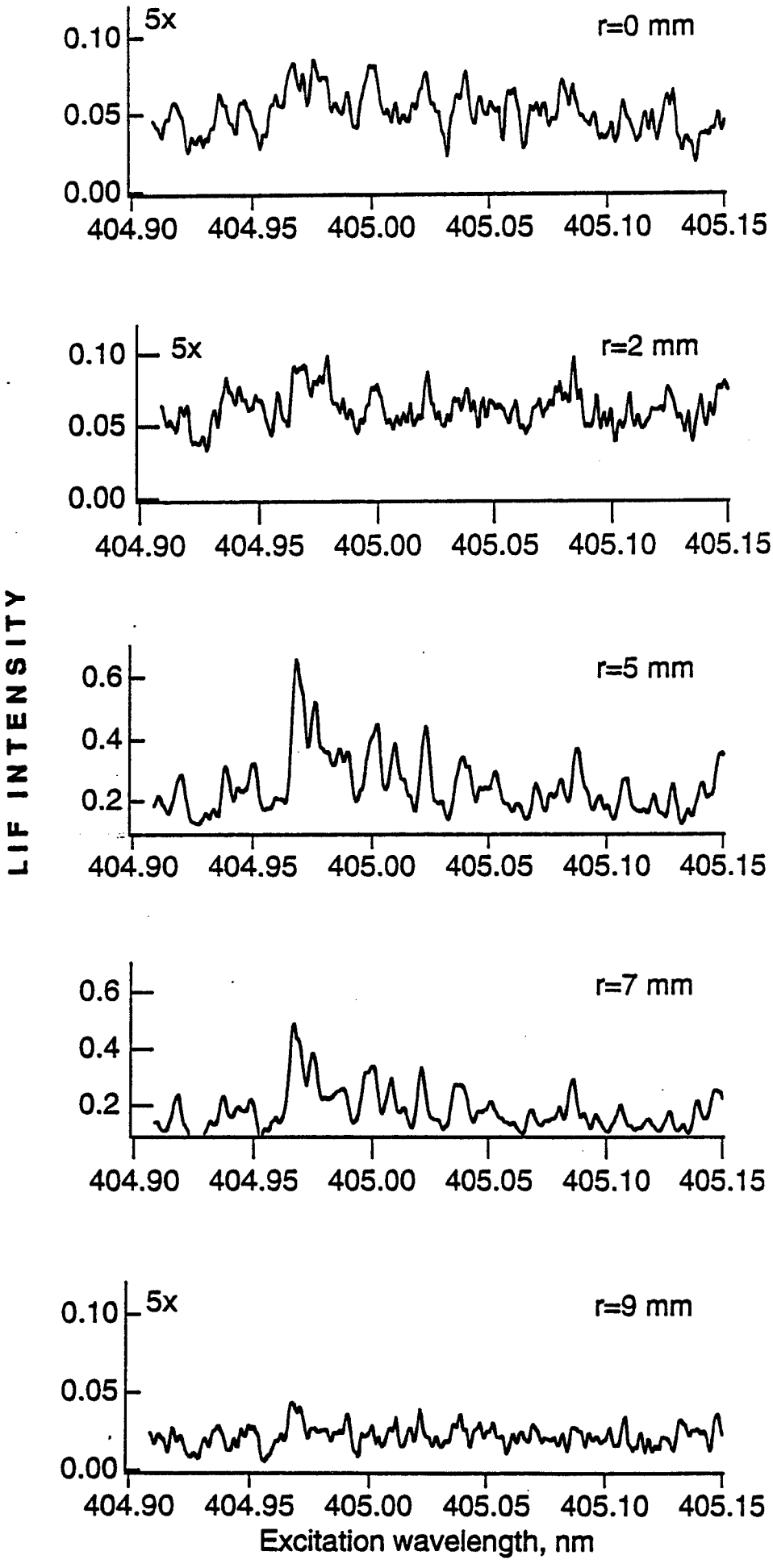
5x
r=0 mm
0.10
0.05
0.00
404.90 404.95 405.00 405.05 405.10 405.15
5x
r=2 mm
0.10
0.05
0.00
404.90 404.95 405.00 405.05 405.10 405.15
LIF INTENSITY
r=5 mm
0.6
0.4
0.2
404.90 404.95 405.00 405.05 405.10 405.15
r=7 mm
0.6
0.4
0.2
404.90 404.95 405.00 405.05 405.10 405.15
5x
r=9 mm
0.10
0.05
0.00
404.90 404.95 405.00 405.05 405.10 405.15
Excitation wavelength, nm

Figure 4

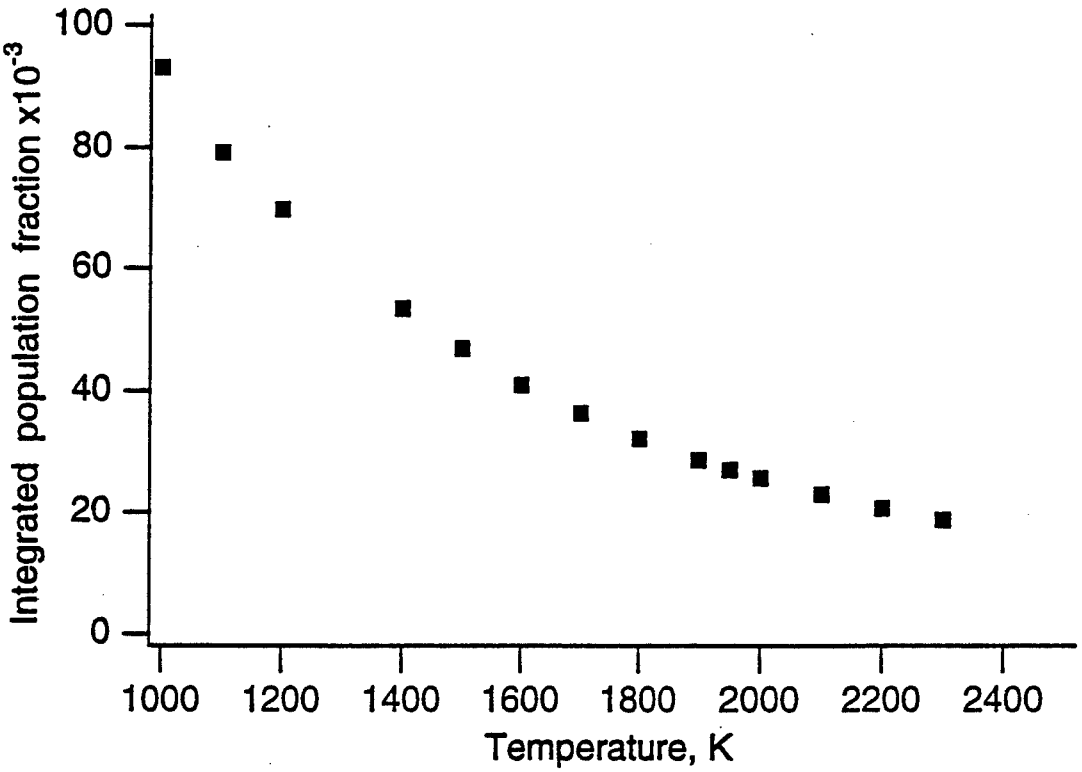
Integrated population fraction x10^{-3}
100
80
60
40
20
0
1000
1200
1400
1600
1800
2000
2200
2400
Temperature, K

Figure 5

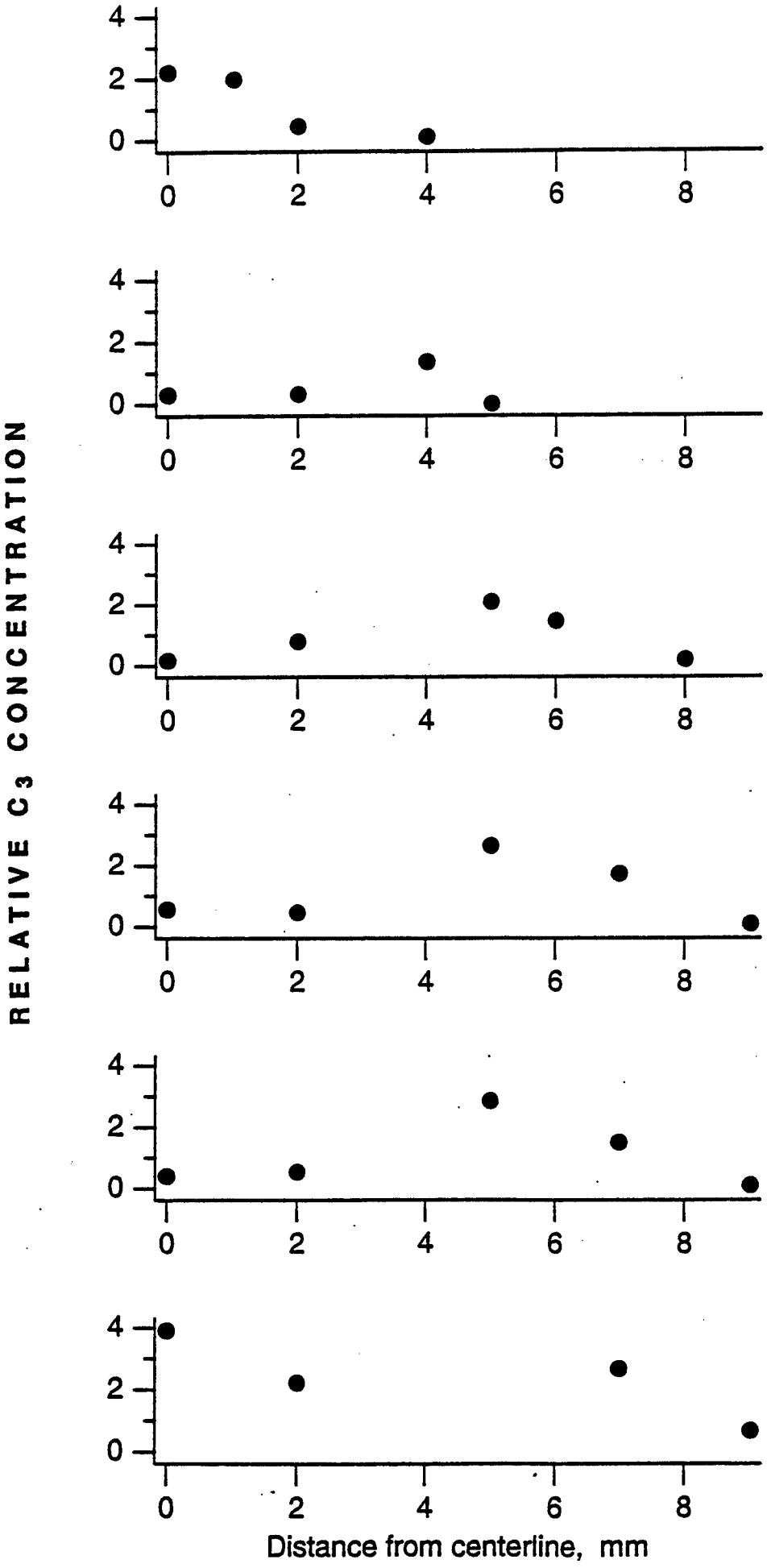
RELATIVE C_3 CONCENTRATION
4
2
0
0
2
4
6
8
Distance from centerline, mm

Figure 6

APPENDIX C

OPTICAL DIAGNOSTICS FOR TEMPERATURE MEASUREMENT IN A DC-ARCJET REACTOR USED FOR DIAMOND DEPOSITION

E. A. Brinkman, G. A. Raiche, M. S. Brown, and J. B. Jeffries

Submitted to *Applied Physics B*

July 1996

OPTICAL DIAGNOSTICS FOR TEMPERATURE MEASUREMENT IN A DC ARCJET REACTOR USED FOR DIAMOND DEPOSITION

Elizabeth A. Brinkman, George A. Raiche,* Michael S. Brown** and Jay B. Jeffries
Molecular Physics Laboratory
SRI International, Menlo Park CA 94025

ABSTRACT

In the plume of a dc arcjet used for the chemical vapor deposition (CVD) of diamond, we determine the gas temperature from laser induced fluorescence measurements (LIF) of the rotational distribution of the X-state of nitric oxide which is seeded into the plume. This temperature is compared with LIF measurements of the rotational distributions of the CH X-state and the C_2 a-state in this plume. LIF measurements of CH are complicated by the presence of C_3 and we discuss strategies to deal with this interference. The gas temperature describing the rotational distributions obtained for NO, C_2 and CH agree within experimental error. Optical emission measurements indicate that the rotational and vibrational distributions of the excited A-state of CH and a-state of C_2 are characterized by vibrational and rotational populations which are at least 1000 K above the ground state distributions. These excited states are collisionally quenched before their population distributions equilibrate with the gas temperature. We also determine relative populations of the ground and excited states along the axis of the plume between the arcjet nozzle and the substrate and relative populations for a cross section of the jet, midway between the nozzle orifice and the substrate. The measured relative ground and excited state populations for both CH and C_2 show different trends along the plume axis, indicating that the ground and excited states of these molecules are products of different chemical mechanisms; such mechanisms are discussed.

*Current address: Department of Chemistry, Hamilton College, Clinton NY 13323
**Current address: MetroLaser Inc., Irvine CA 92714

MP 96-094
June 27, 1996

INTRODUCTION

An arcjet is a high pressure discharge in which an arc is struck in a flowing, high pressure gas, thereby increasing the enthalpy and kinetic energy of the gas. This hot gas expands through a converging-diverging nozzle, forming a luminous beam of reacting gas. These devices are useful for propulsion and have been developed as thrusters for satellite-keeping purposes. An arcjet operating on a hydrogen/methane mix is also ideal for the low pressure synthesis of diamond films. The high temperatures in the plasma result in dissociation of a large fraction of the molecular hydrogen to atomic hydrogen.[1] Low pressure diamond synthesis requires the generation of atomic hydrogen and a high concentration of atomic hydrogen relative to the carbon growth species.[2-4] The high velocities in an arcjet result in reduced boundary layer thickness, and a more efficient delivery of H atoms to the surface. As a result, arcjets produce some of the highest diamond growth rates.

An arcjet reactor provides an excellent environment in which to study the chemical mechanism of diamond CVD growth. The residence time of the gas in the reactor is well defined, allowing for modeling of the gas chemistry if boundary conditions are measured. One parameter which is critical for modeling the chemistry is the temperature distribution of the plume, because many chemical reaction rates have an exponential temperature dependence. Measurement of gas temperature distribution requires a technique which will not perturb the gas flow or chemistry. Insertion of a physical probe to measure the temperature in this environment would both perturb the flow and might not reflect the true temperature, as a result of hydrogen atom recombination on the probe surface. Optical diagnostics can provide non-invasive diagnostics of gas temperature as well as identify and measure concentrations of molecular and atomic species in the plasma.

In this paper we report measurements of the gas temperature using laser induced fluorescence (LIF) measurements with an arcjet operating on a mixture of hydrogen and argon, with <1 % methane added to the effluent of the jet, at a pressure of 18-25 torr. Preliminary reports

of some of this work have previously appeared.[5-7] We perform some LIF temperature measurements using the A-X transition of nitric oxide (NO) seeded into the plasma. Temperature profiles are obtained down the axis of the jet for three different mixtures of argon and hydrogen. We also obtain a temperature profile across the center of the jet for one gas mixture. The temperature obtained using NO LIF is compared with the rotational distributions obtained from LIF of the A-X transition for CH and d-a transition of C_2. These two molecules are produced in the arcjet plume from the reaction of methane with hydrogen. We see that all three molecules yield the same temperature distribution within experimental uncertainties.

We have also observed optical emission of H atoms, CH and C_2 molecules. The optical emission spectra of CH and C_2 can be simulated to obtain rotational and vibrational distributions of the excited states. These distributions can always be characterized by temperatures that are at least 1000 K above the ground state distributions. Therefore, optical emission provides a poor measurement of the gas temperature in our plasma.

LIF and optical emission have also been used to measure the variation of the relative populations of ground and excited state species (CH and C_2) with position in the reactive gas plume. Such variations can be used as a guide for testing chemical models of the plasma, can provide insight into the chemical mechanism of diamond CVD, and can serve as a process control sensor. We see that the ground and excited state species follow different trends down the axis of the jet, and discuss some possible reasons for these differences.

EXPERIMENTAL

A dc-arc is struck in a mixture of argon and hydrogen at the apex of a converging nozzle at a pressure of 6 atmospheres. The effluent expands from a diverging nozzle into a chamber maintained between 4 and 30 torr. Typical flows range from 1 to 6.2 slpm H_2 and 3 to 4.5 slpm Ar. We operate at 1 to 2 kW (90-160 V and 10-12 A; operating voltage depends on percent hydrogen in the mixture). Methane (< 1% of the hydrogen flow) is injected into the plume in the

diverging nozzle. The nozzle assembly is water cooled, and we monitor the water flows, water temperatures and power input for calorimetry. Approximately 4.5 cm downstream of the nozzle exit, diamond grows beneath the stagnation point of the luminous plume, on a water cooled molybdenum substrate.

The excitation laser light for LIF is directed perpendicular to the arcjet plume; fluorescence is detected at right angles to both the gas jet and the laser beam using f/5 collection optics with spatial filtering (2 mm x 2 mm slit) (Figure 1). Output from a Nd:YAG pumped dye laser near 452 nm is frequency-doubled to excite NO $A^2\Sigma^+$- $X^2\Pi$; output near 490 nm is used to excite CH $A^2\Delta$- $X^2\Pi$ (1-0), and output near 474 nm is used to excite C_2 $d^3\Pi_g$-$a^3\Pi_u$ $\Delta v=1$ transitions. The unfocused laser beam is approximately 2 mm in diameter.

To insure that the LIF signal is detected with uniform response for each rotational transition in a given molecular band, different detector arrangements are used for detection of the fluorescence of each electronic transition. For CH and C_2 the LIF signal is focused on the entrance slit of a 0.1 m monochromator with a 0.5 mm entrance slit and a 4 mm exit slit. This yields a trapezoidal bandpass with a flat response of ~ 20 nm. Detection is via a 2" end-on photomultiplier tube (EMI 9558). For NO, the LIF signal is detected using a solar-blind photomultiplier (Hamamatsu R431S) filtered with a UG-5 colored glass filter (Schott). This arrangement, discussed below, produces a slight spectral bias in the detection of the different NO rotational levels.

Optical emission (non-laser-induced) is also collected f/5 at right angles to the flow of the gas plume. Light is focused on the entrance slit of a 0.3 m monochromator and collected in first order (C_2) or second order (CH) to obtain spectra of emission intensity as a function of wavelength; detection is via a photomultiplier (Hamamatsu 4332). Spectral resolution is 1.2 Å for CH and ~ 3 Å for C_2. Relative detection response is obtained using the intensity from a calibrated tungsten lamp. Temperature distributions of the A-state of CH[8] and the d-state of C_2[9] were obtained using spectral simulations of their emission.

Laser-Induced Fluorescence Temperature Measurements in the Arcjet Plume

Laser-induced fluorescence (LIF) in the arcjet plume is produced by illuminating a molecule (or atom) with laser light tuned to an electronic transition. The molecule in the ground electronic state absorbs energy and is promoted to an excited electronic state. The molecules in this excited electronic state may predissociate, be quenched, or fluoresce. Those molecules which fluoresce are detected in the LIF experiment. The rotational and vibrational distributions in the ground electronic state may be mapped by scanning the laser over a wavelength region which covers transitions from several rotational levels. In diatomic molecules, individual rotational transitions will often be resolved. From these distributions, the gas temperature can be determined.

LIF of diatomic molecules provides a convenient, non-intrusive method for measurement of gas temperature. This method is highly sensitive and permits spatial resolution on the order of 0.1 mm. LIF populations will reflect the gas temperature if the ground electronic state is in thermal equilibrium with the gas. Thermalization occurs via rotational energy transfer (RET) and vibrational energy transfer, and competes with chemical reactions that remove molecules from the ground state. Generally, collisional thermalization is rapid compared with chemical reactions of the target molecules and meaningful gas temperatures can be determined using LIF. However, in the arcjet plume we estimate that CH undergoes only 3-4 non-reactive collisions before reacting further. We must therefore test here to insure that CH is rotationally equilibrated with the plume gas temperature.

To measure the temperature in the arcjet plume, we have introduced a small amount of NO along with the methane into the plume, ~0.15% of the total flow. NO has been used to measure LIF temperatures in hot-filament diamond CVD reactors[10] and in flames.[11,12] NO is an attractive molecule to use for temperature measurement in the arcjet plume, since it is relatively unreactive in this environment and is not expected to perturb the gas temperature. There is some reaction of NO with the carbon species in the jet, however, and we see CN $B^2\Sigma$-$X^2\Sigma$ emission after addition of

NO. Addition of NO also degrades diamond production and can not be added when high-quality diamond is desired.

In this environment, NO would perturb the plume temperature mainly via ionization of NO. Of all the major species in the plume, NO has the lowest ionization potential (9.3 eV); charge exchange with other ions produced in the arc will create NO^+. Langmuir probe measurements detect $<10^{13}$ ions/cm^3 (< 0.01 % ionization).[13] This low concentration is not expected to perturb the gas temperature.

We excite NO in the A-X 0-0 vibrational band and detect broadband fluorescence; care is taken to insure the excitation energy is low enough to produce linear excitation. For NO A-X, the Franck-Condon factors are large for the $\Delta v = 0,1,2,3,4$ and 5 transitions. As a result, excitation of the 0-0 band leads to strong fluorescence from the 0-0 through the 0-5 transitions. We excite with a wide range of wavelengths to cover a wide range of energy in the ground state (~3600 cm^{-1}). Rotational energy transfer in the excited state is rapid, but the competition between collisional quenching and RET generates a fluorescence wavelength profile which is slightly dependent on the initial excitation wavelength, i.e., rotational transition. Thus it is crucial that our detector have uniform response for each different rotational transition excited.

We observed fluorescence from these vibrational bands using a filtered PMT. The filter transmission was measured and convoluted with the photomultiplier efficiency over the fluorescence wavelength range to estimate the detection response. We examined the response to the fluorescence from the highest and lowest excited rotational levels to estimate the extent of variation of detector response. Assuming no RET occurs in the upper state, we found an upper limit of 3% underestimation of the temperature. This would produce a worst-case temperature error of 50 K. Althrough collisional rotational energy transfer will reduce this, we have adjusted our results using this estimate.

To excite transitions over a wide range of rotational energies, we scan selected regions then rapidly slew the laser wavelength to the next region. An example of an LIF spectrum is shown in

Figure 2. Peaks are integrated to give the relative fluorescence intensities; these are converted to relative populations using the line absorption coefficients $B_{J"}$. The relative population of the J" rotational level, $N_{J"}$, is related to the temperature T in a Boltzmann distribution, where $g_{J"}$ and $E_{J"}$ are the degeneracy and the energy of the J" level respectively.

$$N_{J"} = g_{J"} \exp(-E_{J"}/kT) \quad (1)$$

T is obtained from the slope of a Boltzmann plot of Eq 1 (Figure 3) .

Temperatures are measured both along and across the arcjet plume for a reactor pressure of 24 torr. For a mixture of ~3 slpm H_2 and ~3.5 slpm Ar, we see that the temperature rises approximately 600 K in the 4.6 cm freestream distance from nozzle exit to the boundary layer (<2 mm) above the substrate (Figure 4). We also have measured the temperature across the width of this plume 20 mm downstream of the jet orifice (Figure 5). We see that the plume is < 25 mm wide and that the temperature varies with position: the temperature peaks at 1950 K in the center of the plume, then drops to approximately 600 K 12 mm from the center. Temperature measurements were also made for two other flow mixes: 1.6 slpm H_2 and 4.7 slpm Ar; 6.1 slpm H_2 and 2.9 slpm Ar. In all cases we see that the temperature rises as the gas moves down the axis.(Figures 6 and 7) We speculate this rise results from collisional slowing of the directed velocity of the plume and energy release due to H atom recombination:

$$H + H \ (+ M) \rightarrow H_2 \ (+ M). \quad (2)$$

LIF temperature measurements were also performed using molecules which are generated in the plasma. CH and C_2 molecules are produced in the plume from reactions of the added methane. There are three choices of electronic transitions in CH to measure the rotational distribution in the ground state: A-X, B-X and C-X. The C state is strongly predissociated in all

vibrational levels and the transition probabilities have a large variation with rotational level, thus making LIF temperature measurements difficult to interpret. Predissociation also occurs in the A-state for N'>11 in v'=1 and in the B state for N'>15 in v'=0 and for N'>6 in v'=1. Therefore, only excitation to v'=0 in the A or B state is suitable at the high temperatures expected in the arcjet plume.

The Franck-Condon factors for excitation to the A and B states are nearly diagonal because the internuclear separation in the ground and excited states is nearly identical. For A-X, the (0,0) band has a Franck-Condon factor of 0.997 and the (0,1) band a factor of 0.003, while for the B-X, the factors are 0.9 for the (0,0) band and 0.1 for the (0,1) band. The most sensitive excitation and detection scheme would normally involve exciting and detecting the (0,0) band for A-X or B-X. However, if we excite and detect in the same band, scattered laser light will interfere with the fluorescence signal. Furthermore, if we collect fluorescence from the (0,0) band of either of these electronic transitions, our fluorescence must compete with the very bright emission from the plume in both of these bands.

Figure 8 compares LIF detection for four different sets of vibrational and electronic transitions, obtained 25 mm above the substrate surface. Three of the four spectra have a non-zero background, due mainly to the excitation of a polyatomic molecule, identified in this laboratory as C_3.[14] The underlying C_3 spectroscopy is complex, containing many populated vibrational levels with overlapping transitions. These produce a background with structure which depends on excitation laser pulse energy. This background interference can be reduced by narrowing the spatial filter (the data in Figure 8 were obtained with a 5 mm spatial filter). Decreasing the laser power also improves the signal to background. Under the conditions used in Figure 8, CH transitions are saturated much more easily than C_3; reducing the laser power will cut the C_3 fluorescence with little sacrifice in the CH signal.

LIF temperature measurements of CH were taken with the conditions in the bottom trace of Figure 8, which does not have C_3 interference: we excite 1-0 and detect 0-0 in the A-X transition.

Exciting the 1-0 band at 490 nm results in a reduction of our signal by a factor of ~ 300, but we no longer excite C_3 at this wavelength. Some of this reduction in signal can be recovered by increasing the excitation laser energy until we saturate the 1-0 transition; previous work from our group has shown that meaningful temperature measurements may be obtained from saturated measurements in CH A-X if the transitions observed all occur in the same branch and there is less than 10% variation in the transition probabilities chosen.[15] The spectrum is shown in Figure 9; a Boltzmann plot yields a temperature of 2100± 200 K.

Measurements of LIF from C_2 were less complicated. We observed C_2 using the d-a transition (Swan bands). The metastable triplet a-state lies 716 cm^{-1} above the singlet ground state. To avoid problems with scattered laser light, we excite the 1-0 band (bandhead 473.7) nm and detect the entire 1-2 transition (bandhead 558.6 nm). The spectrum is congested and we do not resolve individual rotational transitions. Temperature estimates were obtained by simulating the spectrum. The experimental spectrum is shown in Figure 10, overlaid with the simulated spectrum. From the simulation, we determine a temperature of 2000 ± 500 K. This measurement was made with the spatial filter set to collect fluorescence from the center 2 mm of the plume. However, if we remove the spatial filter and observe the fluorescence along the entire laser path through the width of the jet, we obtain a spectrum which appears non-thermal (Figure 10b). This is the result of collecting signal from a region with a large temperature gradient, integrating signal from both the hot central core and the cooler outer wings of the plume. Spectral simulation of this band could not reproduce both the bandhead intensity and the intensities of the other rotational transitions with a single temperature Boltzmann distribution. The temperature gradients in this plume therefore necessitate the use of a spatial filter for the detector.

The CH and C_2 LIF measurements for temperature determination were performed approximately 13 mm downstream of the nozzle in an 18 torr reactor. A series of 3 measurements of the CH LIF give rotational distributions described by 2100 ± 200 K; simulation of the C_2 LIF yields a temperature of 2000 ± 500 K. We compare this directly with a series of measurements

obtained using added NO, under identical conditions. In this case the rotational population is described by a temperature of 1850 ± 100 K. Within experimental error, the three measurements agree.

Our temperature measurements agree well with other measurements in propulsion arcjet thrusters. Several measurements have been made in 1 kW class arcjets operating on pure hydrogen. These measurements used a radiatively cooled arcjet operating on a flow of 8.74 slpm hydrogen at 1.34 kW and a chamber pressure of 55 mTorr . A temperature profile across the nozzle exit plane was determined from the Doppler widths of the fluorescence obtained from two-photon excitation of hydrogen atoms.[16,17] The temperature profile at the nozzle exit shows a peak of 1600-1800 K at the center of the jet, dropping to 1000-1200K over the 5 mm radius of the nozzle exit.

Translational temperatures were also determined for a ~1 kW hydrogen arcjet operating in a chamber of 0.3 torr, from Balmer α hydrogen emission.[18] Translational temperatures were determined from Voigt profiles. The translational temperature for a 0.994 kW arcjet had peak temperature of 2000 ± 400 K at the exit plane, while that for a 1.423 kW arcjet had a peak temperature of 3000 ± 400 K.

An LIF study of excited state H atoms in a ~1.4 kW hydrogen arcjet ,[19] recently re-analyzed to account for Stark broadening,[18] show a peak exit plane translational temperature of 1800 K. This is in good agreement with measurements of Raman scattering of molecular hydrogen, in the same apparatus, on the centerline at the exit plane, which yielded temperatures ranging from 1000 K to 1800 K, for powers from 0.8 to 1.4 kW.[20]

Optical emission temperature measurement in the arcjet plume

The optical emission from the arcjet of hydrogen and argon appears bright red to the eye, due to Balmer α emission of hydrogen at 656 nm. Addition of methane causes the plume to become blue from CH emission near 431 nm. At pressures above 10 torr, the plume becomes green, due to C_2

Swan emission. These emission bands are tempting candidates for gas temperature measurement. However, earlier work in our laboratory with a 220 torr hydrogen arcjet reactor discovered that the rotational and vibrational distributions measured from excited state emission were significantly hotter than the rotational distribution determined in the ground state (5000 K vs 2100 K, respectively).[21]

Emission spectra were obtained from an arcjet operating in a chamber at approximately 18 torr and 3.1-3.3 slpm H_2, 3.6-3.8 slpm Ar and 16 sccm CH_4. Emission from CH A-X R and Q branches ($\Delta v = 0$) and C_2 d-a ($\Delta v = -1$) Swan bands at 13 mm down from the orifice are shown in Figures 11 and 12. These spectra were simulated to determine the vibrational and rotational distributions.

The CH A-X emission spectrum consists of of overlapping 0-0, 1-1, and 2-2 bands. Meaningful temperature simulation of CH requires inclusion of both the predissociation and quenching rates. For CH A-state we find the rotational distribution described by a temperature of 3300 ± 500 K and the vibrational distribution described by 4500 ± 500 K. The distributions for C_2 d-state are much hotter; $T_{rot} = 4000 \pm 700$ K and $T_{vib} = 6000 \pm 700$ K.

Emission measurements were made down the plume axis at 4 locations, for an arcjet operating at 24-24.4 torr. For the C_2 we see a T_{vib} range of ~6000 K and a T_{rot} range of 3500-5000 K while for CH the T_{vib} range is 4500-6000 K and the T_{rot} range is 2800-3500 K. For both molecules, the excited state populations are consistently hotter than the ground state populations, consistent with our previous measurements in a 220 torr arcjet.[21] For both molecules, we also observe that the rotational and vibrational distributions are described by different temperatures. These results are summarized in Table 1.

We are not surprised that the temperatures determined from the excited state emission are substantially hotter than those determined from the ground state populations. Previous measurements in the 220 torr arcjet plasma[21] and in flames[22] have shown that chemiluminescent chemical reactions generate products that can have very hot rotational and vibrational distributions.

These distributions of excited state CH and C_2 can be quenched before rotational energy transfer and vibrational energy transfer collisions bring the distribution into equilibrium with the gas temperature. Collisions generally result in vibrational and rotational quantum number changes of ±1 or 2 and therefore many collisions are required to thermalize the hot populations. Quenching requires only one collision to remove the molecule from the radiating state, so even quenching rates that are smaller than the RET and VET rates can result in non-thermalized excited state distributions. The ground electronic states, removed not by quenching but only by relatively slow chemical reaction are therefore much more likely to have rotational and vibrational state distributions in equilibrium with the gas temperature.

Relative CH and C_2 Populations

Relative populations of CH and C_2 in the ground and excited states have also been determined; populations in the excited state are determined from emission measurements, while populations in the ground state are determined from LIF measurements. A-state populations of CH are determined by integrating the A-X R and Q branch emission. d-state populations of C_2 are determined by integrating the $\Delta v = -1$ a-d transition. Ground state populations for CH X is determined by integration of the Q7 transition of A-X 1-0 band, and populations for C_2 a-state were determined from integration of 2 Å of the $\Delta v = +1$ bandhead. The derived ground-state populations include correction for the temperature dependence of rotational population and LIF signal intensity.

Results down the center axis of the plume are summarized in Table 2. H_γ emission at 4340.47 Å overlaps with the CH A-X emission, so relative H atom excited state populations are also included. We see that all populations decrease down the axis of the plume, with the decreases most dramatic for the excited state species. If we integrate emission across the entire width of the plume we see that the C_2 emission increases down the plume, while the CH emission decreases slightly. The relative populations for the ground states of CH and C_2 across the plume are shown in Figure 13. The CH X-state population peaks in the center of the plume, and drops quickly out

into the wings. The C_2 a-state population is relatively flat over the central several millimeters of the plume, perhaps with a dip in the center, then drops slowly out into the wings of the plume.

We can speculate about the origin of the bright CH and C_2 emission seen in the plume. The relative concentrations of the ground and excited states show different trends: excited state CH decreases by a factor of 100 down the plume while ground state CH is relatively constant. Excited state C_2 decreases by a factor of ~7 down the plume while ground state C_2 decreases by less than a factor of 3. Therefore the pathways which produce the ground- and excited-state species may not be directly related. Also, since the lifetime for CH A in the plume is ~ 40 ns while the transit time down the plume, between the exit plane and the substrate, is ~20 μsec, the excited states whose emission we observe must be generated in flight, either by excitation of ground state species or by chemical reaction.

Three possible methods of exciting ground states to radiating states are metastable energy transfer, thermal excitation, and electron impact excitation. Because argon metastables are rapidly deactivated in this collisional environment,[23,24] we do not expect them to be present in sufficient density to contribute significantly; no argon metastable emission is apparent in our spectra, indicating a low concentration. Thermal excitation would produce excited state distributions characterized by the same temperatures as the ground state distributions. This is not the observed behavior, however.

Electron impact excitation would result in a rotational distribution identical to that in the ground state, while the vibrational distribution would reflect the Franck-Condon overlap between the two vibronic states. Because the CH A-X transition is highly (but not perfectly) diagonal, excitation of a 2000 K X-state distribution would produce a 1900 K vibrational distribution in the A-state. The Franck-Condon pattern for C_2 d-a is not diagonal, and excitation of a 2000 K distribution would produce vibrational distributions of ~2800 K for C_2 d-state. Since our emission distributions are on the order of 4500-6000 K, electron impact also seems an unlikely candidate for an excitation mechanism. However, both the electron density in the plume[13] and the emission

intensities show a similar decrease down the axis, and therefore electron impact excitation probably accounts for at least some of the observed excitation.

Alternatively, chemiluminescent reactions can directly generate excited state species with population distributions quite different from those reflecting the thermal distribution of the gas temperature. Our excited state distributions are consistent with those previously seen for CH and C_2 emission in flames [22] and for C_2 emission in our 220 torr hydrogen arcjet reactor.[21] In the 220 torr arcjet reactor LIF of CH(X) and C_2(a) yielded Boltzmann gas temperatures of 2100 ± 200 K, while the C_2(d) Swan emission yielded an excited state rotational and vibrational population well-described by a 5000 K temperature.

To produce chemiluminescent products, the responsible reactions must be exothermic by at least 55 kcal to produce C_2 d-state, 66 kcal to produce CH A-state, and 74 kcal to produce CH B-state. We estimate that we have high H concentrations (~30 % H_2 dissociation) and that essentially all of the injected methane is transformed in the plume to free atomic carbon. For C_2, a likely production mechanism is via the very exothermic C + C + M = C_2 + M reaction. In flames, excited C_2 is produced via chemiluminescent reactions, although these reactions are not well understood.[22] The origin of CH chemiluminescence in the plume is more speculative. Flame studies indicate that a main route to the production of excited CH is through C_2 + OH = CO + CH.[22] However, this reaction is not expected to be significant in our reactor, since oxygen is present only at trace concentrations (as a feedstock gas impurity). Another possible chemiluminescent pathway for CH is collisional stabilization of CH in C + H collisions (inverse predissociation).

SUMMARY

We have measured the gas temperature in a hydrogen/argon arcjet plume using LIF measurements of both "native" species and NO added to the plume. The temperatures describing the rotational distributions for the X-state of NO agree within experimental error with the LIF measurements of the X-state of CH and the a-state of C_2. Rotational and vibrational distributions obtained from emission of A-state CH and d-state C_2 are consistently hotter, similar to results seen previously in flames and other arcjets. The optical emission from the plasma plume has a significant contribution from chemiluminescent reactions.

ACKNOWLEDGMENTS

This work is supported by ARPA via contract with the Naval Research Laboratory and by the Army Research Office. We thank Dr. Mark Cappelli and Mr. Michael Loh of the High Temperature Gas Dynamics Laboratory at Stanford University for design and operation assistance with the arcjet reactor and for the loan of electrodes for the dc-arc. We thank David Huestis and Greg Smith of SRI International for helpful discussions, and especially thank Jorge Lugue and Wolfgang Juchmann of SRI for sharing their unpublished results.

REFERENCES

1. M. A. Cappelli, in *Handbook of Industrial Diamond and Diamond Films*, edited by M. Prelas (Marcel Decker, New York, in press 1996).

2. D. G. Goodwin, J. Appl. Phys. **74**, 6888 (1993).

3. D. G. Goodwin, J. Appl. Phys. **74**, 6895 (1993).

4. M. E. Coltrin and D. S. Dandy, J. Appl. Phys. **74**, 5803 (1993).

5. E. A. Brinkman and J. B. Jeffries,"Comparison of Optical Emission and Laser-Induced Fluorescence in Arcjet Thruster Plumes Used for Diamond Deposition," AIAA 95-1955 (1995).

6. E. A. Brinkman and J. B. Jeffries, in *Diamond Materials IV*, edited by K. V. Ravi and J. P. Dismukes (The Electrochemical Society, Inc., Pennington, NJ, 1995).

7. J. B. Jeffries, G. A. Raiche and M. S. Brown, "Optical Diagnostics of Diamond CVD Plasmas," in *Laser Techniques for State-Selected and State-to-State Chemistry II*, ed J. W. Hepburn, SPIE **2124**, 270 (1994).

8. J. Luque and D. R. Crosley,"LIFBASE: Database and Spectral Simulation Program," SRI International, MP96-001 (1995).

9. D. L. Huestis, DIATOM Spectral simulation computer Program, Version 7.0 (SRI International, Menlo Park, CA, 1994).

10. N. Heberle, personal communication.

11. J. M. Seitzman, G. Kychakoff and R. K. Hanson, Optics Lett. **10**, (1985).

12. M. P. Lee, B. K. McMillin and R. K. Hanson, Appl. Opt. **32**, 5379 (1993).

13. E. A. Brinkman, K. R. Stalder and J. B. Jeffries, sub 1996.

14. G. A. Raiche and J. B. Jeffries, submitted to Appl. Phys. B, 1996.

15. J. Luque, unpublished results.

16. J. A. Pobst, I. J. Wysong and R. A. Spores, IEPC-95-28 (1995).

17. J. A. Pobst, I. J. Wysong and R. A. Spores,"Laser Induced Fluorescence of Ground State Hydrogen Atoms at Nozzle Exit of an Arcjet Thruster," AIAA 95-1973 (1995).

18. P. V. Storm and M. A. Cappelli,"High Spectral Resolution Emission Study of a Low Power Hydrogen Arcjet Plume," AIAA 95-160 (1995).

19. P. V. Storm and M. A. Cappelli, in press Applied Optics,1996 .

20. D. R. Beattie and M. A. Cappelli,"Raman Scattering Measurements of Molecular Hydrogen in an Arcjet Thruster Plume," 95-1956 (1995).

21. G. A. Raiche and J. B. Jeffries, Appl. Opt. **32**, 4629 (1993).

22. A. G. Gaydon, *The Spectroscopy of Flames* Second Edition (Halsted Press, New York, 1974).

23. L. G. Piper, J. E. Velazco and D. W. Setzer, J. Chem. Phys. **59**, 3323 (1973).

24. M. Bourene, O. Dutuit and J. L. Calve, J. Chem. Phys. **63**, 1668 (1975).

FIGURE CAPTIONS

Figure 1. Experimental Setup

Figure 2. NO A-X LIF excitation spectrum after exciting 0-0 and detecting total fluorescence (details in text). To minimize scan time, we scan a selected region, then rapidly slew wavelength to the next region.

Figure 3. Boltzmann plot of relative NO X-state rotational level populations, corrected for degeneracy, versus rotational energy

Figure 4. Temperature profile along the plume, from LIF measurements of seeded NO. (1.6 kW; 23.9 torr; flows: H_2 3.1 slpm, Ar 3.7 slpm, NO 7-8 sccm; CH_4 16 sccm).

Figure 5. Temperature profile across the plume, 20 mm downstream of the exit plane. (1.6 kW; 23.9 torr; flows: H_2 3.1 slpm, Ar 3.7 slpm, NO 7-8 sccm; CH_4 16 sccm).

Figure 6. Temperature profile along the plume. (2.1 kW; 25.7 torr; flows: H_2 6.1 slpm, Ar 2.9 slpm, NO 7-8 sccm, CH_4 16 sccm)

Figure 7. Temperature profile along the jet. (1.1 kW; 24.9 torr; flows: H_2 1.6 slpm, Ar 4.7 slpm, NO 7-8 sccm, CH_4 16 sccm)

Figure 8. CH LIF rotational excitation spectra

a. Excite B-X 0-0, detect B-X 0-0

b. Excite A-X 0-0, detect A-X 0-0

c. Excite B-X 0-1, detect B-X 0-0

d. Excite A-X 0-1, detect A-X 0-0

Figure 9. CH A-X LIF rotational excitation spectrum after exciting 0-1 and detecting 0-0. Experimental conditions: 1.5 kW; 18.0 torr; flows: H_2 3.1 slpm, Ar 3.6 slpm, CH_4 16 sccm

Figure 10. C_2 d-a LIF rotational excitation spectrum after exciting 0-1and detecting $\Delta v=-1$. Simulation at 2000 K. Experimental conditions: 1.5 kW; 18.0 torr; flows: H_2 3.1 slpm, Ar 3.6 slpm, CH_4 16 sccm

a. 2 mm spatial filter

b. No spatial filter

Figure 11. CH A-X emission from $\Delta v=0$ overlaid with simulation (T_{vib}=4500 K, T_{rot}=3200 K) Experimental conditions: 1.5 kW; 18.0 torr; flows: H_2 3.3 slpm, Ar 3.8 slpm, CH_4 16 sccm

Figure 12. C_2 d-a (Swan band) emission from $\Delta v=-1$, overlaid with simulation (T_{vib}=7000 K, T_{rot}=4000 K) . Experimental conditions: 1.5 kW; 18.0 torr; flows: H_2 3.1 slpm, Ar 3.6 slpm, CH_4 16 sccm

Figure 13. Relative populations, at 20 mm downsteam of the exit plane, obtained from LIF measurements.

a. CH

b. C_2

Table 1

Distance from nozzle exit (mm)	T_{rot} NO LIF ± 100 K	T_{vib} CH emission ± 1000 K	T_{rot} CH emission ± 500 K	T_{vib} C_2 emision ± 1000 K	T_{rot} C_2 emission ± 1000 K
2	1810	6000	3500	6000	5000
14	1970	5000	3000	6000	4000
20					
26	2070				
34	2160	5000	3000	6000	3500
38					
43	2460	4500	2800	6000	4000

All temperatures in K. Conditions: 1.5-1.6 kW, 24-24.4 torr. Flows: 2.9-3.1 slpm H_2, 3.4-3.7 slpm Ar, 16 sccm CH_4

Table 2

Distance from nozzle exit (mm)	CH X-state Intensity (LIF)	CH A-state Intensity (Emission)	C_2 a-state Intensity (LIF)	C_2 d-state Intensity (Emission)	H state Intensity (Emission)
2	1.4	104	2.6	9.5	130
14	1.1	24	1.9	3.4	28
20	1.2		1.5		
26	1.1		1.2		
34		1.3		1.0	1.3
38	1.0		1.0		
43		1.0		1.3	1

All temperatures in K. Conditions: 1.5-1.6 kW, 24-24.4 torr. Flows: 2.9-3.1 slpm H_2, 3.4-3.7 slpm Ar, 16 sccm CH_4

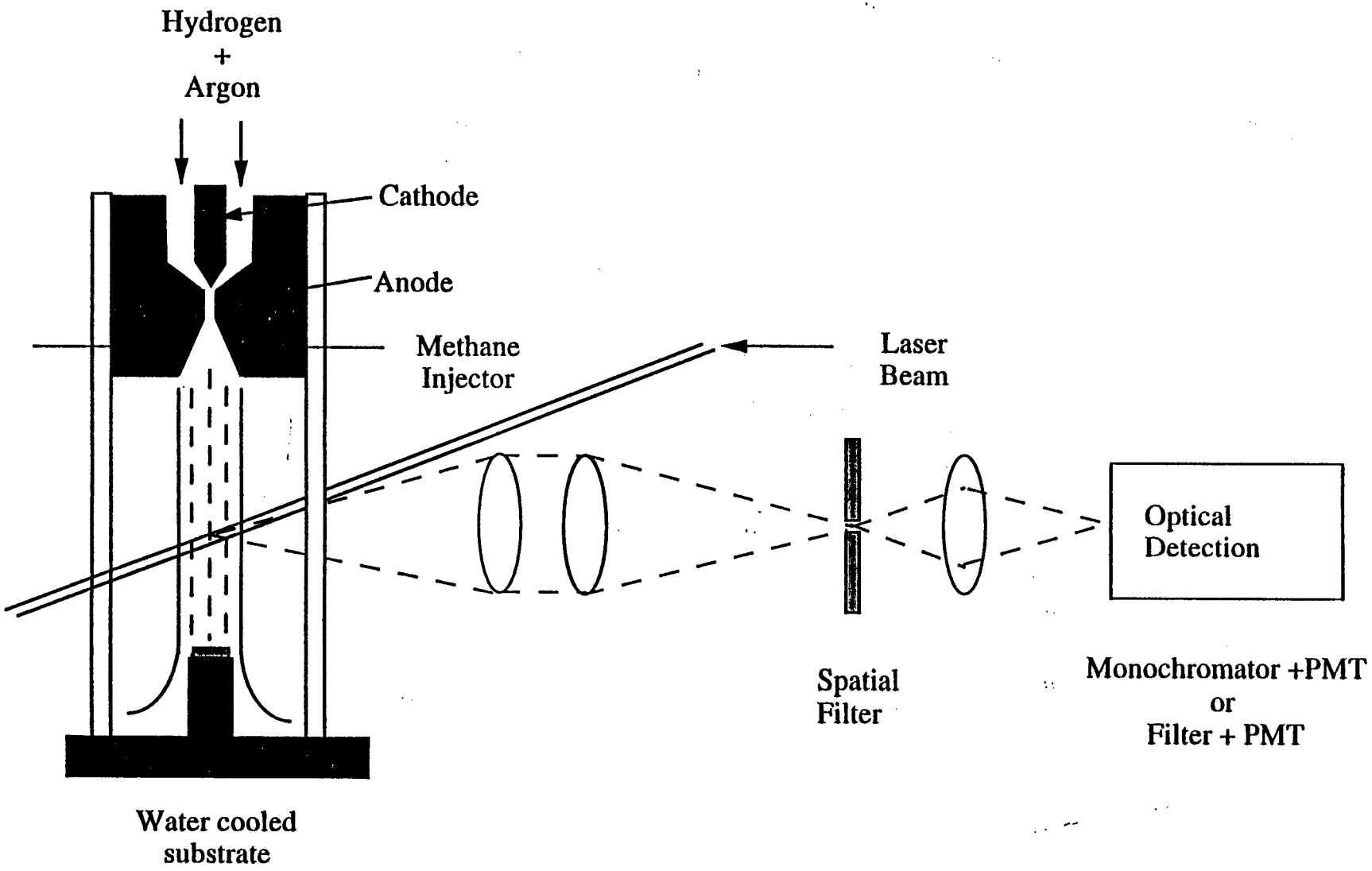
Hydrogen
+
Argon
Cathode
Anode
Methane
Injector
Laser
Beam
Optical
Detection
Spatial
Filter
Monochromator +PMT
or
Filter + PMT
Water cooled
substrate

FIGURE 1

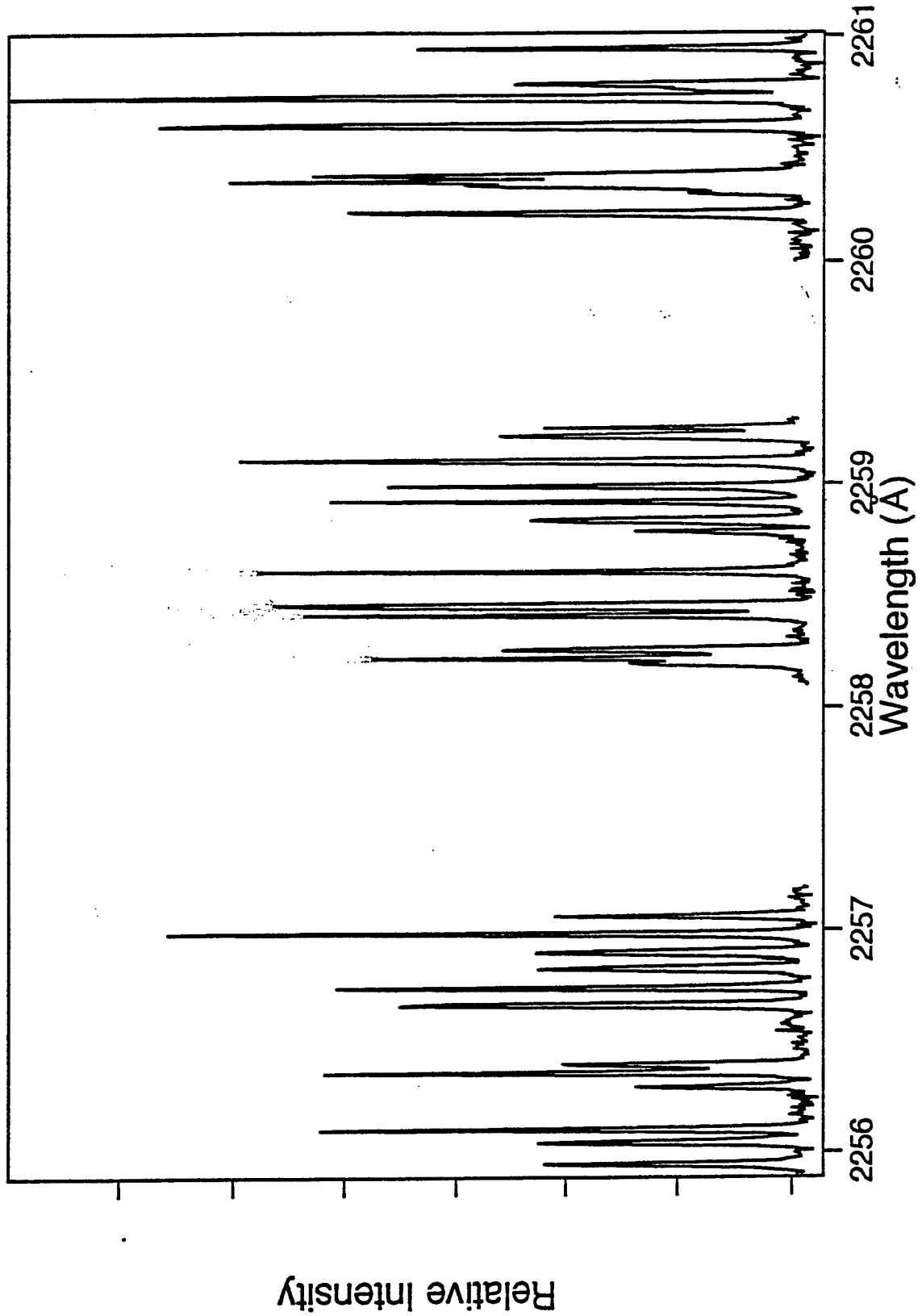
Relative Intensity
2256
2257
2258
2259
2260
2261
Wavelength (Å)

FIGURE 2

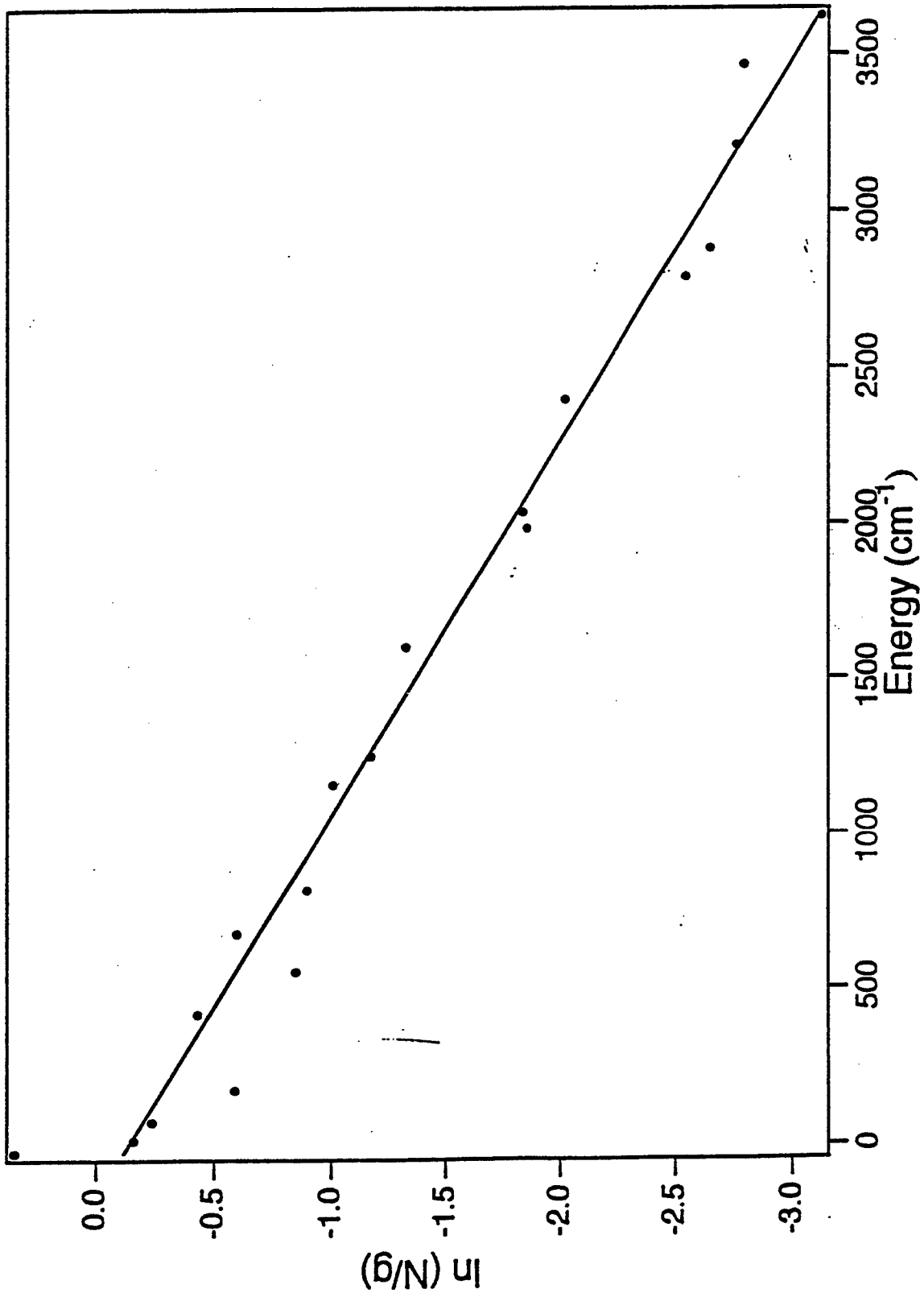
ln (N/g)
0.0
-0.5
-1.0
-1.5
-2.0
-2.5
-3.0
0
500
1000
1500
2000
2500
3000
3500
Energy (cm-1)

FIGURE 3

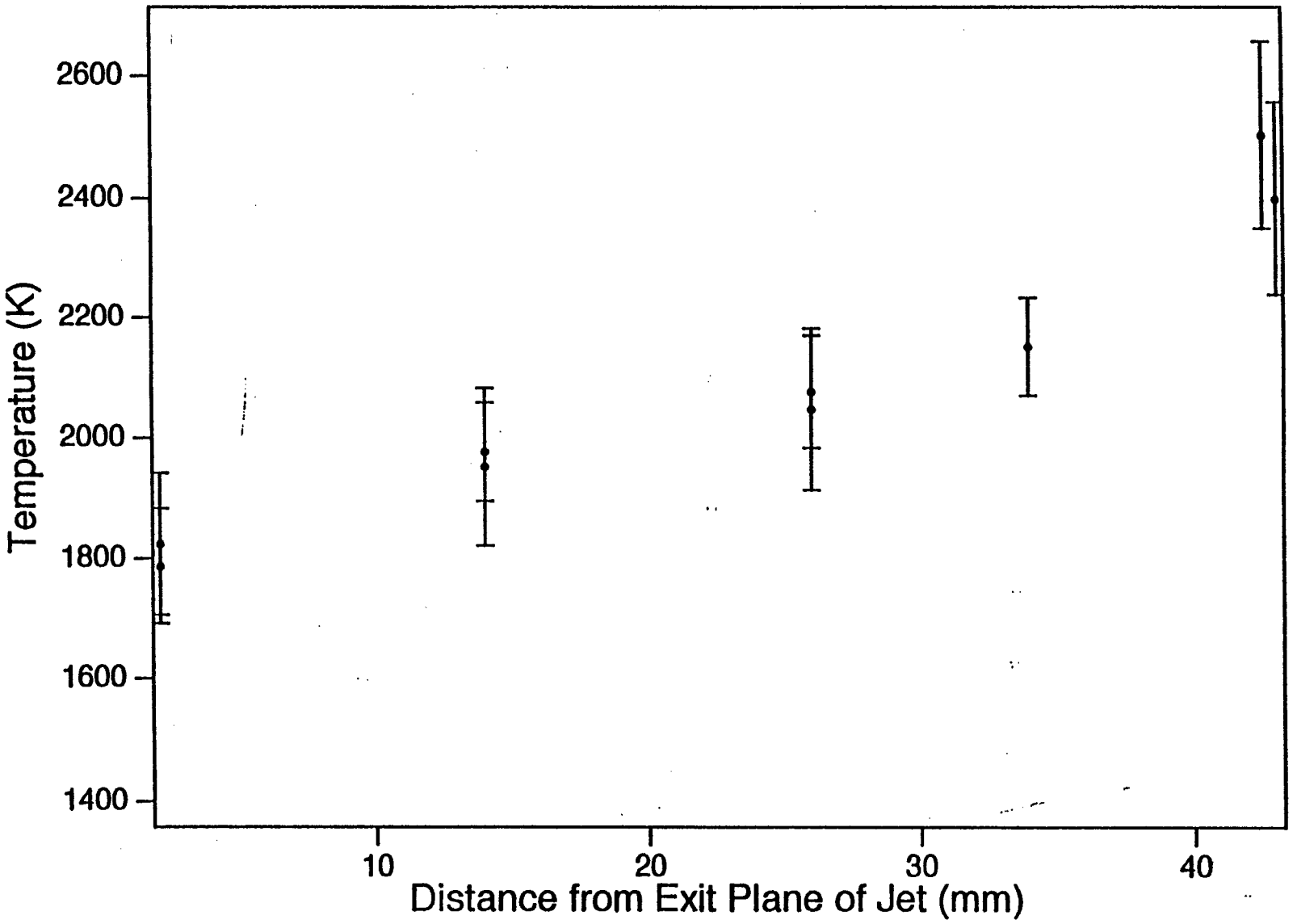
Temperature (K)
2600
2400
2200
2000
1800
1600
1400
10
20
30
40
Distance from Exit Plane of Jet (mm)

FIGURE 4

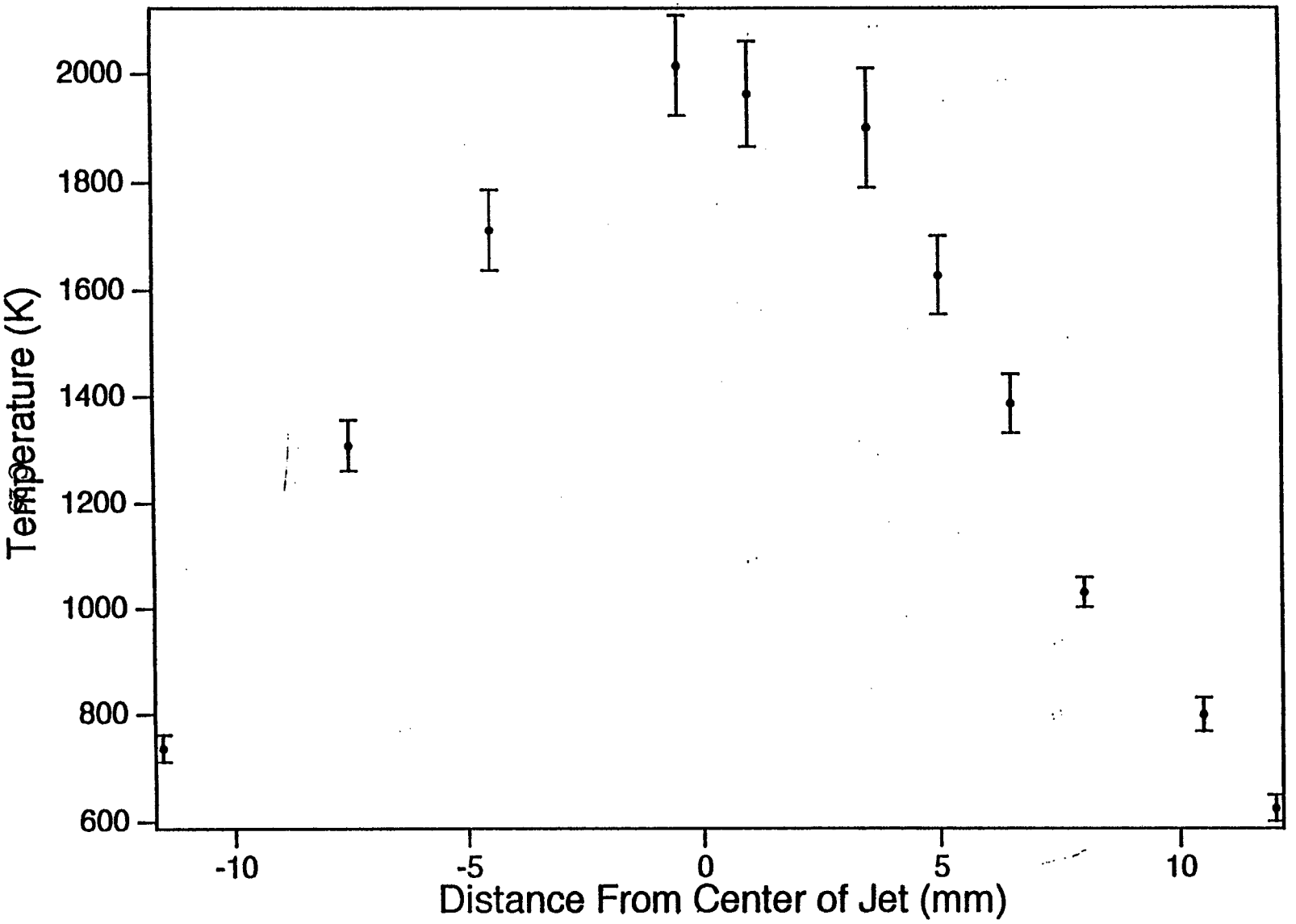
2000
1800
1600
1400
1200
1000
800
600
Temperature (K)
-10
-5
0
5
10
Distance From Center of Jet (mm)

FIGURE 5

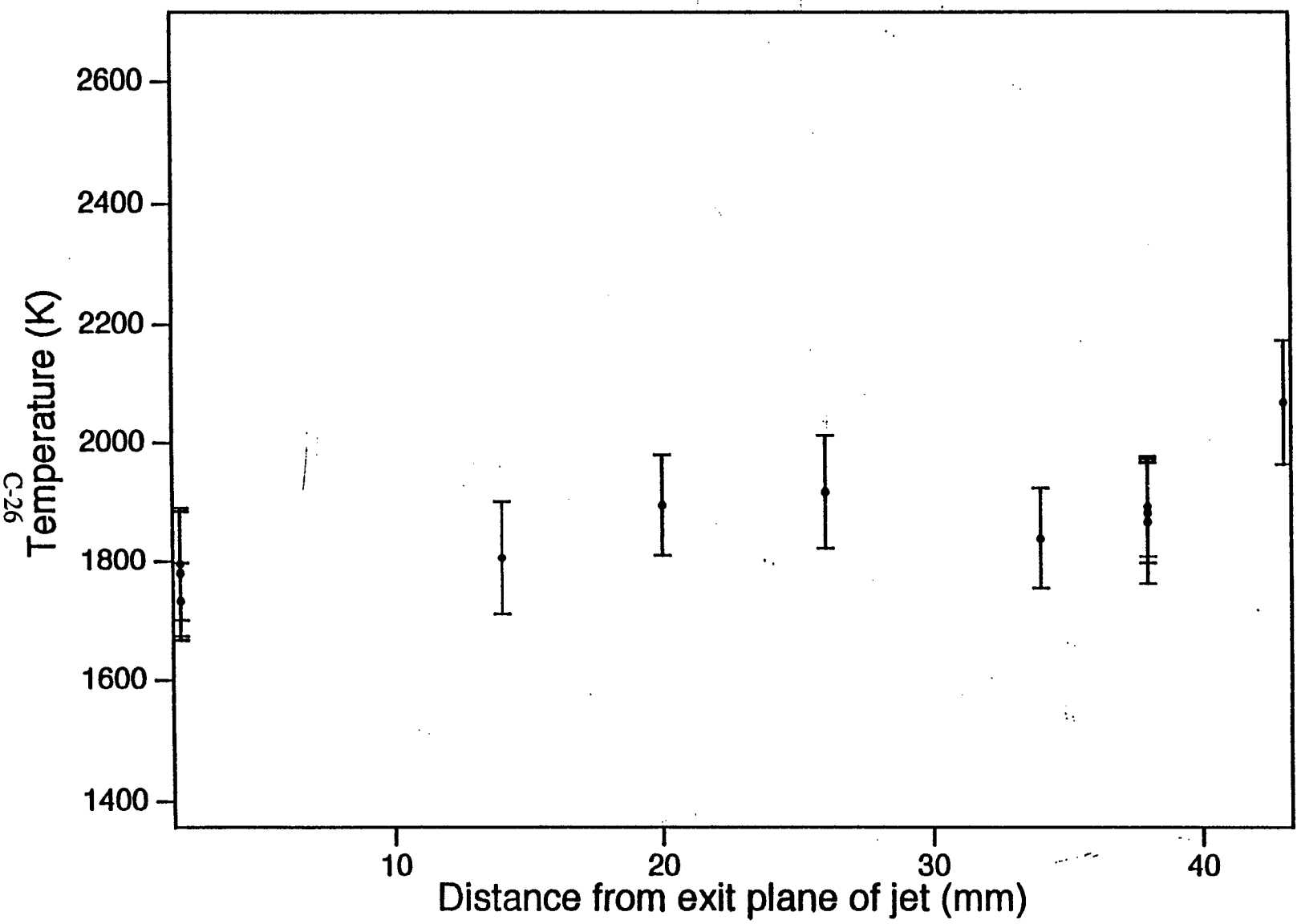
2600
2400
2200
2000
1800
1600
1400
Temperature (K)
10
20
30
40
Distance from exit plane of jet (mm)

FIGURE 6

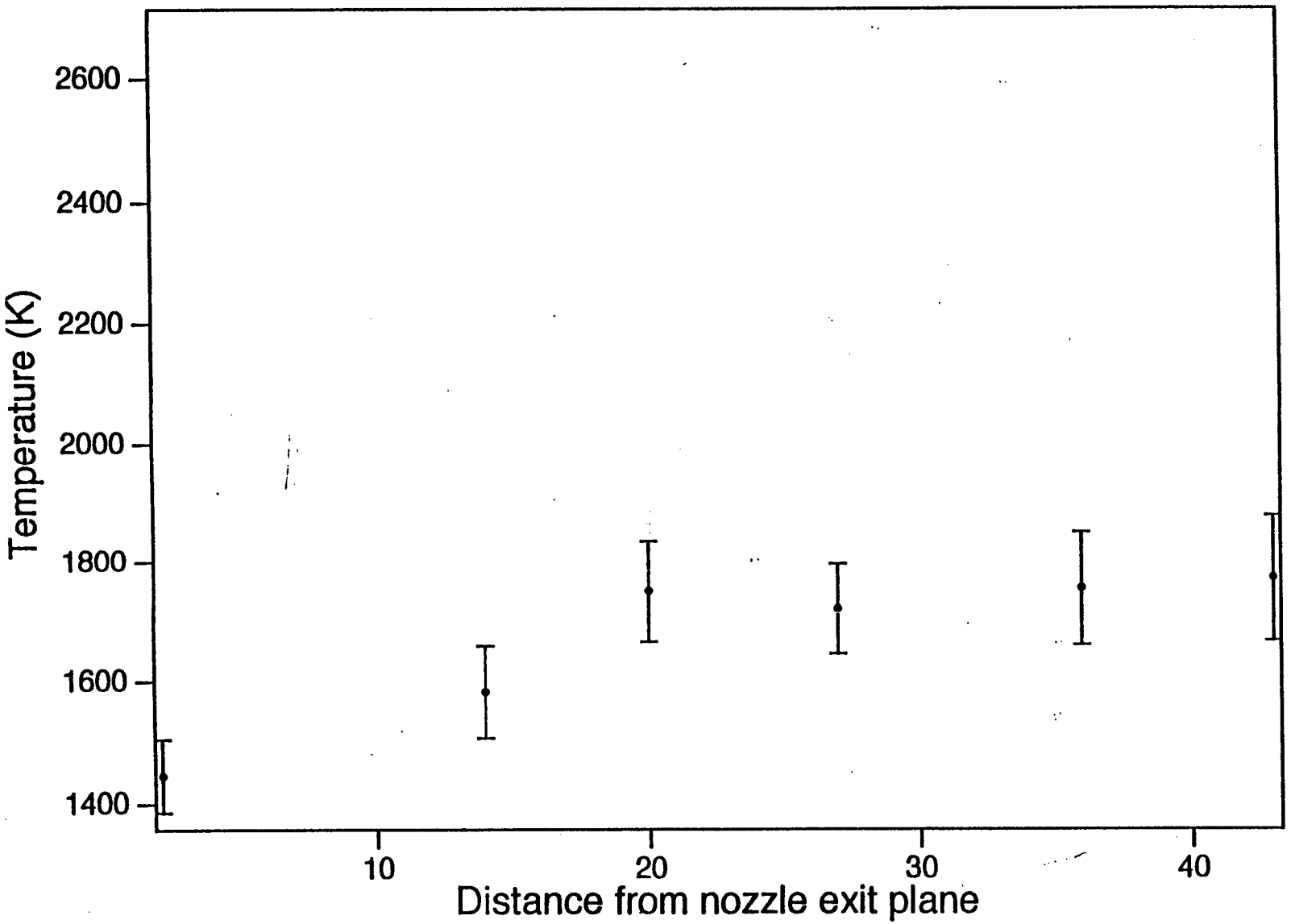
Temperature (K)
2600
2400
2200
2000
1800
1600
1400
10
20
30
40
Distance from nozzle exit plane

FIGURE 7

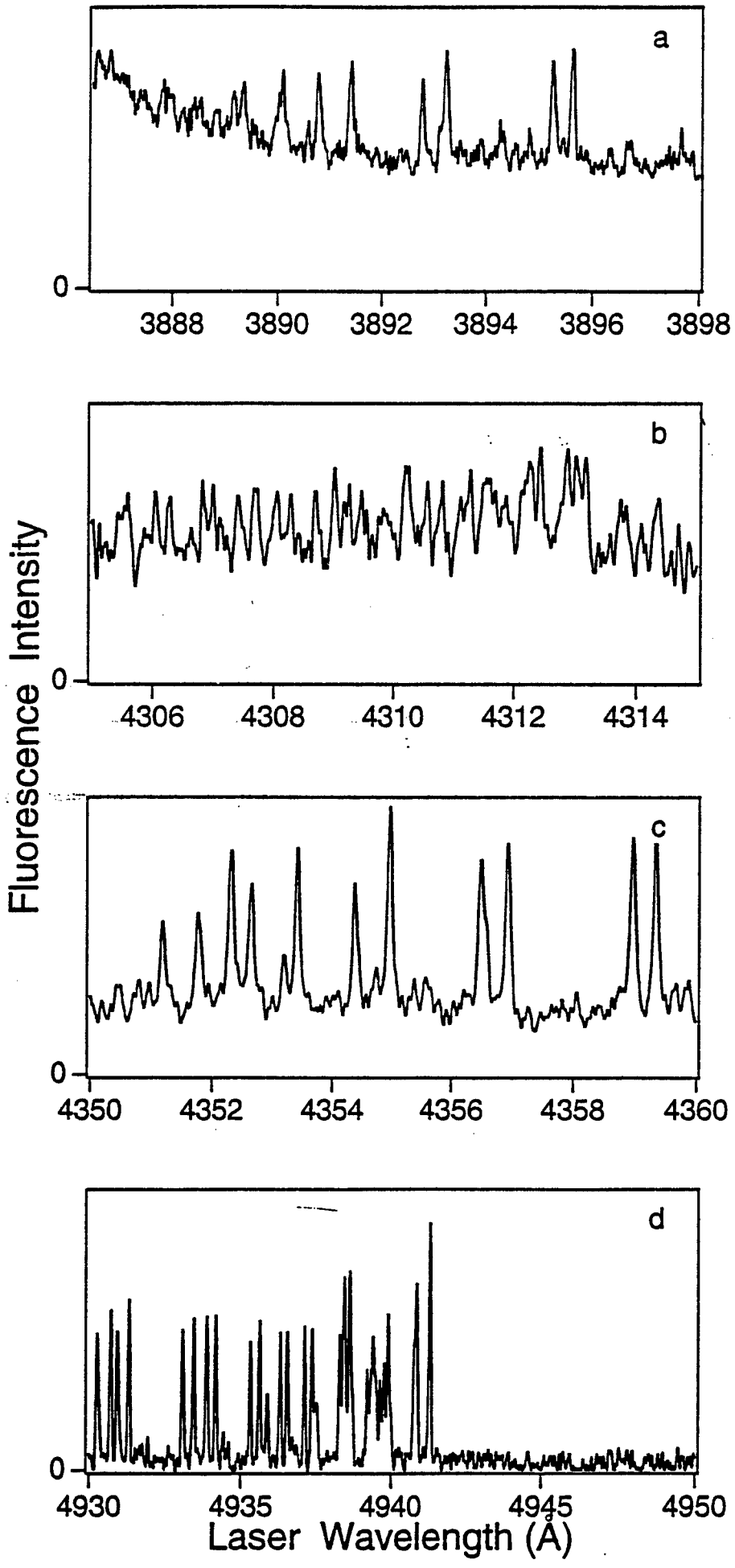
a
0
3888
3890
3892
3894
3896
3898
b
0
4306
4308
4310
4312
4314
Fluorescence Intensity
c
0
4350
4352
4354
4356
4358
4360
d
0
4930
4935
4940
4945
4950
Laser Wavelength (Å)

FIGURE 8

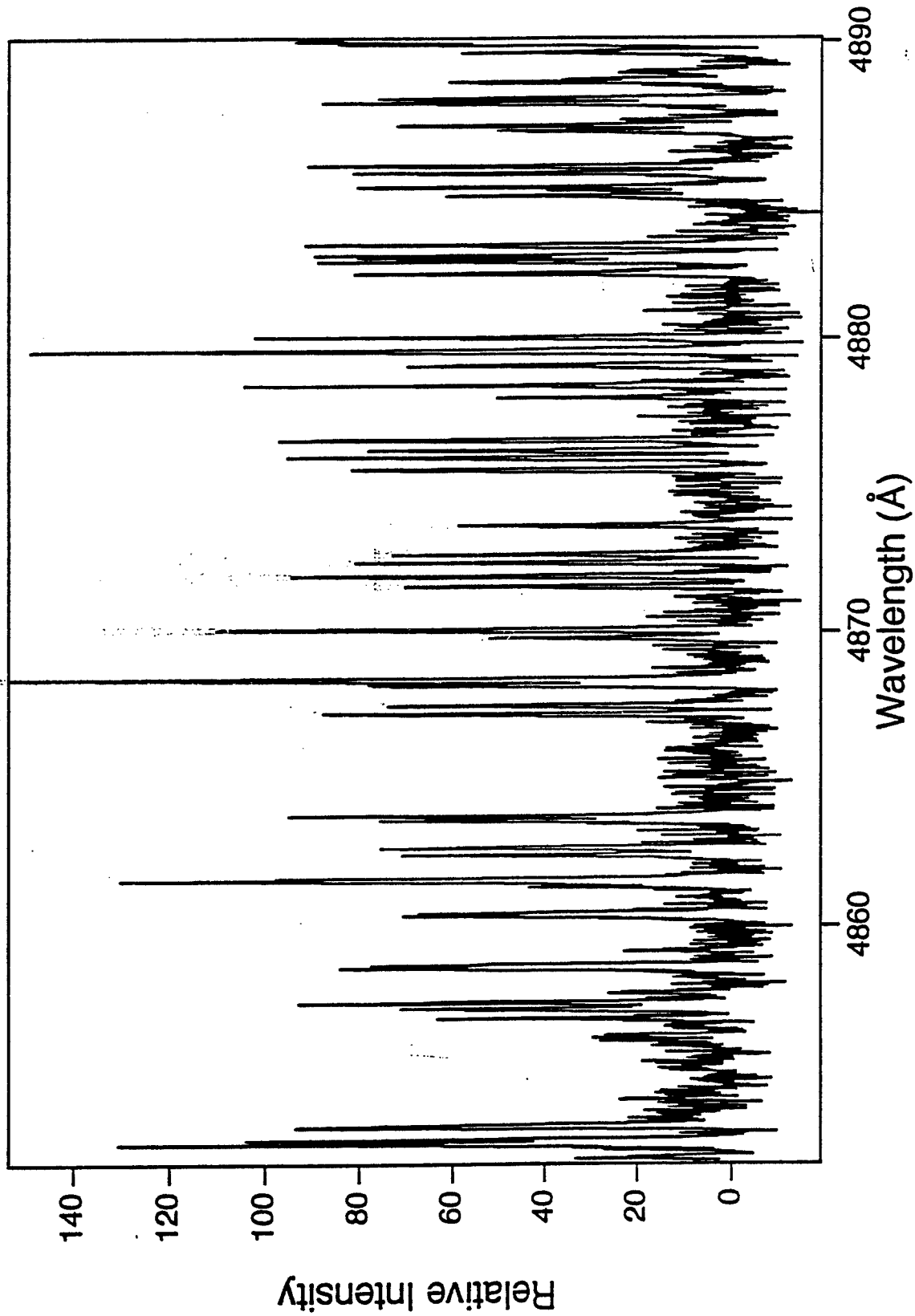
Relative Intensity
140
120
100
80
60
40
20
0
4860
4870
4880
4890
Wavelength (Å)

FIGURE 9

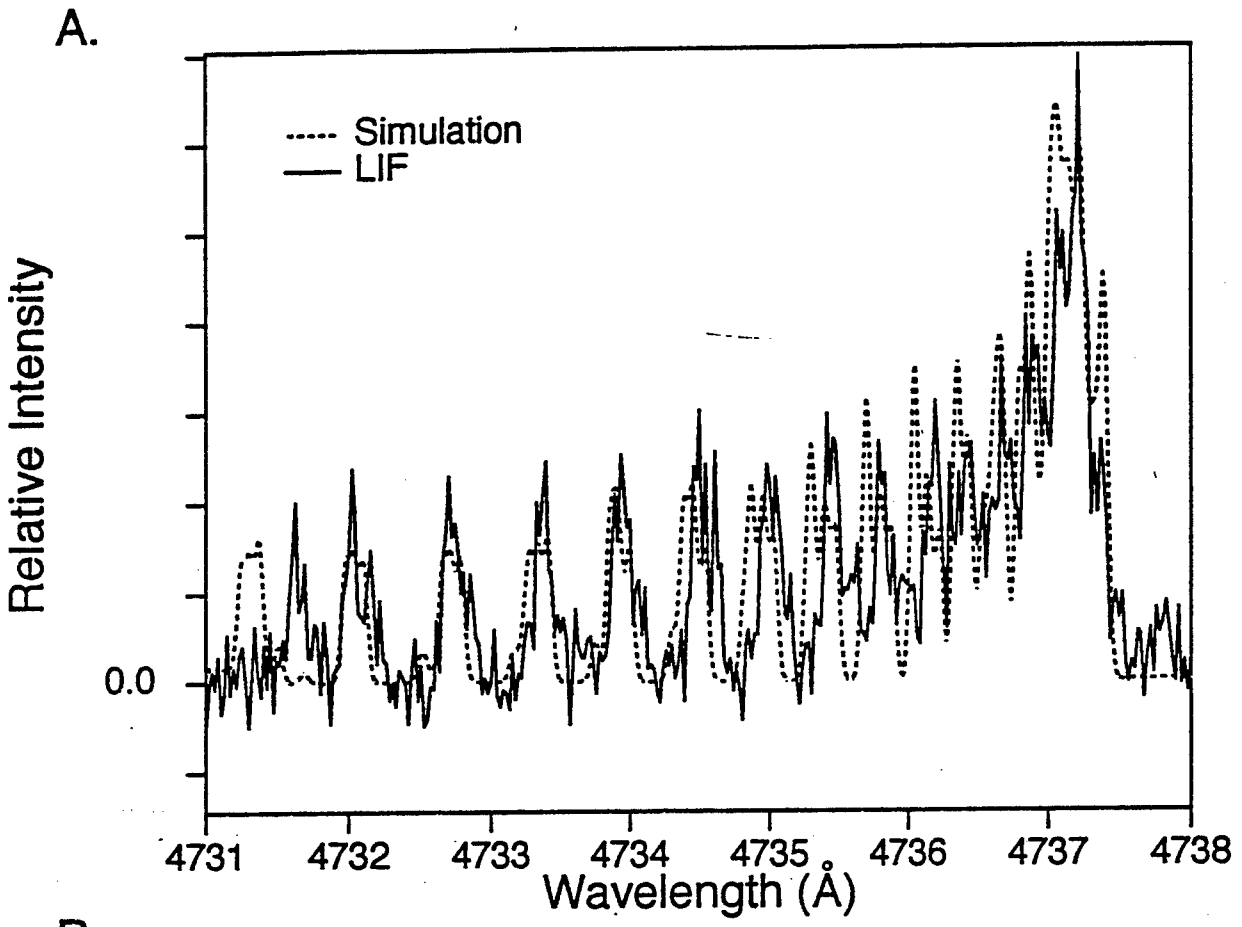
A.
Simulation
LIF
Relative Intensity
0.0
4731
4732
4733
4734
4735
4736
4737
4738
Wavelength (Å)

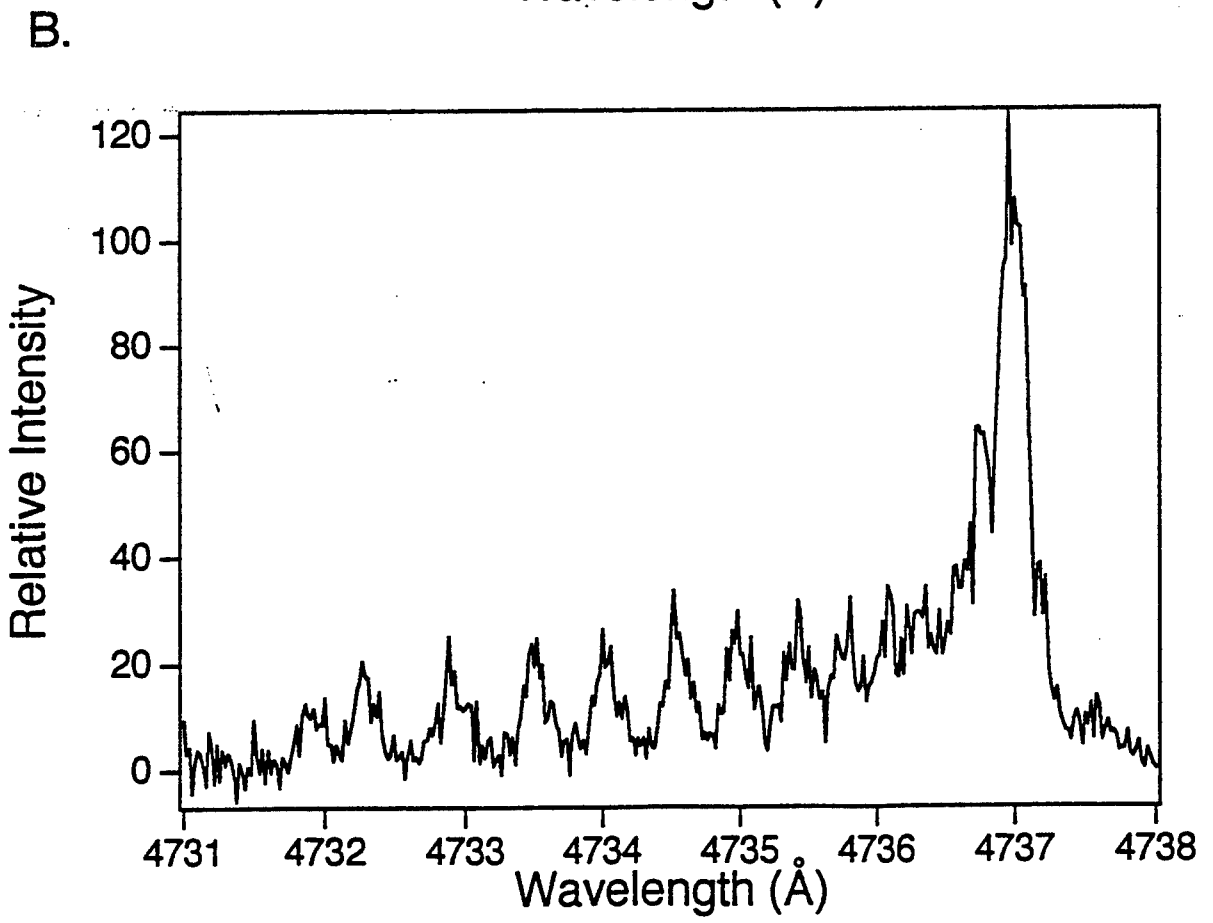
B.
Relative Intensity
120
100
80
60
40
20
0
4731
4732
4733
4734
4735
4736
4737
4738
Wavelength (Å)

FIGURE 10

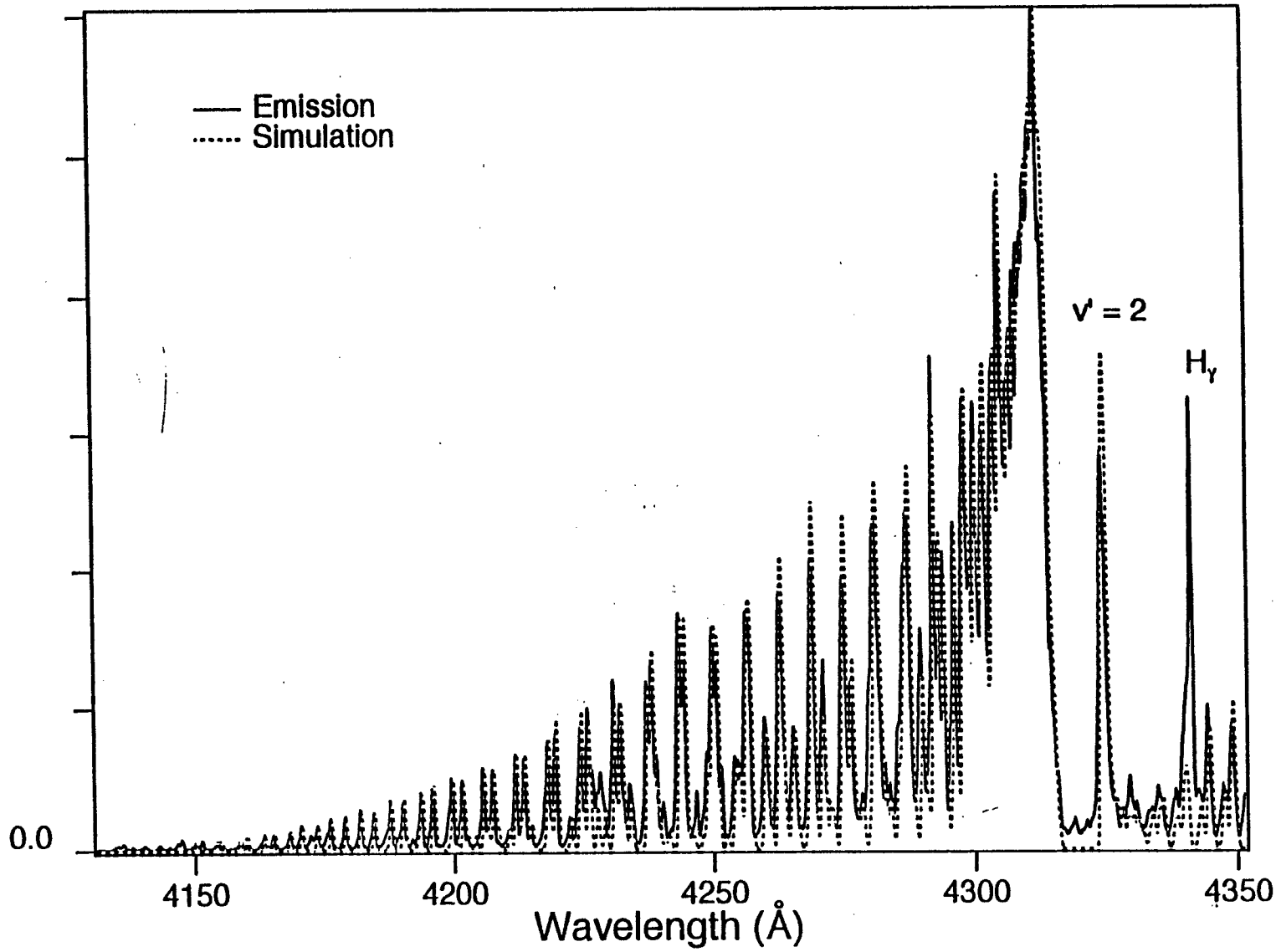
Emission
Simulation
v' = 2
H_γ
Relative Intensity
0.0
4150
4200
4250
4300
4350
Wavelength (Å)

FIGURE 11

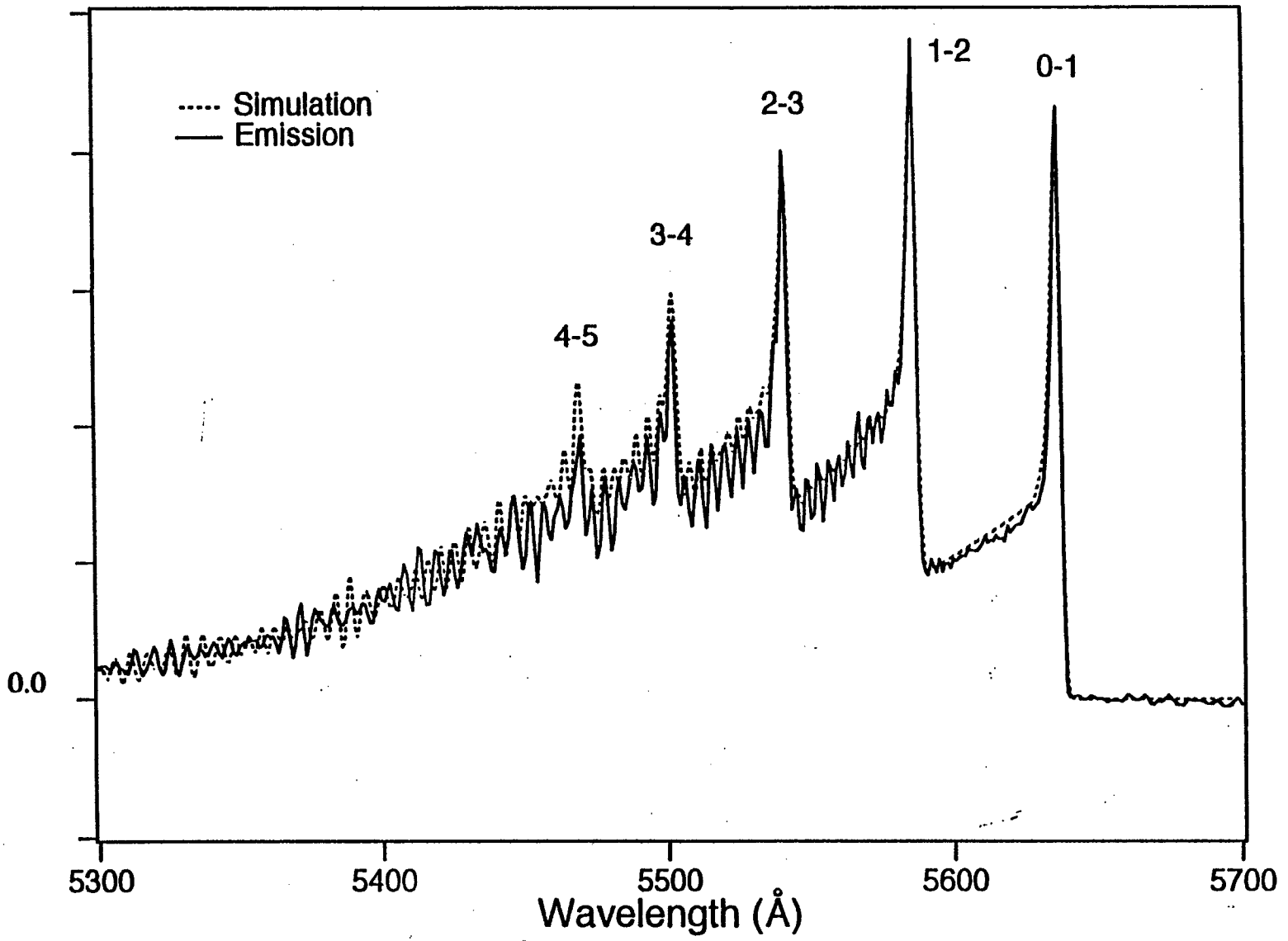
Simulation
Emission
4-5
3-4
2-3
1-2
0-1
Relative Intensity
0.0
5300
5400
5500
5600
5700
Wavelength (Å)

FIGURE 12

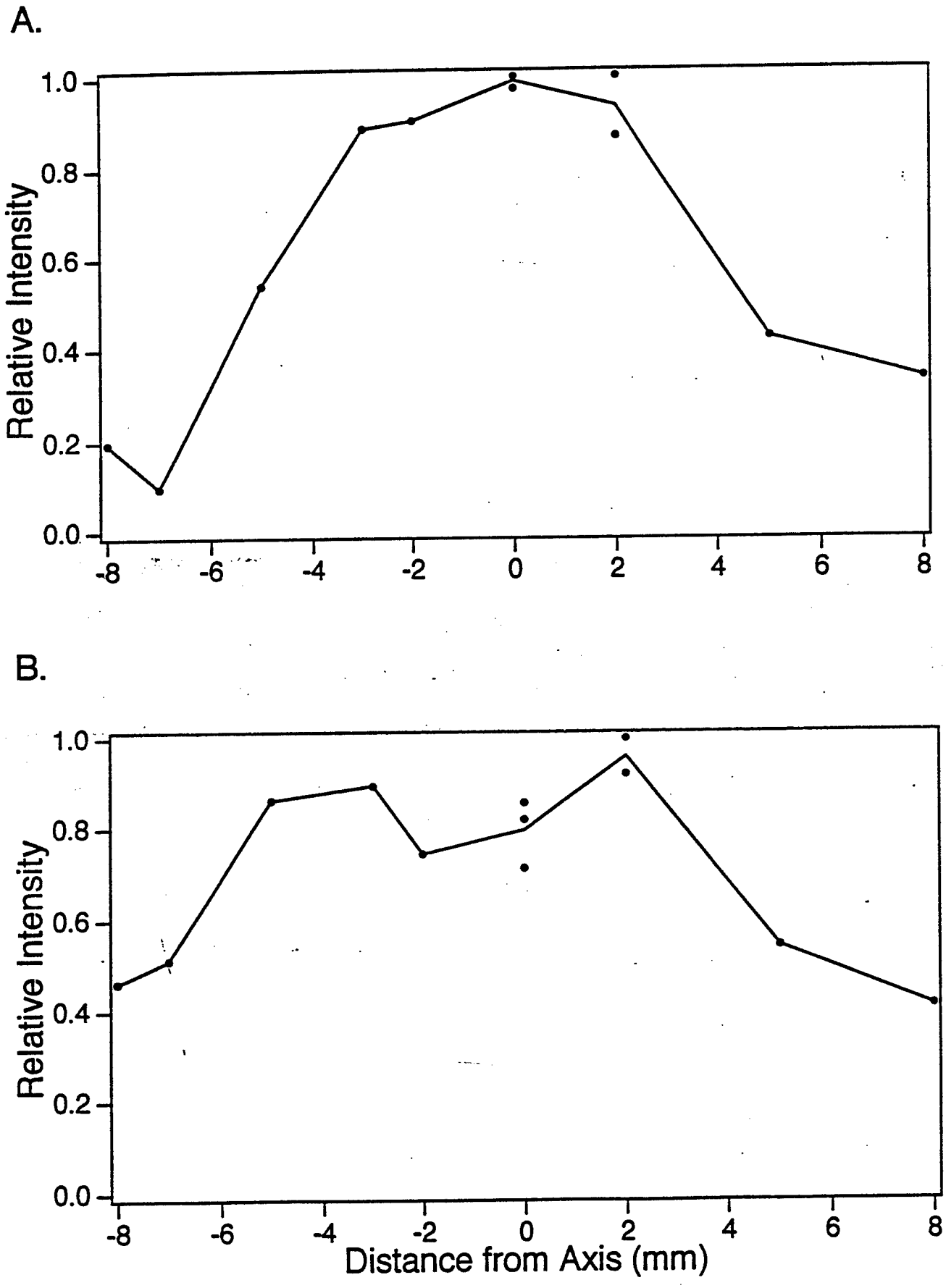
A.
Relative Intensity
1.0
0.8
0.6
0.4
0.2
0.0
-8
-6
-4
-2
0
2
4
6
8
B.
Relative Intensity
1.0
0.8
0.6
0.4
0.2
0.0
-8
-6
-4
-2
0
2
4
6
8
Distance from Axis (mm)

FIGURE 13

APPENDIX D

ELECTRON DENSITIES AND TEMPERATURES IN A DIAMOND-DEPOSITING DC-ARCJET PLASMA

E. A. Brinkman, K. R. Stalder, and J. B. Jeffries

Submitted to *The Journal of Applied Physics*

August 1996

Electron densities and temperatures in a diamond-depositing dc arcjet plasma

E. A. Brinkman, K. R. Stalder, and J. B. Jeffries

Molecular Physics Laboratory
SRI International
Menlo Park, CA 94025

(Received

PACS: 52.70.-m, 52.75.-d, 52.80.-s

Abstract

Langmuir probe measurements of electron density and temperature are made in the plume of a dc-arcjet reactor. A dc-arc is struck in an argon or argon/hydrogen mixture at 6 atmosphere pressure and expands through a converging/diverging nozzle into the reactor with a pressure of 25 torr. Methane and methane/nitric oxide are added in the diverging nozzle, and diamond film grows on a substrate in the gas plume. Electron temperatures of 1-2 eV are significantly hotter than the neutral gas temperature in the plume. Electron densities range from 10^{10} to 10^{13} cm^{-3}, well above the Saha equilibrium for the gas temperature and pressure and well below the equilibrium for the electron temperature.

Introduction

An arcjet is a high pressure discharge in which an arc is struck in a flowing, high pressure gas which expands into a low pressure, forming a luminous plume of reactive gas and thereby increasing the enthalpy and kinetic energy of the gas. Because of the high velocity of the expanding gas plume, which leads to high specific impulse, arcjets have been used for propulsion, especially for satellite station keeping purposes. In addition, an arcjet operating on a hydrogen/argon mixture or pure hydrogen with a small amount of methane added to the effluent of can be used for the chemical vapor deposition (CVD) of polycrystalline diamond films.[1,2] Linear growth rates for diamond in dc-arcjet reactors are among the highest rates reported for diamond CVD, with excellent film quality.

A dc-arcjet provides an excellent environment in which to study the chemical mechanism of diamond CVD. The residence time of the gas in the reactor and the transit time are well defined, allowing for modeling of the gas chemistry if the boundary conditions are measured. These boundary conditions include reactor pressure, the mass flow of the feedstock gases, gas temperature distribution between the nozzle exit plane and substrate, the degree of ionization of the gases and the fraction of hydrogen dissociated.

We have recently measured the gas temperature in a dc arcjet operating with conditions used for the growth of diamond films. This arcjet operates on a mixture of argon and hydrogen, with a small amount of methane introduced into the effluent of the arc; typical

reactor pressures are 20-30 torr.[3] We have used laser-induced fluorescence (LIF) to measure the gas temperature in the plume of this arcjet. LIF is a convenient, non-invasive method to measure gas temperature. LIF has previously been used to measure gas temperatures in a variety of environments, including flames[4,5] and a dc arcjet operating at 220 torr.[6] For some experiments, we introduce a small amount of nitric oxide (NO) along with methane downstream of the arc. NO, which is relatively unreactive in this environment, is a convenient molecule to use for LIF temperature measurement and has previously been used for temperature measurements in hot filament diamond CVD reactors.[7]

In this paper we report a series of Langmuir probe measurements in the plume of this arcjet, to determine the extent of ionization in the plume. We report probe measurements at two positions in the plume of this jet with argon or argon/hydrogen feedstock mixtures and small amounts of methane and/or nitric oxide introduced downstream in the diverging nozzle of the arcjet. Similar measurements have been made in another arcjet plasma diamond CVD reactor,[8] although the operating conditions between the two experiments are somewhat different. In this work, we particularly wish to determine if a significant fraction of the energy imparted into the gas in the arc is partitioned into ionization. We find electron and ion densities to be less than 10 ppm in the plume, which implies that less than 0.1% of the electrical energy in the arc is used to ionize the gas. We also wished to determine if ionization of the added NO perturbs the gas temperature. The ionization potential of NO is 9.25 eV and is therefore smaller than that for the other

species in the plasma, so significant ionization could occur if the plasma was in equilibrium at an energy of 1 or more eV. Although the electron temperature is in excess of 1 eV, we find the ion density to be significantly below the Saha equilibrium with this electron temperature. Thus, even though the added NO may result in a modest increase of the ion density, the gas temperature is not significantly lowered.

Experimental Arrangement

Figure 1 shows the experimental arrangement for these experiments. A dc-arc is struck in pure argon or a mixture of argon and hydrogen at the apex of a converging-diverging nozzle at a pressure of approximately 6 atmospheres. The effluent expands from a diverging nozzle into a chamber maintained between 25 and 30 torr, so the flow is choked. The jet is operated on pure argon or mixture compositions ranging from 24% hydrogen, 76 % argon to 69% hydrogen, 31% argon. Total flows range from 5.6 slm to 9.1 slm respectively. The electrical power dissipated in the arc is 1 to 2 kW (90-160 V and 10-12 A; the operating voltage depends on the percent hydrogen in the mixture). Methane (less than 0.2% of the total flow) is injected into the plume in the diverging nozzle. For some experiments nitric oxide (less than 0.15 % of the total flow) is introduced along with the methane. The nozzle assembly is water cooled and the water flow rate, water temperature and power input are monitored for calorimetric purposes. Approximately 4.5 cm downstream of the nozzle exit diamond grows beneath the stagnation

point of the luminous plume on a water cooled molybdenum substrate.

The Langmuir probe used in these experiments consists of a single 0.10-cm radius tungsten wire, insulated from a 6-mm diameter O.D. stainless steel tube by an alumina thermocouple tube and sealed with Torr-Seal epoxy. The probe tip extends beyond the alumina insulator, forming a cylindrical probe tip 0.20-cm long. The probe tip was centered on the axis of the flowing arcjet plasma plume with the long axis of probe's tip transverse to the plasma flow. Spatial scans are made by moving the arcjet source and its deposition substrate together using an XYZ translator. Thus, once centered on the arcjet plasma axis, the probe itself did not require movement to access various regions of interest in the arcjet flowfield.

Current-voltage (I-V) characteristic curves are obtained by sweeping the bias of the probe tip from -102 volts to + 12 volts relative to the grounded vacuum chamber; a typical measurement is shown in Figure 2. This range of probe voltages covers the entire ion saturation region and most of the transition region, but does not bias the probe into electron saturation. The probe voltage is produced by a ramped voltage from a signal generator and amplified by a four-quadrant operational-amplifier power supply. The probe bias is measured by a high impedance circuit. Both probe current and voltage are recorded, thus forming an I-V curve.

In operation, the probe is subjected to extremely severe thermal conditions. The high temperature of the gas and plasma frequently caused the probe tip to glow with slight incandescence. High concentrations of hydrogen in the arcjet plasma resulted in

rapid H-atom recombination on the surface of the probe tip, causing it to glow extremely bright. In fact, under some conditions of extreme incandescence, thermionic emission from the probe tip is observed and consequently measurements of the ion saturation current are not possible. Probe heating is most severe when the probe tip is 13-mm or closer to the arcjet orifice, and this problem prevented us from conducting measurements closer to the arcjet orifice. Probe heating was less severe as the orifice-probe distance increased.

Data Analysis Methods

The I-V curves were analyzed using collisionless, thin-sheath probe theory.[9] Collisionless theory is valid when the mean free path, λ_C, is significantly greater than the Debye length, λ_D. The mean free path for collisions is $\lambda_C \approx (n_g\sigma)^{-1}$, where n_g is the gas density and σ is an ion-neutral collision cross section. The gas density in the plume is approximately 10^{17} cm^{-3} and we estimate σ as 10^{-15} - 10^{-16} cm^2, resulting in a mean free path of approximately 10^{-2} - 10^{-1} cm. The Debye length is defined as $\lambda_D = \sqrt{kT_e/(4\pi e^2 n_e)}$, where k is Boltzmann's constant, T_e is the electron temperature, e is the electron charge and n_e is the electron density. We will later show that the electron densities were typically at least 10^{11} cm^{-3}, and electron temperatures were on the order of 1 eV, resulting in λ_D less than 2 x 10^{-3} cm. Thus $\lambda_C/\lambda_D \gg 1$, and the use of collisionless probe analysis is justified. Also, the radius of the probe was larger than both the

Debye length and the mean free path, so large probe analysis is applicable for these experiments.

We also neglected plasma flow speed in the probe analysis since the jet velocity is usually below the plasma sound velocity, which is typical of the speed at which ions enter the probe sheath (Bohm criterion) for eventual collection by the probe.[10] Recent Doppler-shift-based measurements[11] indicate with hydrogen in the feedstock that the plasma jet velocity is 2 $x10^5$ cm s^{-1}. The plasma sound speed, $v_s = \sqrt{kT_e/m_i}$, is of about 10 x 10^5 cm s^{-1} if H_3^+ is the predominant ion (see below), and thus flow speed corrections could be safely neglected.

Because both collisional and flow effects are negligible and λ_D is much smaller than the probe radius, we use simple large-probe analysis for cylindrical probes, which relates the ion current to the plasma density through the relation

$$I_i = \frac{1}{2} n_e e A_p \sqrt{\frac{kT_e}{m_i}} \qquad (1)$$

where I_i is the ion saturation current evaluated at plasma potential and A_p is the surface area of the probe.

Since our experiments are conducted with a variety of gases, many different ions are possible, depending on the gas mixtures used. Of course the identity of which ion is predominant in any situation is not possible using probes since ion collection is not mass selective. We use ionization potentials and reaction rates to guide our analysis when gas mixtures are present in the arcjet. In pure

argon (IP=15.8 eV) plasmas, we assume the dominant ion is Ar^+, m_i = 40 u. When molecular hydrogen (IP = 15.4 eV) is added to argon, the dominant ion is expected to be H_3^+ (m_i =3 u), produced from $Ar^+ + H_2 \rightarrow ArH^+ + H$, which has a fast rate constant, 7.4×10^{-10} cm^3 s^{-1}, followed by $ArH^+ + H_2 \rightarrow H_3^+ + Ar$, which also has a fast rate constant, 1.5×10^{-9} cm^3 s^{-1}.[12] Of course the reaction rates are driven by the concentrations of the reactant species as well as the rate constants. If the reactions produce significant concentrations of the product ions in 10 μs, which is a typical transit time of the plasma to the probe, then we use the mass of the product ion in our probe analysis. We expect the ion density to be orders of magnitude larger near the exit orifice of the arcjet, so the reactions are usually driven quite quickly to the expected ion. When NO (IP = 9.25 eV) is added to these gas mixtures, the dominant ions are expected to be either NO^+ (m_i =30 u) (from $H^+ + NO \rightarrow NO^+ + H$; rate constant = 1.9×10^{-9} cm^3 s^{-1}) or HNO^+ (m_i = 31 u) (from $H_3^+ + NO \rightarrow HNO^+ + H_2$; rate constant = 1.4×10^{-9} cm^3 s^{-1}).[12] In these latter examples, the difference in mass between NO^+ and HNO^+ is only about 3% so their exact identity or relative concentration is unimportant given the other uncertainties of the measurement and analysis.

We also examined electron impact ionization processes to determine their efficiency at producing ions. Using measured values of electron densities and temperatures, we determined that the rate of ion production via electron impact was approximately three or four orders of magnitude slower than the charge transfer reactions discussed above, so we neglected these processes. Equilibrium conditions rarely exist in this particular plasma jet because the

transit times are so short. In contrast to our earlier 200-torr arcjet experiments[1,2] this plasma is not close to being in local thermodynamic equilibrium and thus equilibrium calculations using, for example, the Saha equation, to determine the ion densities or even ion identity would be misleading.

Because excessive heating prevented us from biasing the probe to electron saturation conditions, the plasma potential is not measured directly but is derived from the floating potential through the relation

$$V_p = V_f + \frac{kT_e}{2e} \ln\left(\frac{2m_i}{\pi m_e}\right) \qquad (2)$$

Experimentally, V_f is determined by the voltage at which the probe collects no net current. The electron temperature, T_e, is determined from the transitional part of the I-V curve which is usually exponentially rising and varies as

$$I_e \propto \exp\left(\frac{e(V-V_p)}{kT_e}\right) \qquad (3)$$

from which T_e is determined from the reciprocal of the slope of I_e plotted versus the probe potential.

Results

Probe I-V characteristics were obtained for a variety of operating conditions for as many as three different downstream distances. We obtained I-V characteristics for the jet operating on pure argon at 32 torr chamber pressure, at 3 different distances. An example of a typical IV curve obtained in pure argon is shown in Figure 2. I-V curves were also obtained after adding hydrogen. For the Ar/H_2 mix, curves were also obtained with small amounts of either CH_4 (~.2 % of the total flow), or NO (~0.1 % of the total flow), or both, introduced downstream of the arc. Electron temperatures were obtained by plotting the logarithm of the electron current versus the probe voltage as shown in Figures 3a and 3b. The slope of the line thus obtained yields the electron temperature. The electron temperatures generally range from 0.8 to 2.6 eV. In some cases, as depicted in Figure 3a, there is a bimodal electron energy distribution with a high-energy tail whose electron temperature ranges from 5.6 to 11.8 eV.

Ion densities were obtained as described above. The ion densities measured closest to the orifice, 13 mm downstream, are 10^{12} to 10^{13} ions cm^{-3}, while densities 42 mm downstream of the nozzle are generally about an order of magnitude lower. The measured ion density decreases downstream from the orifice. In Figure 4, we show the variation of ion density versus downstream distance for various mixtures. Some observations can be made with respect to the spatial variation. In hydrogen plasmas, the ion density

decreases even though the gas temperature actually increases as a function of downstream distance.[3] The gas temperature increases in this case because of the large exothermicity of the hydrogen atom recombination. We believe the results show that the ionized component of the plasma is far out of equilibrium with the gas.

The electron temperature as a function of various gas compositions and distance is shown in Figure 5. There is very little variation in T_e as a function of distance, but it does depend more strongly on gas composition. Adding CH_4 with or without NO tends to decrease Te, due to efficient vibrational energy excitation by electrons in these molecules.

A primary reason for conducting these experiments was to determine if NO addition significantly altered the ionization levels in the plasma, or upset the plasma's normal energy balance. Although the apparent change in ion density from the ion saturation current alone is usually less than 20%, our assumption that adding NO to a hydrogen-containing plasma changes the ion mass from 3 u to 30 u causes the derived density from Eq. 1 to increase by a large factor of $\sqrt{10} = 3.2$. Thus the apparent ion density is much more strongly influenced by the assumption of a particular ion mass than by the change in measured ion saturation current.

Under the conditions we grow diamond films (49% H_2/ 51 % Ar/ 0.2% CH_4) the electron temperature is 1.1 eV and the ion density is 6×10^{11} cm^{-3} 13 mm from the nozzle exit plane. Addition of 0.15% NO results in an electron temperature of 1.0 eV and an ion density of 1.4×10^{12} cm^{-3}, which is an increase in ionization levels of about a factor of two. If we assume that all of the ions arise from the

NO (NO^+ or HNO^+), then approximately 1% of the NO is converted to ions at this position in the plume. Over a wider range of operating conditions, the addition of 0.1% NO modestly increases the ionization level, depending on position in the arcjet plume or gas composition.

The energy required to ionize the NO is only about 1% of the total electrical energy dissipated in the arc. Thus, the energy balance is not strongly influenced by NO addition, even though the ionization level can be markedly influenced.

Discussion

In either pure argon plasmas or argon/hydrogen plasmas with H_3^+ assumed to be the dominant neutral species, the Saha equation predicts the electron density to be insignificant at 1800 K, rising to only 4×10^4 cm^{-3} in hydrogen-containing plasmas at 2400 K. We find the measured electron density is at least 6 orders of magnitude larger. Therefore the electron/ion density is not in equilibrium with either the gas temperature or the electron temperature. Conversely, using the measured electron temperature of 1-2 eV, then the predicted electron density is greater than 10^{16} cm^{-3} in 25 torr hydrogen, which is 4 orders of magnitude greater than measured. We conclude, that the ionization is produced primarily in the arc region itself, and the resulting free electrons are convected downstream with the gas jet. This plasma is strongly out of equilibrium for the gas temperatures and pressures that prevail in jet.

Both the level of ionization and the electron temperatures in either unseeded or seeded arcjets is found to depart markedly from equilibrium levels using the measured gas temperature. Although the addition of NO appears to increase the ion density significantly is some cases, the increase is not as great as predicted from equilibrium considerations using, for example, the Saha equation. The electron temperature appears to be significantly hotter than the gas temperature and small uncertainties in it provide some flexibility in trying to fit the measured electron density with that predicted by the Saha equation. However we cannot achieve a reasonable agreement between a thermal equilibrium model and experiment using either the electron temperature or the gas temperature. The Saha equation relates the electron density to the ionization potential and electron temperature assuming Boltzmann equilibrium applies to both the neutral and ionized species of a plasma. Applying this analysis to our case in which the NO acts as a seed molecule in the bath of argon and atomic and molecular hydrogen, we write

$$\frac{n_e^2}{n_s - n_e} = 2\frac{Z_i}{Z}\left(\frac{2\pi m_e kT_e}{h^2}\right)^{3/2} \exp\left(\frac{-\varepsilon_i}{kT_e}\right) \qquad (4)$$

where n_s is the total number density of neutrals and ions of the ionizable seed species, Z_i and Z are the corresponding partition functions of the ion and neutral, h is Plank's constant, and ε_i is the ionization potential of the seed species.[13] In these experiments, the ionizable seed molecule, NO, was injected into the jet below the arcjet orifice, and its density based on flow rates and gas temperatures is

estimated to be no greater than 10^{13} cm^{-3}. Since the ionization potential of NO is 9.25 eV, and kT_e is about 1-2 eV, we estimate that the additional ionization provided by NO is essentially complete. Since our observations only show increases in ion density of between 50% to a factor of seven, the measured ionization is below that predicted in equilibrium. We conclude, therefore, that there is not enough time for equilibrium to be established from the time the NO enters the gas jet until it reaches the probe.

The electrons produced in the arc region are energetic, and remain hot as the gas convects downstream. Based on gas flow rates and the orifice diameter, the gas velocity in the jet is estimated to be 10^5 cm s^{-1}, and recent measurements[11] indicate that it is less than 2×10^5 cm s^{-1}. The electron thermalization rate is given by

$$\frac{dT_e}{dt} = 2\frac{m_e}{m_n} \nu_{en} (T_n - T_e) \qquad (5)$$

where T_n is the neutral gas temperature, m_n is the mass of a neutral gas particle, and ν_{en} is the electron neutral collision frequency. Under conditions relevant to this arcjet plasma, we estimate ν_{en} is about 3×10^9 s^{-1}, which leads to a time constant for electron thermalization, $\tau = m_n/(2\nu_{en}m_e) \approx 10$ μs. Again, since the transit time for the arcjet plasma to convect from the nozzle to the probe is of order 10 μs, the electrons simply do not have enough time to thermalize significantly with the hot gas, even though the gas is actually heating as a result of recombination of the atomic hydrogen. Thus, the electrons can cause significant excitation, dissociation, and

ionization along the entire length of the jet, and their temperature is more reflective of the plasma conditions in the arc region well within the arcjet source.

A comparison of ion densities with emission from the plume[3] shows some interesting similarities and differences. Emission from CH and H atom Balmer-γ drops by a factor of ~25-30 from 13 mm to 42 mm downstream in the plume, while the ion density drops by about a factor of ten over this same distance and the high energy electron energy distribution is depleted. The emission from the C_2 d-state shows a much smaller decrease, dropping by only a factor of ~3 over this same distance. These results suggest that electron impact excitation may be responsible for the H and CH emission but not C_2 emission. The electron energies appear not to be critical: H atom excitation requires ~11 eV while CH excitation requires ~2 eV, yet the emission drop is very similar for both CH and H atoms. The rotational and vibrational distributions in the CH A-state suggest that electron impact is not the only excitation mechanism for this state and that chemiluminescent reactions probably account for some of its excitation.[3] Chemiluminescent reactions probably account for most of the C_2 excitation.

We can compare our results with measurements in other arcjets. Sankovic[14] has used Langmuir probes to study a 1 kW H_2/N_2 (33% H_2, 67 % N_2) arcjet . In his studies, the electron densities ranged from 2 x 10^{11} to approximately 7 x10^{10} cm^{-3} on the centerline at 3 cm to 5 cm downstream of the nozzle, similar to our results. Electron temperatures were lower than those in our jet,

approximately 0.15-0.35 eV. This arcjet is directed into a low-pressure chamber and by the time the plasma reaches the probe there is the opportunity for rapid cooling of the electrons by vibrational excitation of N_2.

Reeve and Weimer[8] have used a floating double probe to measure plasma parameters in an arcjet used for the deposition of diamond. This jet operates on argon, with hydrogen (28% of total flow) and methane (<1% of total flow) injected into the plume in the diverging section of the nozzle; chamber pressure is 60 torr. They made measurement approximately 1.2 cm to 7 cm downstream of the nozzle and 9 mm to 22.2 mm from the centerline, and found electron temperatures ranging from 2.3 eV near the nozzle exit to 0.4 eV in the downstream peripheral regions of the plume. Their electron densities range from 7×10^{11} cm^{-3} to 1×10^{9} cm^{-3} respectively. Even though this jet operates under quite different conditions from our jet, the results are very similar: ion densities less than 10 ppm and electron temperature much greater than the gas temperature. In this jet, the argon is ionized in the arc; the ions and electrons are then convected downstream along with the reacting hydrogen and methane.

Storm and Cappelli[15] infer electron densities near 10^{13} cm^{-3} in a 1.4 kW hydrogen arcjet at the exit plane. This level of ionization is roughly ten time larger than our measurements 13-mm downstream from the exit plane in our arcjet. We find these measurements to be consistent with the drop in ion density with axial distance.

Conclusions

Our arcjet has a low degree of ionization (less than 10 ppm) and the ion density and electron temperature are not in Saha equilibrium. We see a drop in electron densities of about a factor of ten, as we move 3 cm downstream in the jet, while the electron temperatures remain fairly constant. The addition of methane to the argon/hydrogen jet results in an increase in the ion density and with the addition of NO, the ion density rises even more. In any event, an insignificant amount of input energy of this jet results in ionization compared to dissociation and gas heating.

Acknowledgments

This work is supported by the Army Research Office under Contract DAAH04-93-K-0001.

References

1 A. W. Phelps and K. R. Stalder, Appl. Phys. Lett. **57**, 1090 (1990)

2 K. R. Stalder and R. L. Sharpless, J. Appl. Phys. **68**, 6187 (1990)

3 E. A. Brinkman, G. A. Raiche, M. Brown ,J. B. Jeffries, submitted to Appl. Phys. B

4 D. R. Crosley, Combust. Flame, **78**, 153 (1989).

5 D. R. Crosley, in *Turbulence and Molecular Processes in Combustion*, T. Takeno, Ed., Elsevier, Amsterdam, 1993, p.221.

6 G. A. Raiche and J. B. Jeffries, Appl. Opt., **32**, 4629 (1993).

7 N. Heberle, Ph.D. thesis, University of Bielefeld, 1994

8 S. W. Reeve and W. A. Weimer, J. Vac. Sci. Technol. A **12**, 3131 (1994)

9 N. Hershkowitz, in *Plasma Diagnostics*, Vol 1, ed. by O. Auciello and D. L. Flamm (Academic Press, Boston, 1989)

10 P. M. Chung, L. Talbot, and K. J. Touryan, AIAA Journal, **12**, 133 (1974)

11 W. Juchmann and J. B. Jeffries, private communication.

12 D. L. Albritton, Atomic Data and Nuclear Data Tables, **22**, 1 (1978)

13 M. Mitchner and C. Kruger, *Partially Ionized Gases* (John Wiley & Sons, New York, 1973)

14 J. M. Sankovic, NASA Technical Memorandum 103638 (1990)

15 P. V. Storm and M. A. Cappelli, Appl. Optics, in press (1996)

Figure Captions

1. Experimental arrangement.

2. Typical current-voltage (I-V) characteristic curve. Gas flow = 7 standard liters per minute (slm) argon; gas pressure = 32 torr; nozzle-probe distance = 42 mm.

3. Electron current versus probe bias showing a) BiMaxwellian electron energy distribution; 7.7 standard liters per minute argon, gas pressure= 32 torr, nozzle-probe distance =, and b) single Maxwellian electron energy distribution.

4. Ion density versus gas composition and distance downstream. Argon and hydrogen plasma, at z=13 mm (closed circles); plasma seeded with CH_4 only, at z=13 mm (closed squares); plasma seeded with both CH_4 and NO, at z=13 mm (closed triangles). Argon and hydrogen plasma, at z=42 mm (open circles); plasma seeded with CH_4 only, at z=42 mm(open squares); plasma seeded with both CH_4 and NO, at z=42 mm (open triangles).

5. Electron temperature versus gas composition and distance downstream. Argon and hydrogen plasma, at z=13 mm (closed circles); plasma seeded with CH_4 only, at z=13 mm (closed squares); plasma seeded with both CH_4 and NO, at z=13 mm (closed triangles). Argon and hydrogen plasma, at z=42 mm (open circles); plasma seeded with CH_4 only, at z=42 mm(open squares); plasma seeded with both CH_4 and NO, at z=42 mm (open triangles).

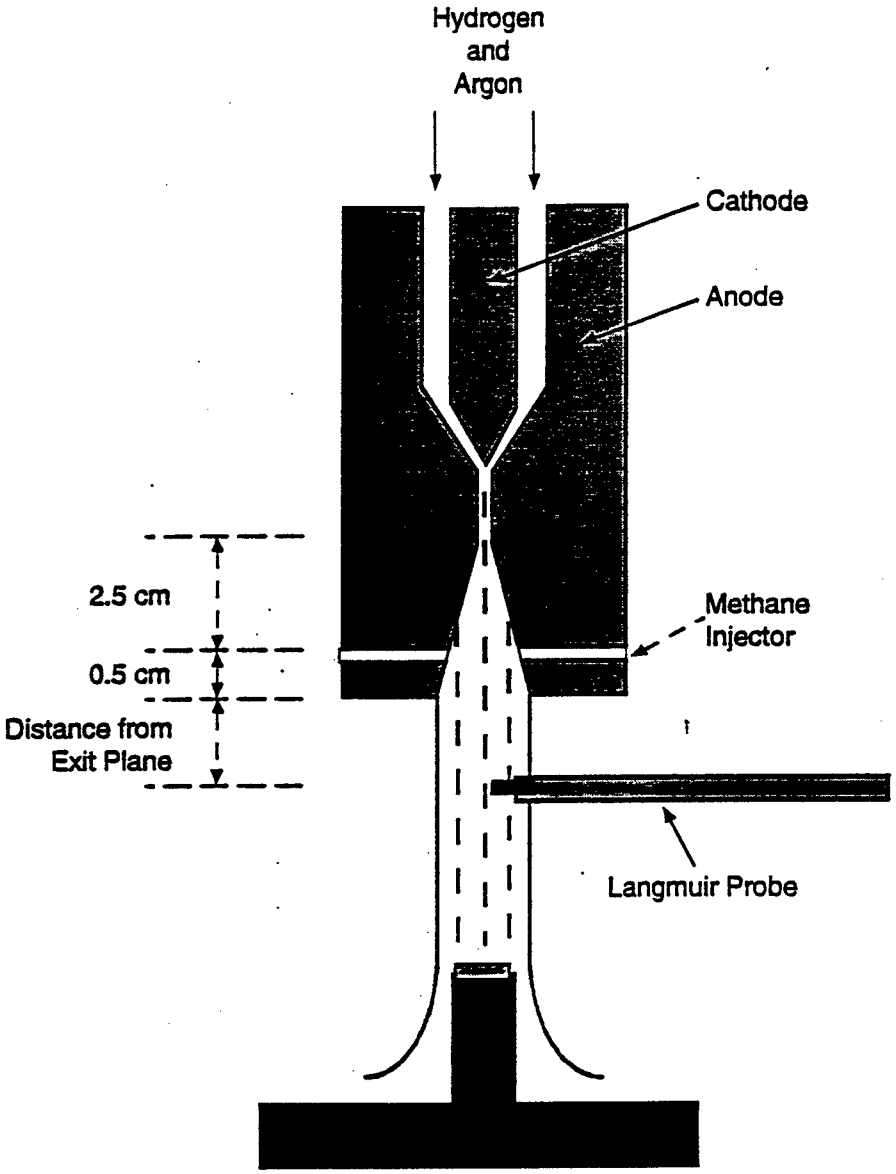
Hydrogen
and
Argon
Cathode
Anode
2.5 cm
0.5 cm
Distance from
Exit Plane
Methane
Injector
Langmuir Probe
Water Cooled Substrate
NAM-333581-1

Figure 1.

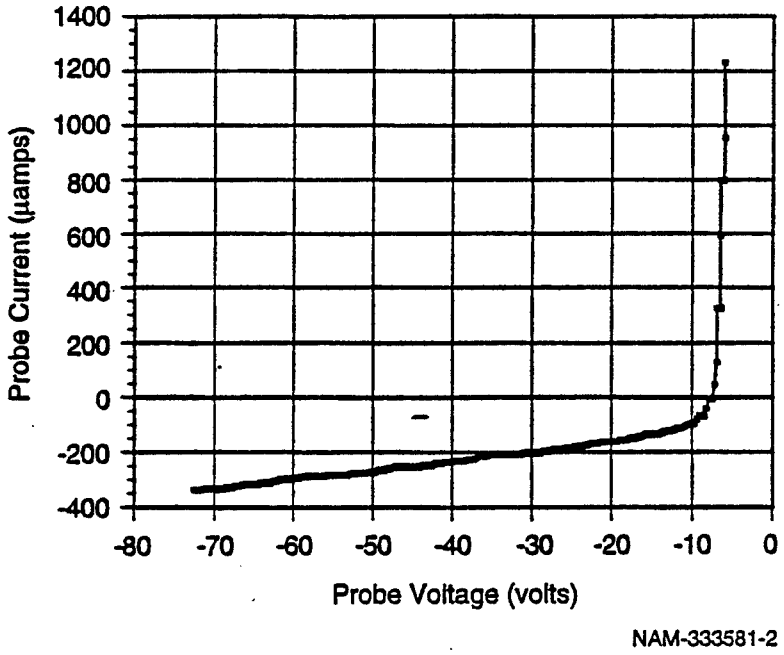
1400
1200
1000
800
600
400
200
0
-200
-400
Probe Current (µamps)
-80
-70
-60
-50
-40
-30
-20
-10
0
Probe Voltage (volts)
NAM-333581-2

Figure 2.

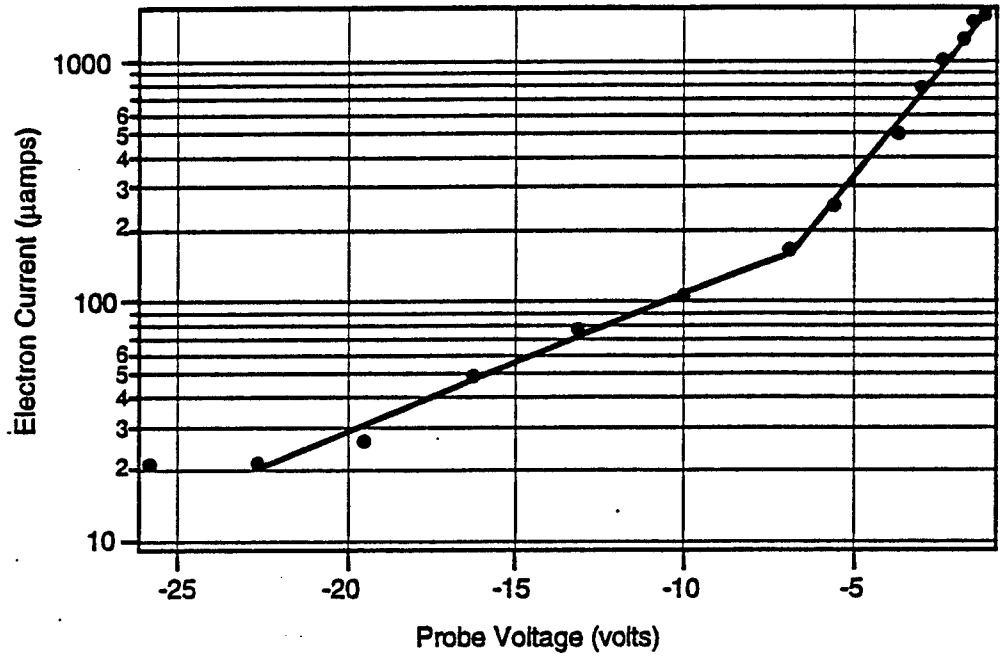

Figure 3a.

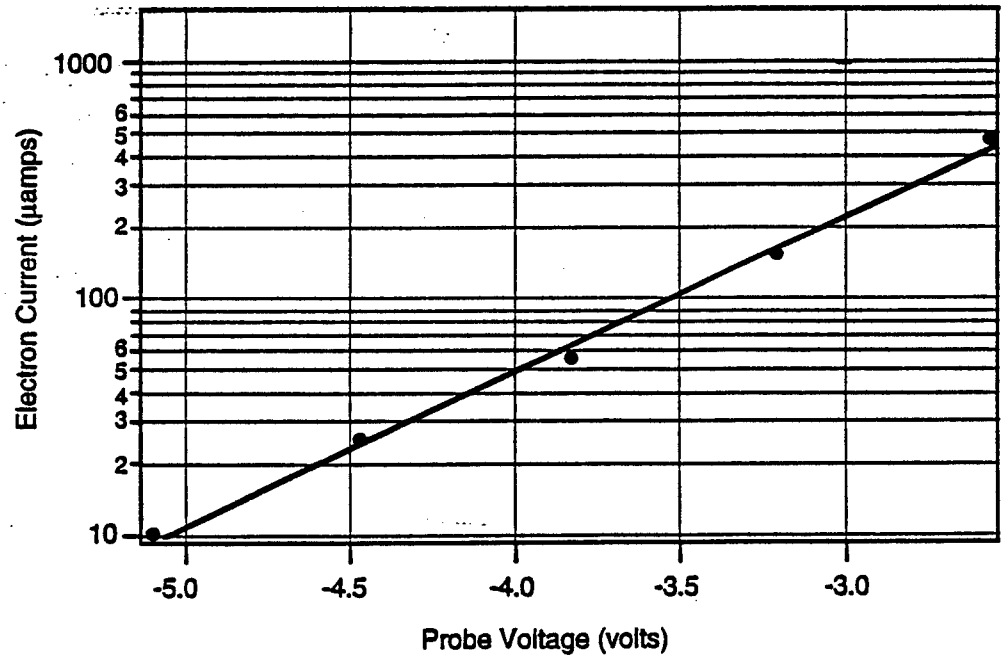

Figure 3b.

NAM-333581-3

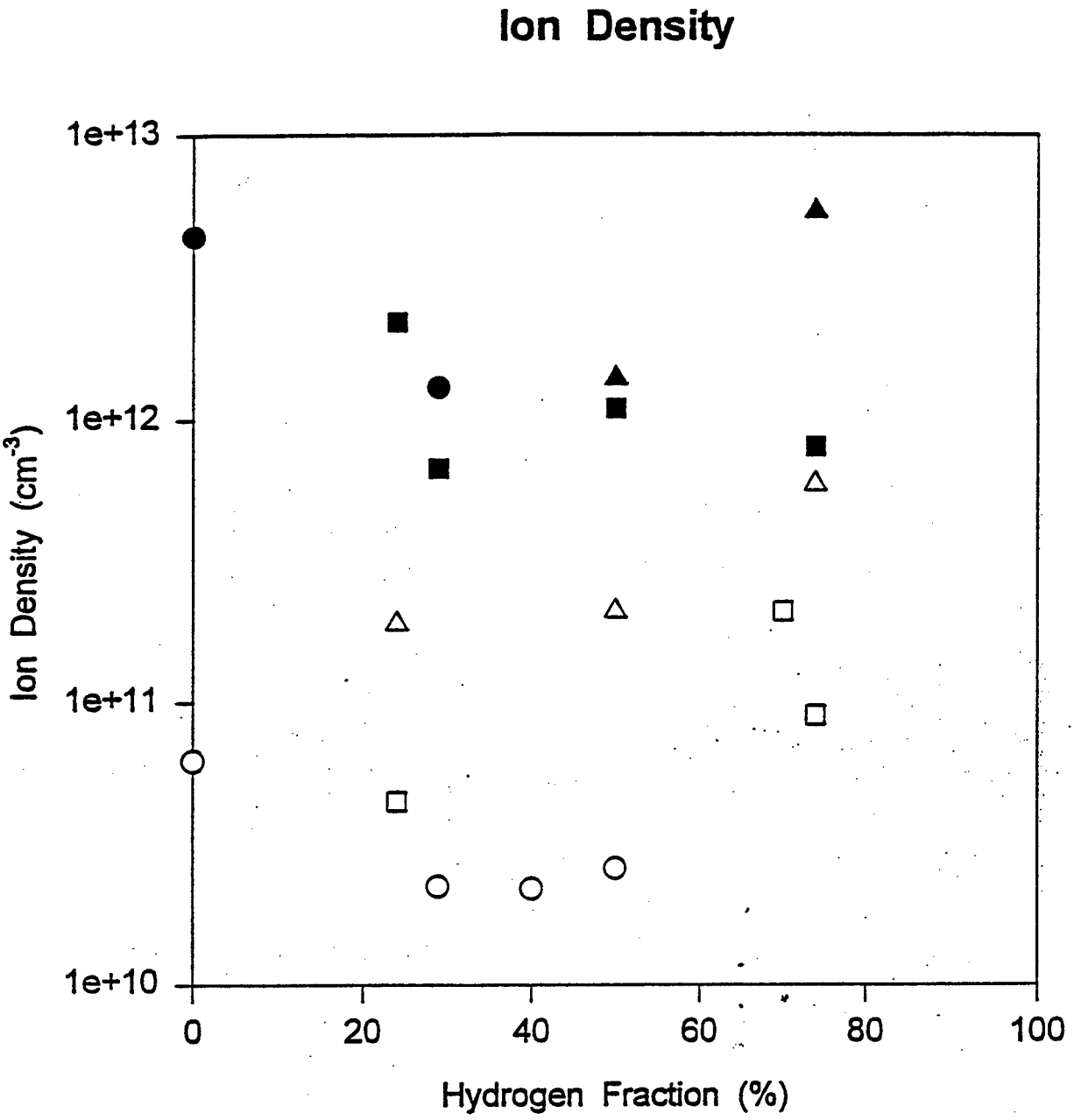
Ion Density
1e+13
1e+12
1e+11
1e+10
Ion Density (cm-3)
0
20
40
60
80
100
Hydrogen Fraction (%)

Figure 4

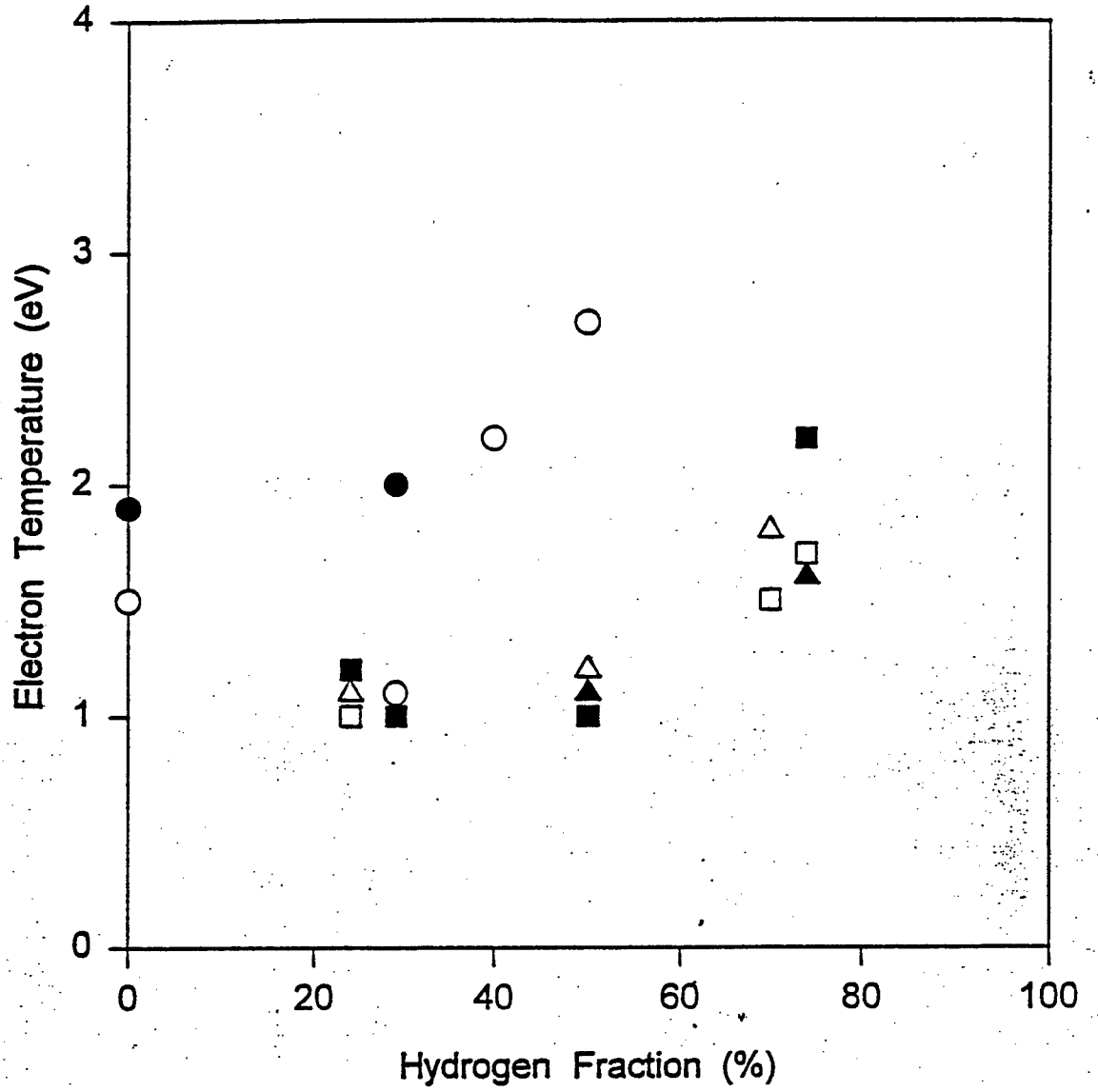
Electron Temperature
Electron Temperature (eV)
Hydrogen Fraction (%)
0
1
2
3
4
0
20
40
60
80
100

Figure 5